

## REVIEW

[View Article Online](#)  
[View Journal](#) | [View Issue](#)



Cite this: *Chem. Sci.*, 2024, **15**, 15023

Received 30th April 2024  
Accepted 2nd August 2024  
DOI: 10.1039/d4sc02888k  
[rsc.li/chemical-science](http://rsc.li/chemical-science)

## Four-electron reduction of CO<sub>2</sub>: from formaldehyde and acetal synthesis to complex transformations

Sarah Desmons,<sup>†a</sup> Julien Bonin,<sup>\*bc</sup> Marc Robert<sup>ID \*bcd</sup> and Sébastien Bontemps<sup>ID \*a</sup>

The expansive and dynamic field of the CO<sub>2</sub> Reduction Reaction (CO<sub>2</sub>RR) seeks to harness CO<sub>2</sub> as a sustainable carbon source or energy carrier. While significant progress has been made in two, six, and eight-electron reductions of CO<sub>2</sub>, the four-electron reduction remains understudied. This review fills this gap, comprehensively exploring CO<sub>2</sub> reduction into formaldehyde (HCHO) or acetal-type compounds (EOCH<sub>2</sub>OE, with E = [Si], [B], [Zr], [U], [Y], [Nb], [Ta] or -R) using various CO<sub>2</sub>RR systems. These encompass (photo)electro-, bio-, and thermal reduction processes with diverse reductants. Formaldehyde, a versatile C<sub>1</sub> product, is challenging to synthesize and isolate from the CO<sub>2</sub>RR. The review also discusses acetal compounds, emphasizing their significance as pathways to formaldehyde with distinct reactivity. Providing an overview of the state of four-electron CO<sub>2</sub> reduction, this review highlights achievements, challenges, and the potential of the produced compounds – formaldehyde and acetals – as sustainable sources for valuable product synthesis, including chiral compounds.

### 1. Introduction

Research in CO<sub>2</sub> transformations conducted by the Carbon Capture and Utilization (CCU) community is driven by both fundamental and applicative motivations. On the fundamental side, the goal is to find the keys to transform this thermodynamically and kinetically stable molecule. On the practical side, there is a desire to emulate nature by using CO<sub>2</sub> either as a synthetic building block or as an energy carrier. These objectives gain urgency due to the increasing concentration of atmospheric CO<sub>2</sub> and the inevitable depletion of fossil

<sup>a</sup>LCC-CNRS, Université de Toulouse, CNRS, 205 route de Narbonne, 31077 Toulouse Cedex 04, France. E-mail: [sebastien.bontemps@lcc-toulouse.fr](mailto:sbastien.bontemps@lcc-toulouse.fr)

<sup>b</sup>Laboratoire d'Electrochimie Moléculaire, Université Paris Cité, CNRS, F-75013, Paris, France. E-mail: [julien.bonin@sorbonne-universite.fr](mailto:julien.bonin@sorbonne-universite.fr); [marc.robert@sorbonne-universite.fr](mailto:marc.robert@sorbonne-universite.fr)

<sup>c</sup>Institut Parisien de Chimie Moléculaire, Sorbonne Université, CNRS, F-75005, Paris, France

<sup>d</sup>Institut Universitaire de France (IUF), F-75005, Paris, France

† Present address: Laboratory of Inorganic Synthesis and Catalysis, Institute of Chemical Sciences and Engineering, Ecole Polytechnique Fédérale de Lausanne (EPFL), EPFL-ISIC-LSCI, BCH 3305, Lausanne, CH 1015 Switzerland.



Sarah Desmons

Her current research focuses on the enantioselective production of chiral amines via tailored bio-catalyzed hydroamination reactions.

Sarah Desmons is currently a postdoctoral researcher in the Laboratory of Inorganic Synthesis and Catalysis (LSCI) at École Polytechnique Fédérale de Lausanne (EPFL) in Switzerland. She obtained her PhD in Chemistry and Biochemistry for the chemo-enzymatic conversion of CO<sub>2</sub> into carbohydrates from the Laboratoire de Chimie de Coordination (LCC) and the Toulouse Biotechnology Institute (TBI) in Toulouse, France.



Julien Bonin

Julien Bonin received his PhD in molecular physical chemistry from the Université Paris-Sud 11 in 2005. He then joined the Radiation Laboratory at the University of Notre Dame as a Postdoctoral Research Associate for one year. From 2006 to 2024, he has been an Associate, then a Full Professor of Chemistry at the Université Paris Cité, and he has now joined Sorbonne Université. His current research interests are related to photo-

chemistry, redox catalysis and CO<sub>2</sub> reduction.



resources. Given its significance and broad scope, the field of  $\text{CO}_2$  transformation has been extensively covered in numerous reviews and books. Early reviews<sup>1</sup> and comprehensive perspectives<sup>2</sup> provide authoritative insights. Other reviews focus specifically on the use of  $\text{CO}_2$  as an energy carrier<sup>3</sup> or as a synthetic reagent.<sup>4</sup> From an applied perspective, the importance of Life Cycle Assessment (LCA)<sup>5</sup> has been considered to evaluate the industrial potential of various processes.<sup>6</sup> From a thermodynamic standpoint, this expansive field can be categorized into reactions involving a redox event at the carbon atom of  $\text{CO}_2$  ( $\text{CO}_2$  Reduction Reaction:  $\text{CO}_2\text{RR}$ ) or those that do not.<sup>4a</sup> Motivations for the  $\text{CO}_2\text{RR}$  include using  $\text{CO}_2$  as an energy carrier, as energy is formally stored during  $\text{CO}_2$  reduction, and as a sustainable source of carbon. In the  $\text{CO}_2\text{RR}$ , comprehensive reviews have focused on the type of reduction used, whether it involves thermal reduction with dihydrogen,<sup>7</sup> hydroboranes,<sup>8</sup> or hydrosilanes,<sup>9</sup> (photo)electro reduction<sup>10</sup> or bio-catalysed reduction.<sup>11</sup> Other reviews explore the homogeneous<sup>12</sup> or heterogeneous<sup>13</sup> nature of the catalytic system.

Within the  $\text{CO}_2\text{RR}$ , the level of reduction of  $\text{CO}_2$  is arguably the most important parameter to consider. Since the carbon atom of  $\text{CO}_2$  is fully oxidized (+IV), it can be reduced by as much as  $8\text{e}^-$  giving rise to four possible even reduction states shown (Scheme 1). The +II, 0, -II and -IV carbon atom oxidation states can be reached by electroreduction or hydrogenation of  $\text{CO}_2$ . The corresponding  $\text{C}_1$  reduction products are represented in Scheme 1(a):  $\text{CO}^{14}$  and  $\text{HCOOH}^{15}$  ( $2\text{e}^-$ ),  $\text{HCHO}$  and  $\text{ROCH}_2\text{OR}$  ( $4\text{e}^-$ ),  $\text{CH}_3\text{OH}^{15a,16}$  ( $6\text{e}^-$ ) and  $\text{CH}_4$  (ref. 17) ( $8\text{e}^-$ ). As shown in Scheme 1(b), the same oxidation states are reached with hydroelementation (E-H) reactions. Using mostly hydroborane ( $\text{E} = \text{BR}_2$ ) and hydrosilane ( $\text{E} = \text{SiR}_3$ ),  $\text{HCOOE}$  ( $2\text{e}^-$ ),  $\text{EOCH}_2\text{OE}$  and  $\text{HCHO}$  ( $4\text{e}^-$ ),  $\text{CH}_3\text{OE}$  ( $6\text{e}^-$ ) and  $\text{CH}_4$  ( $8\text{e}^-$ ) have indeed been reported. Although it does not correspond to a formal hydroelementation, the catalytic formation of  $\text{CO}$  ( $2\text{e}^-$ ) was reported with hydroborane<sup>18</sup> and with diborane.<sup>19</sup> The  $4\text{e}^-$  reduction products of  $\text{CO}_2$  – namely formaldehyde and acetal compounds

– occupy a distinct position compared to other  $\text{C}_1$  reduction products (Scheme 1c). The reasons for this are explained below.

### 1.1. Why reducing $\text{CO}_2$ by $4\text{e}^-$ to formaldehyde?

In the context of an increasing demand for complex transformations of  $\text{CO}_2$  beyond the simple  $\text{C}_1$  building blocks mentioned earlier<sup>20,21</sup> and the desire for long-term  $\text{CO}_2$  storage, formaldehyde offers unparalleled potential in terms of reactivity and versatility.<sup>22</sup> More than 30 million tons of formaldehyde are produced and used annually by the chemical industry. This commodity compound is typically synthesized from the partial oxidation of methanol under energy-demanding conditions, representing over 35% of the total methanol transformation.<sup>22a,23</sup> A mild and sustainable synthesis of formaldehyde from  $\text{CO}_2$  would thus represent a significant advancement for the chemical industry. Most industrial applications use formaldehyde as a reticulating agent in condensation reactions leading to various  $\text{C-N}$ ,  $\text{C-O}$ ,  $\text{C-S}$ , and  $\text{C-C}$  bonds.

Furthermore, formaldehyde serves as a precursor to more complex molecules, including chiral ones,<sup>24</sup> being a  $\text{C}_1$  and a  $\text{C}_n$  source in aldol<sup>25</sup> and formose reactions,<sup>26</sup> notably. These transformations are beyond the reach of other  $\text{CO}_2$  reduction products.

However, there is still no selective and sustainable synthesis of formaldehyde from  $\text{CO}_2$ . This can be attributed to two major issues: (i) the  $4\text{e}^-$  reduction stage requires any catalytic system to overcome the energy barriers for both the 2 and  $4\text{e}^-$  reduction steps while preventing the  $6\text{e}^-$  reduction, and (ii) the detection of formaldehyde ( $\text{HCHO}$ ) is challenging due to its intrinsic instability, limiting further development and optimization. Depending on the reaction media (pH, solvent, co-substrates), formaldehyde can polymerize, precipitate, or react with other chemicals present in the mixture, making its characterization difficult. Several detection methods have been used, such as optical methods, chemical derivatization for HPLC and GC analysis, or chemical conversion for colorimetric method analysis (established by Nash in the 1950s).<sup>27</sup> Recently,



Marc Robert

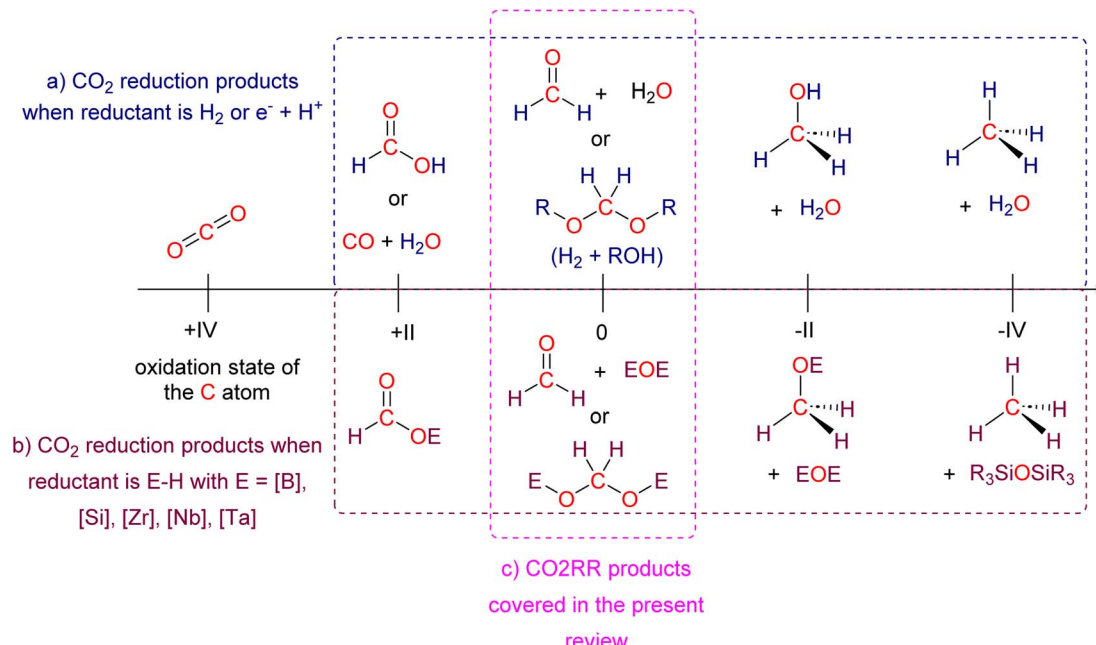
Advisory Board member at *Angewandte Chemie International Edition*, *ChemSusChem* (Wiley), *Artificial Photosynthesis* and *ACS Electrochemistry* (ACS).



Sébastien Bontemps

Sébastien Bontemps has received his PhD in 2006 from the University Paul Sabatier in Toulouse and carried out postdoctoral stays at the University of Chicago and McGill University. Since 2009, he has been a CNRS researcher in LCC-CNRS in Toulouse developing research studies directed at  $\text{CO}_2$  transformations, boron and hydride chemistry and at the synthesis of new first row metal complexes.





**Scheme 1**  $\text{C}_1$  products generated from  $\text{CO}_2$  reduction by (a) hydrogenation or electroreduction or (b) hydroelementation reactions. (c) Formaldehyde and acetal compounds as the products of four-electron reduction of  $\text{CO}_2$  covered in the present review.

a new and simple method for trapping and quantifying formaldehyde in aqueous solutions by  $^1\text{H}$  NMR was designed, otherwise allowing for isotope labelling experiments and thus unambiguous demonstration that the  $\text{HCHO}$  production arises from  $\text{CO}_2$  reduction.<sup>28</sup>

## 1.2. Why reducing $\text{CO}_2$ by $4\text{e}^-$ to acetal compounds?

The formation of acetal ( $\text{EOCH}_2\text{OE}$ ) from hydroelementation of  $\text{CO}_2$  is an important process linked to formaldehyde, because

(i) Some of these acetal compounds were shown to quantitatively release formaldehyde, offering an efficient and selective access to it under particularly mild conditions and with isotope labelling proving the origin of formaldehyde. The generated formaldehyde was subsequently used as  $\text{C}_1$  and also  $\text{C}_n$  sources,<sup>29</sup> and notably in the first enantioselective transformation of  $\text{CO}_2$  into a  $\text{C}_4$  carbohydrate,<sup>30</sup> representing the highest level of complexity obtained from  $\text{CO}_2$  at that time.<sup>31</sup>

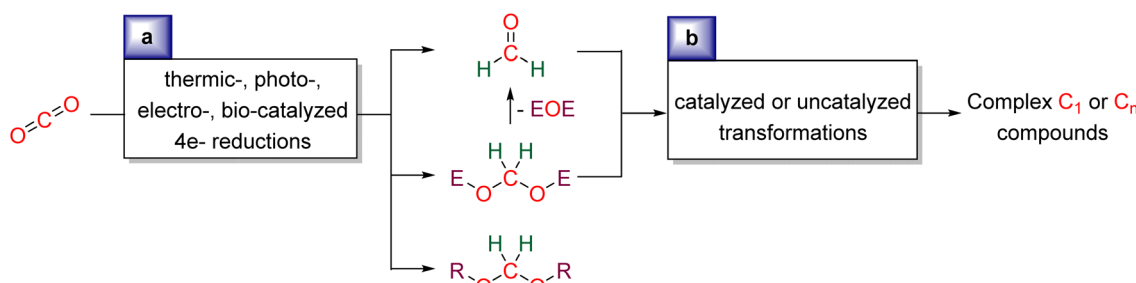
(ii) Beyond the release of formaldehyde, acetal compounds were also involved in transformations related to but distinct

from formaldehyde, notably when used as a  $\text{C}_n$  source. Interestingly, in one case, boryl moieties remained on the product, demonstrating a difference in reactivity compared to formaldehyde.<sup>32</sup> This finding should open opportunities to use the boryl or silyl functional groups as an integral part of new compounds as opposed to a waste moiety.

(iii) Finally, mild conditions and organic solvents used in hydroelementation enable *in situ* NMR monitoring leading to easier proofs of the origin of the acetal or formaldehyde by isotopic labelling experiments.

## 1.3. Objective and organization of the review

We aim at presenting the challenges and mechanistic considerations associated with formaldehyde<sup>33</sup> and acetal synthesis from  $\text{CO}_2$  (Scheme 2a), as well as highlighting the reactions in which these reduction products have been involved (Scheme 2b). This review is organized by the type of reduction system: Hydrosilylation (Section 2), Hydroboration (Section 3), Other hydroelementation reactions (Section 4), Hydrogenation



**Scheme 2** General scheme presenting the current review: (a) synthesis of formaldehyde or acetal compounds from  $\text{CO}_2\text{RR}$  and (b) utilisation of formaldehyde and acetal as  $\text{C}_1$  and  $\text{C}_n$  sources.

(Section 5), Electroreduction (Section 6), Photo(electro)reduction (Section 7), and Bio-catalysed reduction (Section 8). In each section, the reduction and subsequent transformations of the  $4e^-$  reduction products are presented, with special attention drawn to the mechanisms involved.

## 2. Hydrosilylation

Hydrosilylation of multiple C=C, C=O and C=N bonds has been intensely investigated, fuelling applications in the silicon industry as well as in synthetic chemistry, in asymmetric reductions in particular.<sup>34</sup> Hydrosilylation of CO<sub>2</sub> involves the addition of a Si–H bond to the C=O bond, transferring the hydride to the carbon atom and forming a Si–O bond. This reaction is favoured kinetically and thermodynamically by the polarity of the Si–H bond (electronegativity (E. N.) of H = 2.2, Si = 1.9) and the formation of a strong Si–O bond (>500 kJ mol<sup>-1</sup>),<sup>35</sup> respectively. As a consequence, CO<sub>2</sub> hydrosilylation usually operates under mild conditions of temperature and pressure.

CO<sub>2</sub> hydrosilylation was first reported in 1981 with Ru- and Pd-based catalysts, independently.<sup>36</sup> In both cases, the reduction process led to formoxysilane (2e<sup>-</sup> reduction product). Hydrosilylation beyond the 2e<sup>-</sup> reduction stage was hypothesized in these two initial reports based on the observation of bis(silyl) ether (R<sub>2</sub>SiOSiR<sub>3</sub>) and of a small amount of formaldehyde (<4% yield) with the Ru-based catalyst.<sup>36b</sup> In 1989, an Ir-based catalyst enabled unambiguous observation of the hydrosilylation of CO<sub>2</sub> beyond the 2e<sup>-</sup> reduction stage. In this pioneering study, it was remarkable that the 2, 4 and 6e<sup>-</sup> reduction products – formoxysilane, bis(silyl)acetal (BSA) and methoxysilane, respectively – were subsequently observed.<sup>37</sup> Finally, the first report of CO<sub>2</sub> hydrosilylation into methane was published in 2006 by Matsuo and Kawaguchi with a [Zr]/B(C<sub>6</sub>F<sub>5</sub>)<sub>3</sub> catalytic system.<sup>38</sup>

Since these initial reports, the reduction of CO<sub>2</sub> by 4e<sup>-</sup> with hydrosilane witnessed a growing attention. The present section aims to cover in detail (i) the formation of BSA and formaldehyde in part 2.1, (ii) the mechanisms accounting for their generation in part 2.2, (iii) the proposed origin of the selectivity toward BSA in part 2.3, and (iv) their use as reactive intermediates in reductive functionalization reactions leading to more complex products in part 2.4 (Scheme 3).

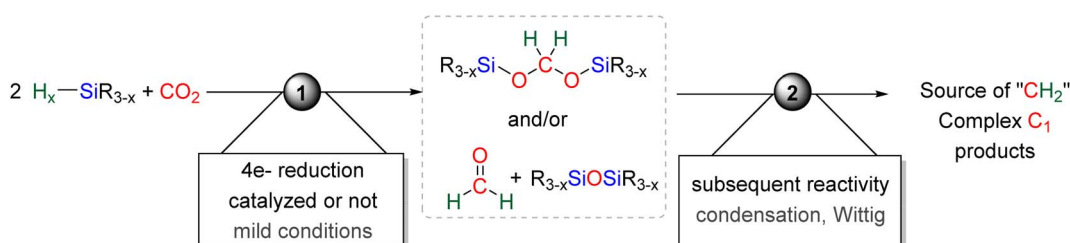
### 2.1. Hydrosilylation of CO<sub>2</sub> into bis(silyl)acetals (BSAs) and formaldehyde

**2.1.1. Description of BSA 1 to BSA 11.** Bis(silyl)acetals (BSAs) are obtained from the double hydrosilylation of one

molecule of CO<sub>2</sub>. They feature an acetal core with two stabilizing silyl moieties attached to both oxygen atoms. Reported BSAs are depicted in Scheme 4 and their NMR characterizations are given in Table 1. Currently, eleven BSAs (BSA 1–11) have been reported in the literature. BSA 1–6 have been generated from tertiary silanes HSiMe<sub>3</sub>, HSiEt<sub>3</sub>, HSiPh<sub>3</sub>, HSiMe<sub>2</sub>Et, HSiPh<sub>2</sub>Me and HSiPhMe<sub>2</sub>, respectively, in excellent NMR yields (79 to 99%) regardless of the nature of silane substituents (trialkyl, triaryl or mixed silanes). Among them, only BSA 2 and 3 were isolated with best yields of 94 and 95% with C4 and C17, respectively. The utilization of secondary and primary silanes led to the formation of BSA 7–10. None of them was isolated. BSA 10a was characterized from a quasi-stoichiometric control experiment between a Co–formate complex and phenylsilane.<sup>42</sup> The use of only three equivalents of silane enabled the characterization of BSA 10a as the sole (silyl)acetal, in contrast to the observation of several BSA signals under the catalytic conditions. The presence of more than one hydride as reductive entities on the silicon atom with primary or secondary silanes indeed leads to the observation of multiple (silyl)acetal signals. This was clearly exemplified by Eisenberg *et al.* when using the dialkylsilanes, Me<sub>2</sub>SiH<sub>2</sub> and Et<sub>2</sub>SiH<sub>2</sub> (BSA 7–8, respectively).<sup>37</sup> In both cases, three <sup>13</sup>C and <sup>1</sup>H NMR signals characteristic of BSA were observed. Despite the ill-defined nature of the acetal mixture, the characteristic NMR chemical shifts and the absence of other signals in this area enable not only the detection but also the quantification of the (silyl)acetal entities. As shown in Table 1, a narrow range of methylene chemical shifts was observed in <sup>1</sup>H NMR (4.96 to 5.80 ppm) and in <sup>13</sup>C NMR (83 to 85.7 ppm) with <sup>1</sup>J<sub>CH</sub> coupling constants between 161.5 and 164.4 Hz. In addition, conclusive labelling studies were reported with <sup>13</sup>CO<sub>2</sub>. <sup>29</sup>Si NMR data are restricted to BSA 2, 4–6, and 11 with chemical shifts of 18.3, 17.7, -2.74, 6.99 and 24.0 ppm, respectively.

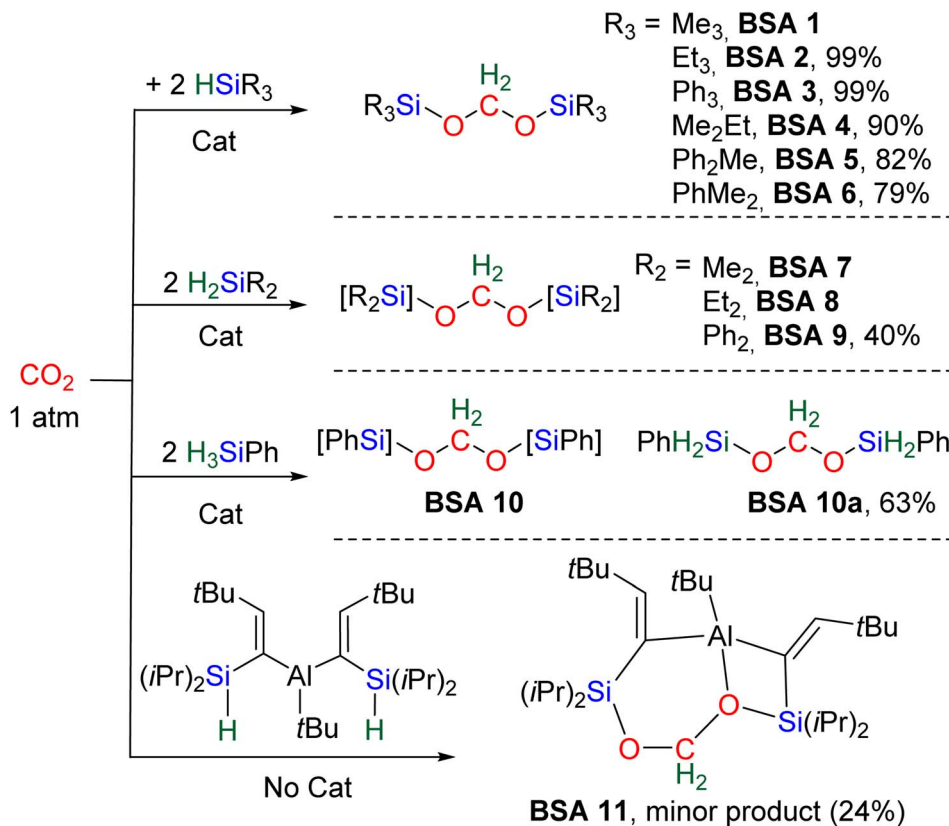
Most of the characterized BSA features tertiary silane moieties (BSA 1–6 and BSA 11). Three of them were isolated (BSA 2, 3 and 11) and the latter two were characterized by XRD. The higher stability of (silyl)acetals featuring tertiary silyl moieties is discussed in the mechanism section, Section 2.2. Catalysts were necessary to generate BSA but for BSA 11, which was derived from the hydrosilylation of CO<sub>2</sub> by an aluminum complex featuring two hydrosilane pendent moieties. BSA 11 was generated as a minor product in 24% yield and features an acetal fragment stabilized by the Lewis acidic alane moiety.<sup>43</sup>

**2.1.2. Catalytic systems.** Selective (C1–C25) and non-selective (C26–C36) catalytic systems leading to the formation of BSA 1–10 are described separately below. We consider



Scheme 3 General scheme of Section 2: CO<sub>2</sub> hydrosilylation.





Scheme 4 Synthesis of BSA 1–11. The yields indicated are the best reported yields.

Table 1 NMR characterization of BSA 1–11

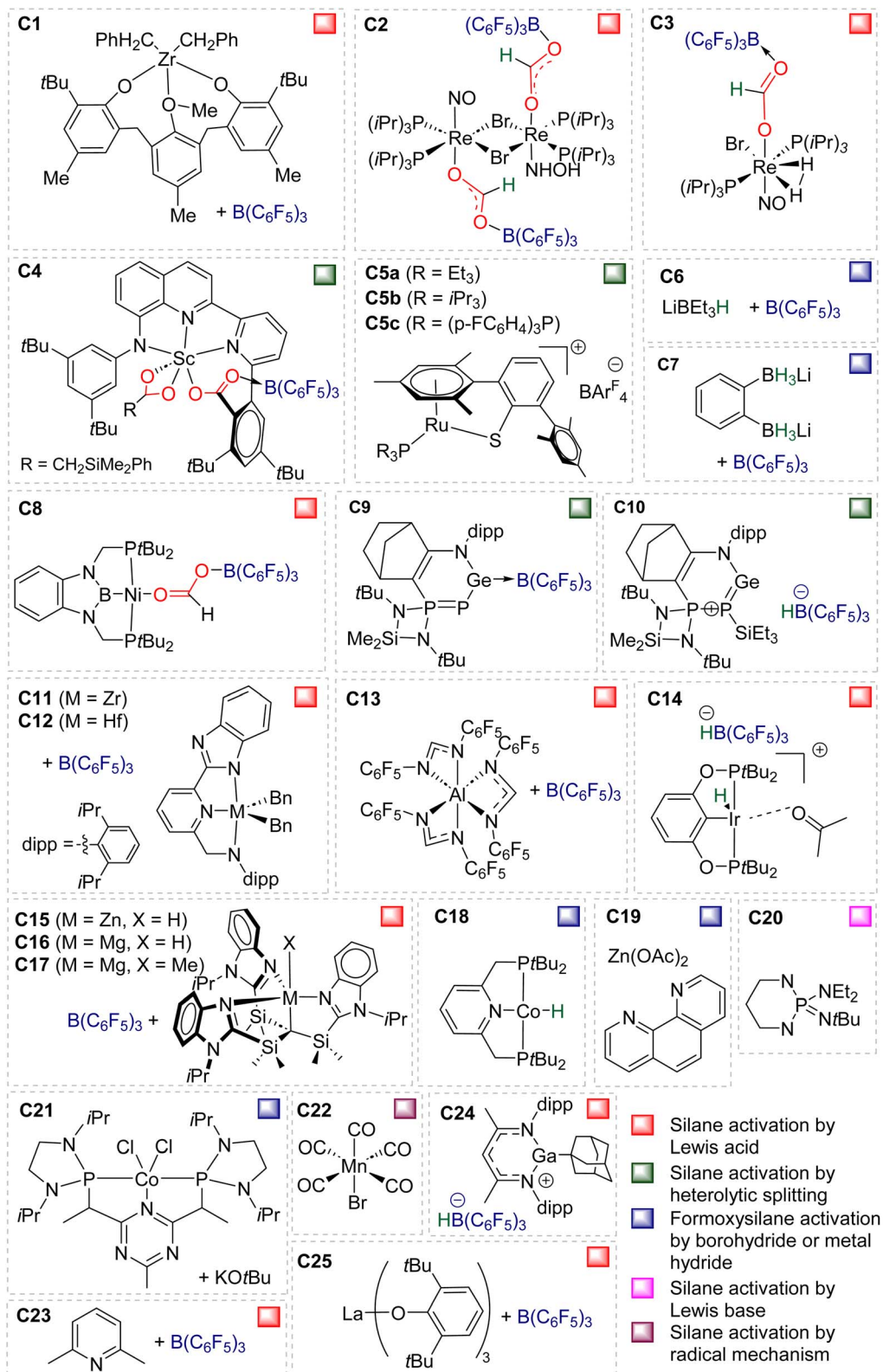
BSA	Solvent	$^{13}\text{C}(\text{CH}_2)$		$\delta^{29}\text{Si}$ (ppm)	Ref.
		$\delta$ (ppm)	$^1\text{J}_{\text{CH}}$ (Hz)		
<b>1</b>	$\text{C}_6\text{D}_6$	—	164	5.03	37
<b>2</b> <sup>a</sup>	$\text{C}_6\text{D}_6$	84.6	—	5.03	39
<b>3</b> <sup>a</sup>	$\text{C}_4\text{D}_5\text{Br}$	85.5	—	5.55	38
	$\text{C}_6\text{D}_6$	85.7	164.4	5.45	38
<b>4</b>	$\text{C}_6\text{D}_6$	84.0	—	5.02	40
<b>5</b>	$\text{C}_6\text{D}_6$	84.9	—	5.21	40
<b>6</b>	$\text{C}_6\text{D}_6$	84.5	—	5.06	40
<b>7</b>	$\text{C}_6\text{D}_6$	85.4	164	5.02	37
		84.5	—	5.08	
		83.8	—	5.12	
<b>8</b>	—	—	—	—	37
<b>9</b>	$\text{CD}_3\text{CN}$	83	—	5.8	41
<b>10</b>	$\text{C}_6\text{D}_6$	85.6	—	—	42
<b>11</b> <sup>a</sup>	$\text{C}_6\text{D}_6$	87.6	—	5.04	43
			—	5.18	

<sup>a</sup> Isolated.

a system selective when it affords BSA as the major product even if at a low conversion rate of silane. Catalysts C1–C25 are depicted in Fig. 1. The specific mode of action of these catalysts indicated with a colour code in Fig. 1 (bottom right) are discussed in detail in the mechanism section, Section 2.2.

Table 2 gathers the catalytic performances (turnover number – TON, turnover frequency – TOF, yield) of catalysts C1–C25. Key features are the mild conditions in terms of temperature (ranging from 25 to 80 °C) and  $\text{CO}_2$  pressure (from stoichiometric quantities to 6 atm). We have selected the conditions affording the best performances in terms of TON, TOF and/or yield for each catalytic system. TOFs are not given at the initial rate because such data were available only for C5 (Table 2). All BSA derivatives were obtained selectively with the exception of BSA 1, 7 and 8. Most of the TON values are in between 10 and 89. The catalysts C1, C8, C11, C12, C17 and C25 afford high TONs of 203, 395, 285, 620, 178 and 670, respectively. Only catalysts C4 and C8 led to exceptionally high TON values of 3400 and 1200, respectively. Moreover, C8 and C25 led to maximum TOFs of 55.8 and 52  $\text{h}^{-1}$ , respectively, while all the other catalysts led to TOFs between 0.1 and 10.4  $\text{h}^{-1}$ .

In addition to TON and TOF, yields are important to assess the selectivity of a given system. This is particularly important when the synthesized BSA is intended to be used as an intermediate in one-pot transformation (see reductive functionalization, Section 2.4). Most of the catalysts afforded BSA in yields higher than 73%. BSA 2 was notably isolated from C8-catalyzed  $\text{CO}_2$  hydrosilylation on the NMR scale, while larger scales of BSA 2 (570 mg, 2.1 mmol) and BSA 3 (2.67 g, 4.7 mmol) were isolated with C4- and C17-catalyzed reactions, in 94 and 95% yield respectively. This preparative scale notably facilitated the utilization of BSA 3 in subsequent transformations (see reductive



- Silane activation by Lewis acid
- Silane activation by heterolytic splitting
- Formoxysilane activation by borohydride or metal hydride
- Silane activation by Lewis base
- Silane activation by radical mechanism

Fig. 1 Catalysts C1–C25 leading to the selective formation of BSA.

functionalization, Section 2.4). The yields for hydrosilylation of CO<sub>2</sub> are given based on the hydrosilane and not on the CO<sub>2</sub> conversion in the vast majority of the cases. This is due to the

difficulty in controlling the amount and conversion of CO<sub>2</sub> as a gas with <sup>13</sup>C NMR titration and to the fact that silane is considered to be the most expensive reactant. Yields based on

Table 2 Catalytic performances of the selective catalysts C1–C25 for the synthesis of BSA 2–6, 9 and 10

BSA	Catalyst	TON <sup>a</sup>	TOF (h <sup>-1</sup> )	Yield <sup>b</sup> (%)	P <sub>CO<sub>2</sub></sub> <sup>f</sup>	T (°C)	Time (h)	[Cat] (%)	Ref.
2	C1	203	1.2	82	1	25	165	0.9	38
	C2	89	5.9	87	5	80	15	1	44
	C3	95	7.3	89	5	80	13	1	
	C4	1000	10.4	94 <sup>e</sup>	4	65	96	0.1	45
		3400	n.d	94 <sup>e</sup>	4	65	n.d	0.02	
	C5a	25	6.2/11 <sup>c</sup>	99	5	80	4	4	40
		49	1.5/8.6 <sup>c</sup>	80	5	80	32	2	
	C5b	25	0.51/<0.01 <sup>c</sup>	89	5	80	48	4	
	C5c	25	0.34/0.00 <sup>c</sup>	>99	5	80	72	4	
	C6	n.d	n.d	91	1	50	24	10	46
	C7	n.d	n.d	54	1	50	41	10	
	C8	1200	55.8	60 <sup>d</sup>	4	70	21.5	0.05	39
		910	26.8	91 <sup>d</sup>	4	70	34	0.1	
	C9	20	0.8	82	3	60	24	5	47
	C10								
	C11	395	6.6	76	1	22	60	0.24	48
	C12	285	5.9	55	1	22	48	0.24	
	C13	9	0.69	60	6	80	13	1.5	49
3	C22	57	57.3	86	4	50	1	1.5	50
	C24	17	0.3	85	2	60	58	10	51
	C25	99	99	99	5	25	1	1	52
	C1	50	0.13	64	1	25	384	2	38
	C14	36	2	100	1	23	22.7	2.5	53
	C15	12	0.1	n.d	1	25	120	2 : 10	54
	C16	83	1.2	n.d	1	25	69	0.5 : 2.5	
4	C17	178	2.5	n.d	1	25	72	0.5 : 2.5	29a
		n.d	n.d	95 <sup>e</sup>	1	25	672	1	
5	C25	670	52	67	5	80	13	1	52
	C5a	31	0.57/7.8 <sup>c</sup>	64	5	80	55	2	40
6		25	2.3/12 <sup>c</sup>	90	5	80	11	4	
	C5a	17	0.23/3.9 <sup>c</sup>	24	5	80	73	2	40
		25	0.69/12 <sup>c</sup>	79	5	80	36	4	
7	C8	620	16.5	62 <sup>d</sup>	4	70	37.5	0.1	40
		137	18.3	82 <sup>d</sup>	4	70	7.5	0.6	
	C5a	32	0.44/6.2 <sup>c</sup>	55	5	80	73	2	40
8		24	0.32/9.5 <sup>c</sup>	79	5	80	75	4	
	C8	121	40	78	4	70	3	0.6	39
	C13	3.5	0.07	31	6	80	48	1	49
9 <sup>g</sup>	C19	40 <sup>i</sup>	1.7 <sup>i</sup>	40 <sup>i</sup>	1 mmol	25	24	1	55
	C20	5.6	1.4	7	5	25	4	1.25	56
10 <sup>h</sup>	C18	32/126 <sup>j</sup>	1.2/4.8 <sup>j</sup>	63	0.4 mmol	25	26	2	42

<sup>a</sup> TON = silane converted/catalyst loading unless otherwise stated. <sup>b</sup> *In situ* yield unless otherwise stated. <sup>c</sup> Initial rate measured after 1 hour. <sup>d</sup> No other product detected. <sup>e</sup> Isolated yield. <sup>f</sup> atm unless otherwise stated. <sup>g</sup> 2 eq. vs. CO<sub>2</sub>. <sup>h</sup> 4 eq. vs. CO<sub>2</sub>. <sup>i</sup> Based on hydrosilane and on CO<sub>2</sub> conversion. <sup>j</sup> Based on CO<sub>2</sub> conversion.

CO<sub>2</sub> conversion are nonetheless significant because (i) it allows for more complete description of a given catalytic system by reporting its performances based on both reactants and (ii) silane is not necessarily the most expensive substrate, notably when isotopically labelled CO<sub>2</sub> is used. Performance data based on CO<sub>2</sub> conversion are particularly important when <sup>11</sup>CO<sub>2</sub> and <sup>14</sup>CO<sub>2</sub> are used for radiochemistry.<sup>57</sup>

Compounds C26,<sup>58</sup> C27,<sup>37</sup> C28,<sup>59</sup> C29,<sup>60</sup> C30,<sup>61</sup> C31,<sup>41</sup> C32,<sup>62</sup> C33,<sup>49</sup> C34,<sup>49</sup> C35<sup>63</sup> and C36<sup>64</sup> were shown to catalyse the hydrosilylation of CO<sub>2</sub> affording BSA as a minor product (Fig. 2). Most of these systems were optimized for the generation of methoxysilane and/or methane and not for BSA. The observation of BSA as intermediates in many cases confirms that (silyl)

acetals are very often on the reaction pathway to the 6 and 8e<sup>-</sup> reduction products in hydrosilylation processes.

**2.1.3. Formaldehyde.** The observation of formaldehyde from CO<sub>2</sub> hydrosilylation was only reported at 100 °C with Ru(Cl)<sub>2</sub>(PPh<sub>3</sub>)<sub>3</sub> as the catalyst in 1981 (Scheme 5).<sup>36b</sup> It was however observed in less than 4% yield and detailed experimental data are lacking to know if free formaldehyde was observed by a direct or indirect method after derivatization. Based on current knowledge, one can wonder if the detected formaldehyde may result from BSA evolution, although the authors explicitly indicated that no experimental proofs were found for BSA generation.

More recently, BSA was utilized as an intermediate to selectively access formaldehyde (Scheme 6). The air stable BSA 3



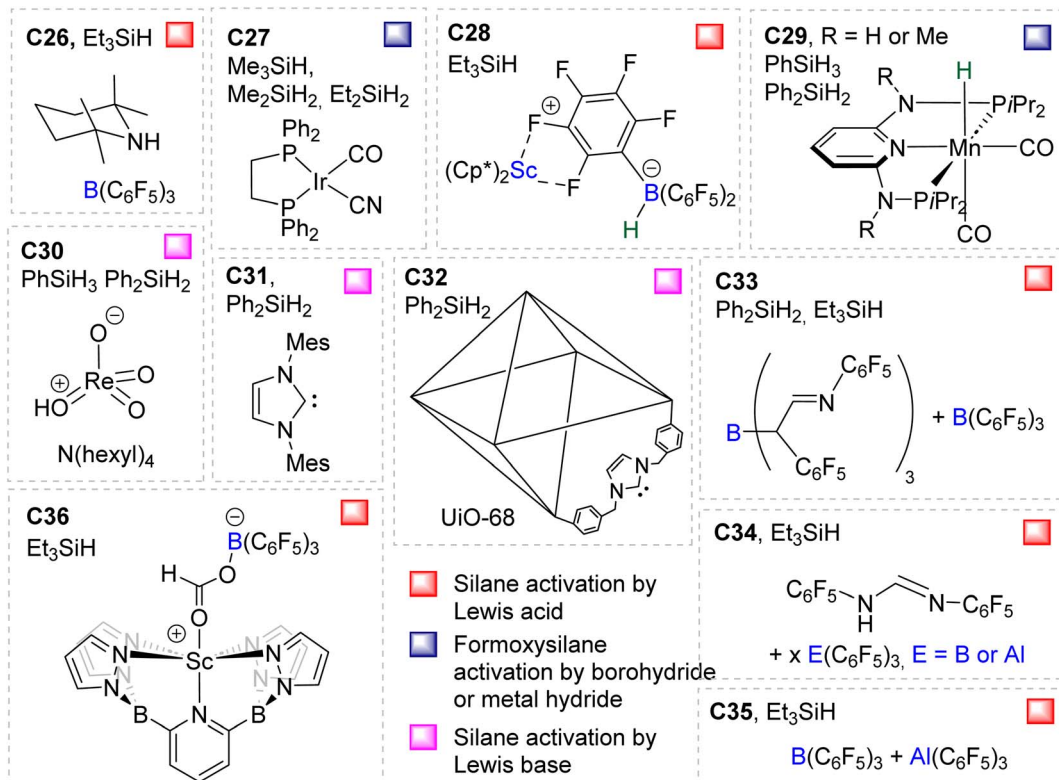
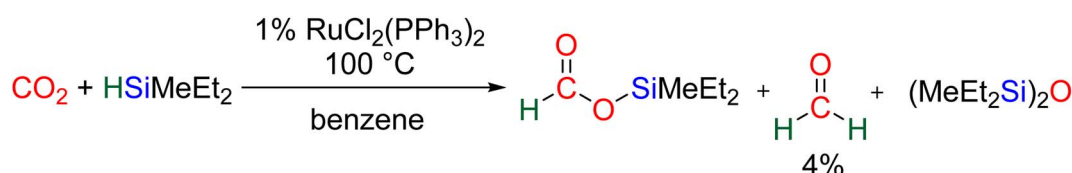
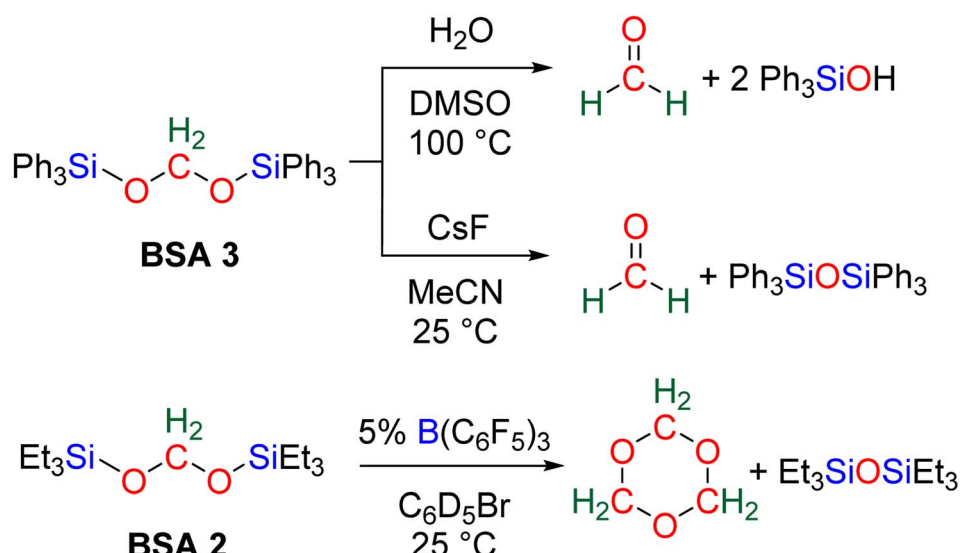


Fig. 2 Unselective catalytic systems C26–C36 and hydrosilane employed.

Scheme 5 Early observation of formaldehyde from  $\text{CO}_2$  hydrosilylation.

Scheme 6 Quantitative generation of formaldehyde from BSA 2 and 3.



featuring triphenylsilyl groups was shown to quantitatively deliver formaldehyde in  $\text{DMSO}/\text{H}_2\text{O}$  at 100 °C or in the presence of  $\text{H}_2\text{SO}_4$  at room temperature.<sup>29a</sup> Alternatively, CsF promoted the generation of formaldehyde at room temperature, presumably *via* the breaking of the Si–O bond after fluoride attack on the silicon centre.

In another study, **BSA 2** featuring triethylsilyl moieties was shown to quantitatively release formaldehyde in the form of trioxane within 1 h in the presence of 5 mol% of  $\text{B}(\text{C}_6\text{F}_5)_3$  as the catalyst at room temperature.<sup>63</sup> Conversely, **BSA 3** did not release formaldehyde in the presence of 22 mol% of  $\text{B}(\text{C}_6\text{F}_5)_3$  in 10 days at room temperature.<sup>29a</sup> These contrasting reactivities between **BSA 2** and **BSA 3** highlight the influence of the silyl fragment on the reactivity of the BSA.

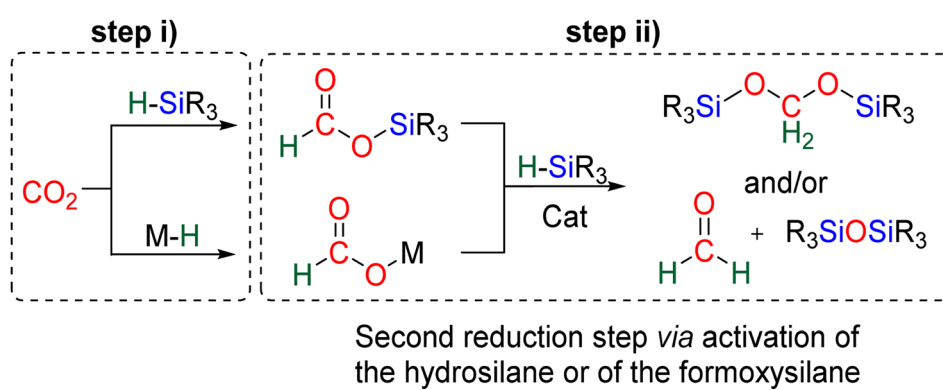
## 2.2. Mechanistic considerations

The  $4\text{e}^-$  reduction of  $\text{CO}_2$  into bis(silyl)acetal (BSA) or formaldehyde by hydrosilane takes place along two steps: (i) the  $2\text{e}^-$  reduction of  $\text{CO}_2$  into either formoxysilane or metal formate (Scheme 7, step (i)), followed by (ii) the hydrosilylation of the intermediate into the corresponding  $4\text{e}^-$  reduction products (Scheme 7, step (ii)). The elementary reactions accounting for step (i) have been already investigated both experimentally and theoretically in reviews focusing on  $\text{CO}_2$  hydrosilylation.<sup>9</sup> We will focus here on the less investigated second reduction step leading to the  $4\text{e}^-$  reduction products. A thorough evaluation of

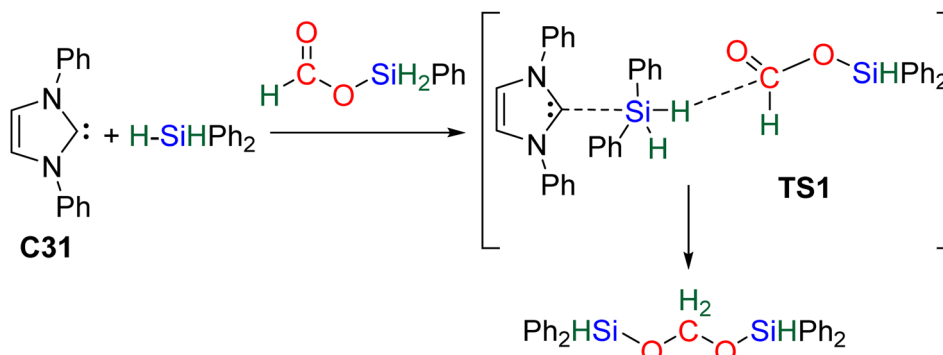
the different mechanisms showed that the role of the catalyst is to activate either the hydrosilane or the formoxysilane, along different activation modes depending on the nature of the catalyst which are described hereafter for the catalysts **C1–36**. A summary of the different activation modes is given in Section 2.2.7 with a general scheme, Scheme 13.

**2.2.1. Activation of the hydrosilane by a Lewis base.** The N-Heterocyclic Carbene (NHC) **C31** has been shown to catalyse the hydrosilylation of  $\text{CO}_2$  into methoxysilane with the observation of BSA as an intermediate.<sup>41</sup> DFT investigations have suggested that the NHC activates the hydrosilane to trigger a hydride transfer to the formoxysilane and the generation of the BSA (Scheme 8).<sup>65</sup> The calculated transition state (TS1) of the rate determining step involves three key components: **C31** acting as the LB activator,  $\text{Ph}_2\text{SiH}_2$  as the reductant and finally the formoxysilane intermediate. A subsequent – almost barrier less – step regenerates the catalyst **C31** along with the BSA release. Although not yet proven, the action mode of **C20**,<sup>56</sup> **C30**<sup>61</sup> and **C32**<sup>62</sup> may be similar to that of **C31** because of their high Lewis basicity. Theoretical investigations on the hydrosilylation of  $\text{CO}_2$  catalysed by the perhenenate anion **C30** also support such views with a similar activation pathway of the hydrosilane for the first reduction step to formoxysilane.

**2.2.2. Activation of the hydrosilane by a Lewis acid.** Hydrosilanes are typically activated by strong Lewis acids promoting the transfer of a silylum “ $\text{Si}^+$ ” moiety. The cationic



Scheme 7 Two mechanistic pathways for the  $4\text{e}^-$  reduction of  $\text{CO}_2$  by hydrosilanes.



Scheme 8 Schematic view of the computed transition state (TS1) of the Lewis basic activation of hydrosilane by catalyst **C31**.

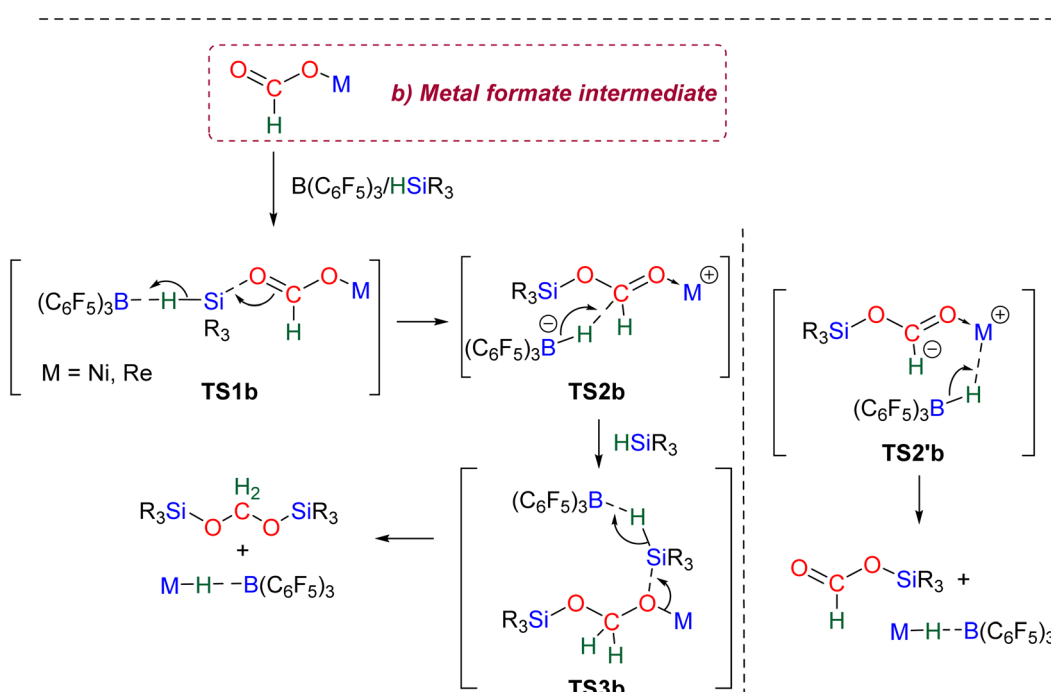
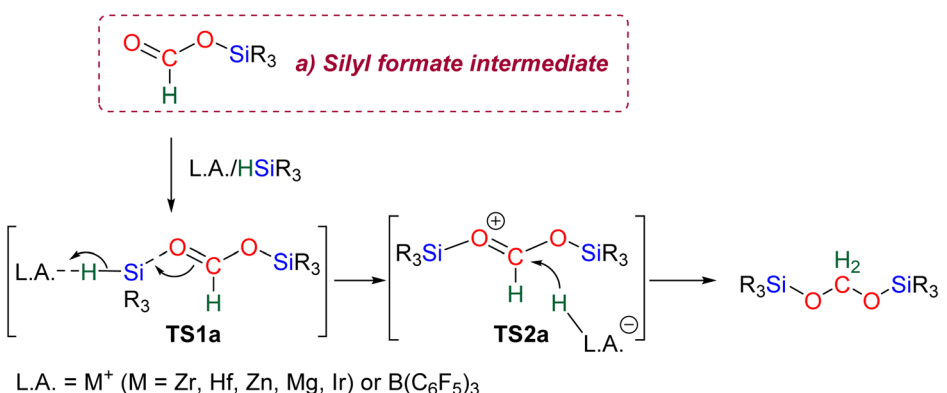


Ir-based complex **C14** and  $B(C_6F_5)_3$  are two prototypical compounds known to catalyse the activation of hydrosilanes in various transformations.<sup>66</sup> In such Lewis acid-catalysed generation of BSA, combined cationic TM-based complexes and  $B(C_6F_5)_3$  were proposed to catalyse hydrosilylation either of a silylformate or of a metal formate as illustrated in Scheme 9a and b, respectively.

**2.2.2.1. Silyl formate intermediate.** Scheme 9a describes the mechanism associated with a Lewis acidic system promoting the silylum “ $Si^+$ ” transfer to *silyl formate* species. Such a reaction occurred in an  $SN_2$ -type activation going through the transition state **TS1a**. The resulting intermediate is then involved in a second elementary step through the transition state in which the hydride abstracted by the Lewis acid (H-LA) is transferred to the carbon atom of the carbonyl function to form the corresponding BSA derivative while regenerating the Lewis acid. Such a mechanism was computed for **C14**,<sup>53,67</sup> **C26**,<sup>58,68</sup> and **C35**.<sup>63</sup>

In the cases of **C14** and **C26**, **TS1a** was found to be higher in energy than **TS2a**, while the reverse was found with **C35**. The catalysts **C1**, **C11–13**, **C15–17**, **C24–25**, **C28** and **C36** are proposed to follow a similar pathway. The catalysts **C18**, **C33** and **C34** could also follow a similar pathway but the observed induction period points toward a more complex process.

**2.2.2.2. Metal formate intermediate.** Scheme 9b describes the mechanism associated with the Lewis acidic system promoting the silylum “ $Si^+$ ” transfer to metal formate species. In the cases of **C2**, **C3** and **C8**, the second reduction step indeed occurred at a metal formate intermediate. The mechanism involving **C8** has been investigated by DFT (Scheme 9b).<sup>69</sup> Both **TS1b** and **TS2b** are similar to **TS1a** and **TS2a** respectively (Scheme 9a). The acetal obtained after these two first steps is a metal silyl acetal. After a second activation of the hydrosilane by  $B(C_6F_5)_3$ , this metal silyl acetal intermediate is converted into the corresponding BSA derivative along with the regeneration of the



**Scheme 9** Calculated Lewis acid activation of (a) silylformate or (b) metal formate intermediates. Only TS are shown for the sake of simplicity, and the movement of the electrons is schematically shown with arrows.



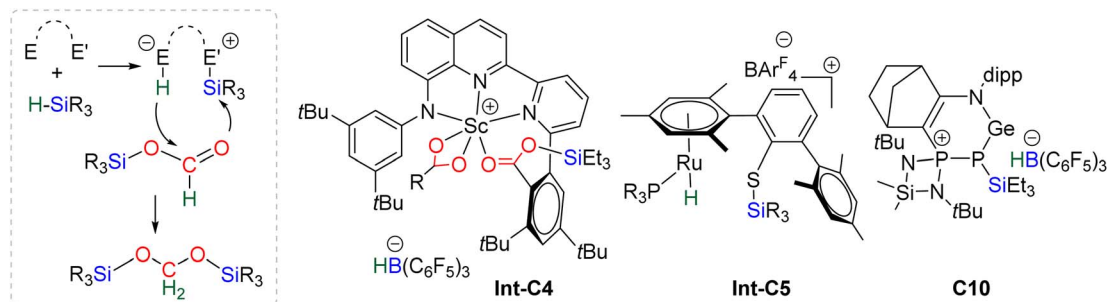


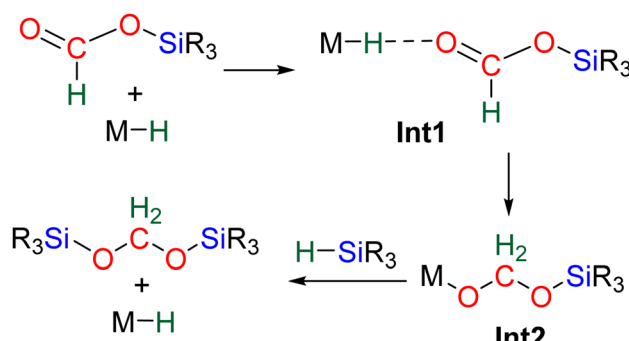
Fig. 3 Complexes resulting from the heterolytic splitting of hydrosilane prior to  $\text{CO}_2$  hydrosilylation.

active catalyst. An alternative pathway involving **TS2/b** was also calculated to be iso-energetic.<sup>69</sup>

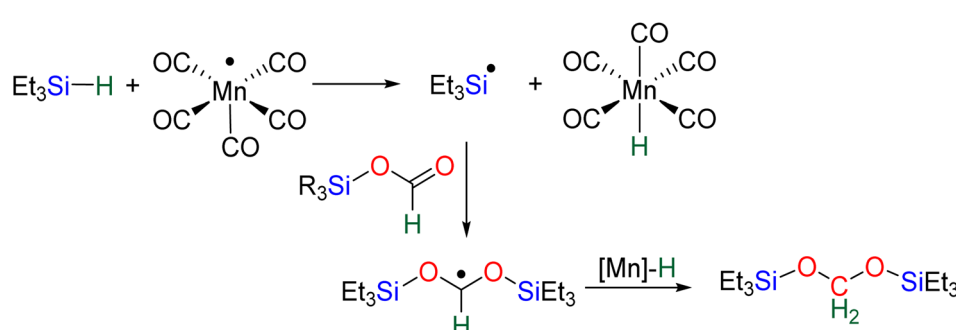
**2.2.3. Heterolytic cleavage of the hydrosilane by bifunctional activation.** While the catalytic systems **C4–5**<sup>40,45</sup> and **C9**<sup>47</sup> are structurally different systems, the proposed mechanism of activation is similar: heterolytic cleavage of the hydrosilane prior to the reduction of the formoxysilane (Fig. 3, left). To support this assumption, catalysts **C4–5** and **C9** were shown to heterolytically cleave hydrosilanes to afford the three species **Int-C4**,<sup>45</sup> **Int-C5**<sup>70</sup> and **C10** (Fig. 3).<sup>47</sup> In addition, **C10** was isolated and used as a catalyst in place of **C9**, showing similar catalytic activity toward  $\text{CO}_2$  hydrosilylation to that of **C9**. These compounds are proposed to transfer both silylum and hydride moieties to the formoxysilane intermediate to form the corresponding BSA derivative. Based on previous results concerning the hydrosilylation of other substrates, Oestreich *et al.* proposed the initial transfer of the silylum moiety followed by hydride transfer in a two elementary step mechanism with **Int-C5**.<sup>40</sup> Such a two-step pathway would be very similar to the calculated pathway for the Lewis acid activation of hydrosilane described above.

**2.2.4. Homolytic cleavage of the hydrosilane by a radical initiator.**  $\text{Mn}(\text{CO})_5\text{Br}$  complex **C22** was shown to catalyse the hydrosilylation of  $\text{CO}_2$  into BSA 2 with triethylsilane.<sup>50</sup> **C22** was proposed to generate a radical complex upon loss of a bromine atom which would then activate triethylsilane in a homolytic manner (Scheme 10). Although no mechanism for the second step was proposed, following the logic of the first reduction step suggests that addition of the silyl radical to the silylformate could take place, followed by hydrogen transfer from a Mn hydride species.

**2.2.5. Activation of the formoxysilane by a metal-hydride moiety.** As shown in Scheme 11, formoxysilane may be activated by metal hydride species by its formal addition into the M–H bond, leading to a metal(silyl)acetal which will then release the corresponding BSA. Catalytic systems **C18**, **C21**, **C27** and **C29** are proposed to follow this pathway. Detailed pathways were calculated with **C29**<sup>60</sup> and **C21**.<sup>71</sup> The in-depth theoretical investigation on catalyst **C21** points toward the insertion of the formoxysilane into the Co–H bond leading to the formation of a metal silyl acetal intermediate.<sup>71</sup> Following this addition, the metal centre is able to activate the hydrosilane *via* an oxidative addition leading to the transfer of the silyl ligand to produce BSA. Moreover, calculations enabled comparison of the three distinct catalytic cycles leading to the formoxysilane, the BSA and the methoxysilane products. The authors compared the



Scheme 11 Computed pathway for the hydrosilylation of formoxysilane to BSA with M-H catalyst **C29** and **C21**.



Scheme 10 Proposed mechanism for the radical activation of  $\text{Et}_3\text{SiH}$  by **C22** based on experimental results.



energy gap values  $\delta E$  between the most stable intermediate and the highest transition state for each cycle. The smaller value (24.2 kcal mol<sup>-1</sup>) found for the formation of the formoxysilane compared to the values for the BSA (28.9 kcal mol<sup>-1</sup>) and the methoxysilane (29.9 kcal mol<sup>-1</sup>) explain why formoxysilane could be obtained selectively. The small difference between the  $\delta E$  of BSA *vs.*  $\delta E$  of methoxysilane explains the difficulty in selectively generating BSA in these systems. These calculations reproduced the experimental selectivity obtained under different reaction conditions of temperature and pressure. We hypothesize that the catalytic system **C19** followed this pathway as well, based on the assumption that the combination of the bidentate ligand (*i.e.*, 1,10-phenanthroline) and Zn(OAc)<sub>2</sub> would generate a Zn–H moiety in the presence of a hydrosilane under catalytic conditions.

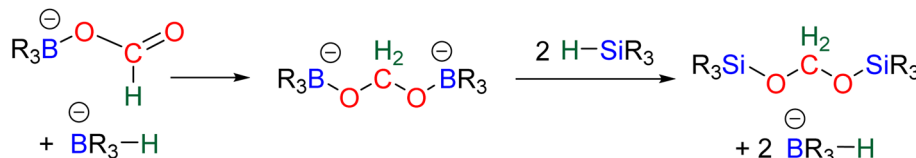
**2.2.6. Activation of the formate by a borohydride.** Catalyst systems **C6** and **C7** are the only borohydride compounds reported so far to catalyse the hydrosilylation of CO<sub>2</sub> into BSA.<sup>46</sup> No theoretical investigations were conducted. Based on experimental findings, the proposed mechanism involves the insertion of CO<sub>2</sub> into two B–H bonds of borohydride catalyst leading to a dianionic acetal intermediate (Scheme 12). This assumption is based on the observed reactivity of **C7** with CO<sub>2</sub> and bromobenzoic acid as the CO<sub>2</sub> surrogate. The reactivity of **C7**

toward CO<sub>2</sub> was indeed immediate but led to an insoluble material difficult to analyse. However, the reactivity toward bromobenzoic acid led to the reaction of the two borohydride fragments with two equivalents of the carbonyl part. While no further insights were gathered with theoretical investigations for these specific systems, the ability of borohydride to insert CO<sub>2</sub> was observed previously in various studies.<sup>72</sup> An alternative BR<sub>3</sub>/SiR<sub>3</sub> exchange after each borohydride addition may also be at play and would avoid any charge build-up.

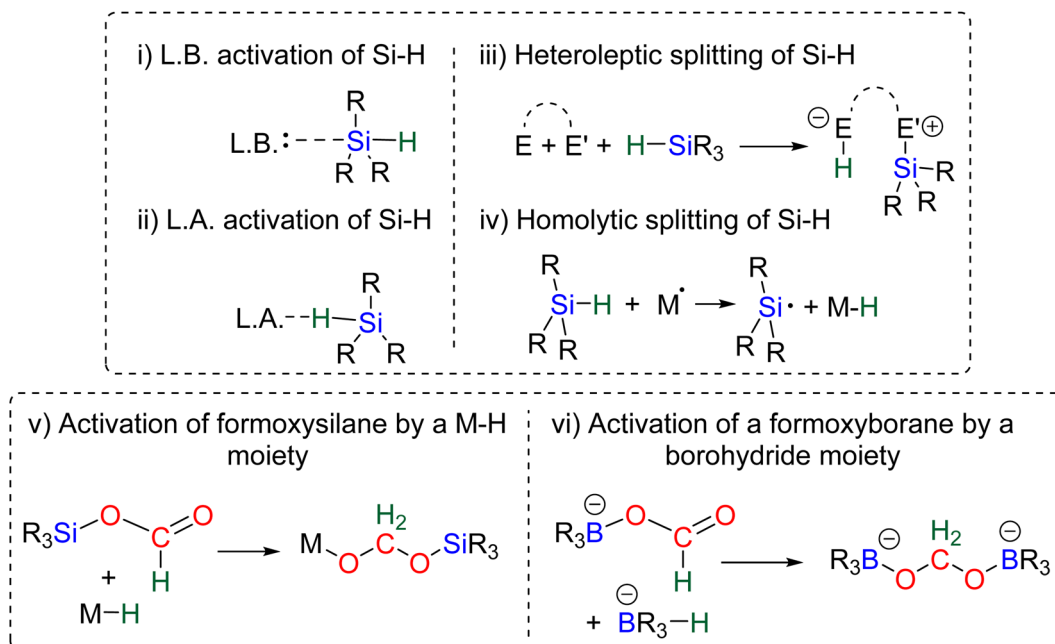
**2.2.7. Summary of the activation modes of hydrosilane or formoxysilane.** Most of the catalytic systems activate the hydrosilane reductant either *via* (i) Lewis base (LB), (ii) Lewis acid (LA), (iii) heterolytic splitting of the Si–H bond in a bifunctional manner or (iv) homolytic cleavage by a radical initiator. The Lewis acid activation is at play in the majority of the examples. In fewer cases, the silyl- or boryl-formate intermediates are activated by (v) a metal or (vi) a borohydride species. The different activation modes are summarized in Scheme 13.

### 2.3. Origin of the selectivity for BSA

The control or simply the understanding of the selectivity for bis(silyl)acetal (BSA) is a challenge. In this section we describe some of the main parameters which have been shown to favour



Scheme 12 Proposed mechanism for **C6** and **C7** catalytic systems based on experimental results.



Scheme 13 Activation modes of hydrosilane or formoxysilane leading to (silyl) acetals BSA (LB = Lewis base, LA = Lewis acid).

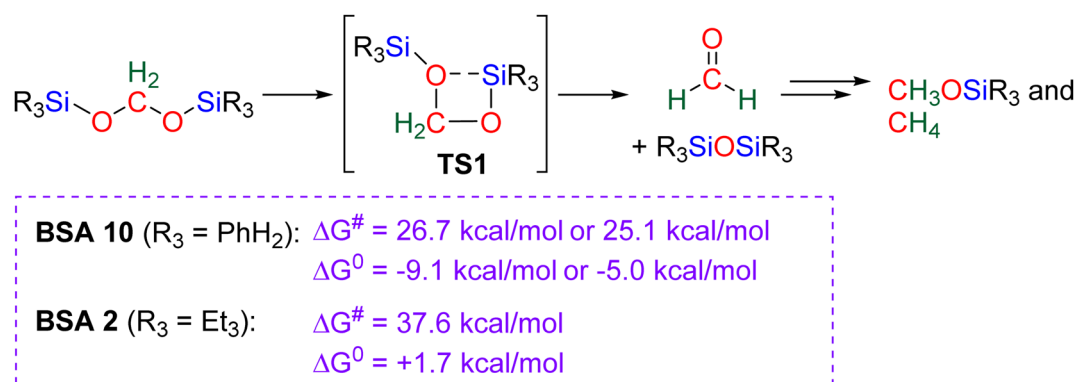


BSA accumulation either upon thermodynamic stabilization or by disfavouring further reduction to methoxysilane or methane.

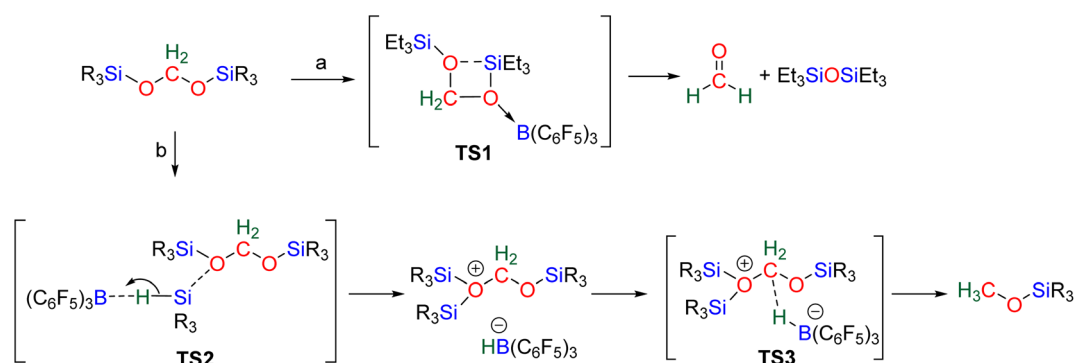
**2.3.1. Thermodynamic and kinetic stabilization of BSA by the nature of the silyl groups.** Although no specific study was conducted on the role of the silyl group in the stabilization of BSA, two theoretical investigations provided some reactivity trends. These calculations suggested that BSA evolves to formaldehyde *via* TS1, and the formaldehyde is then further reduced to methoxysilane and/or methane (Scheme 14). This process was calculated in two independent studies with phenylsilyl groups ( $\text{SiH}_2\text{Ph}$ ) to be thermodynamically favoured by  $-9.1$  and  $-5.0$  kcal mol $^{-1}$ , with an activation barrier of  $25.1$  and  $26.7$  kcal mol $^{-1}$ .<sup>65,73</sup> When the same transformation was calculated with triethylsilyl ( $\text{SiEt}_3$ ) groups, the reaction was then thermodynamically disfavoured by  $+1.7$  kcal mol $^{-1}$  with a barrier of  $37.6$  kcal mol $^{-1}$ .<sup>63</sup> It thus appears that  $\text{SiEt}_3$  groups bring both kinetic ( $>10$  kcal mol $^{-1}$ ) and thermodynamic (about  $8$  kcal mol $^{-1}$ ) stability compared to phenylsilyl moieties. Although care must be taken while comparing different theoretical studies, these investigations point toward a higher stability of a BSA featuring tertiary silyl moieties as compared to BSA featuring primary silyl moieties. This corroborates the predominance of tertiary silanes for the selective generation of BSA 1–6, and 11. Moreover, some catalysts were shown to favour BSA when tertiary silanes were employed, but methoxysilane and methane when secondary and primary silanes were

employed. This is the case for example with C1 and C15–17, while most of the other selective catalysts have not been tested with primary or secondary silanes. Finally, every isolated BSA featured trisubstituted silyl groups (BSA 2, 3 and 11).

**2.3.2. Sequestration of  $\text{B}(\text{C}_6\text{F}_5)_3$ .** The origin of selectivity for BSA of the catalytic systems C4 and C8 employing  $\text{B}(\text{C}_6\text{F}_5)_3$  is proposed to be the result of the formation of a Lewis pair between  $\text{B}(\text{C}_6\text{F}_5)_3$  and an oxygen atom present on the complex. This so-called sequestration of  $\text{B}(\text{C}_6\text{F}_5)_3$  during the process is proposed to prevent further reduction.<sup>39,45,69</sup>  $\text{B}(\text{C}_6\text{F}_5)_3$  has indeed been shown to favour further reduction to methoxysilane or methane. Two modes of action were calculated (Scheme 15, paths a and b). In path a,  $\text{B}(\text{C}_6\text{F}_5)_3$  catalyses the transformation of BSA into formaldehyde *via* TS1. This result was obtained within the same study presented just above with BSA 2 featuring triethylsilyl moieties.<sup>63</sup> The  $\text{B}(\text{C}_6\text{F}_5)_3$ -catalyzed reaction was calculated to be  $10$  kcal mol $^{-1}$  lower in energy compared to the uncatalyzed transformation. Moreover, the reaction was probed experimentally: while BSA 2 was stable for a day in solution, it was transformed into formaldehyde within  $1$  h in the presence of  $5\%$  of  $\text{B}(\text{C}_6\text{F}_5)_3$ . The second mode of activation b occurs *via* an  $\text{SN}_2$ -type activation of the hydrosilane by the Lewis acid  $\text{B}(\text{C}_6\text{F}_5)_3$  leading to silylum transfer (TS2) and finally hydride (TS3) transfer to form methoxysilane (Scheme 15, path b). These transformations were calculated in the cases of C14 (ref. 67) and C26.<sup>68</sup> In accordance with this mechanism proposal, various

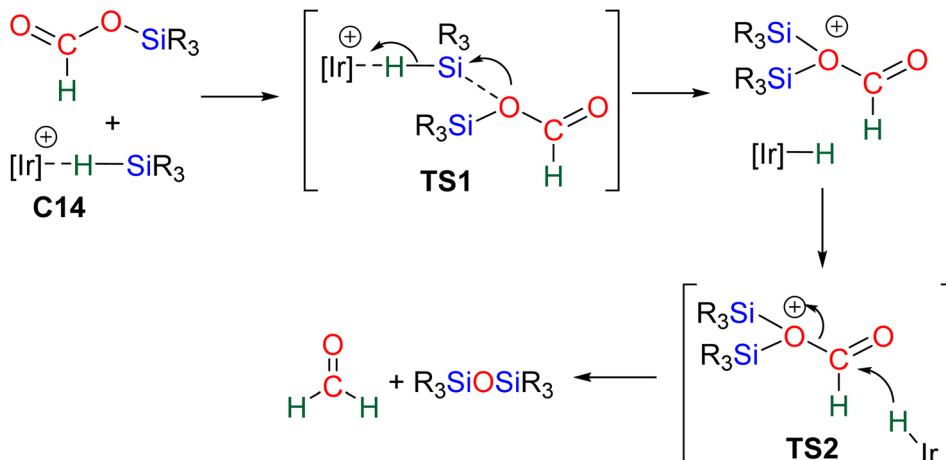


Scheme 14 Computational findings regarding the capability of BSA to liberate HCHO based on the type of silyl moiety.



Scheme 15 Computed  $\text{B}(\text{C}_6\text{F}_5)_3$ -catalyzed conversion of BSA into formaldehyde or methoxysilane.





Scheme 16 Calculated pathway for the generation of formaldehyde from formoxysilane with the Ir-based catalytic system C14.

selective systems reported further reduction when an additional catalytic amount of  $B(C_6F_5)_3$  was added to the system. This was notably the case for C4, C8 and C15–17.

**2.3.3. Stoichiometry.** In most of the  $CO_2$  hydrosilylation reactions reported, an excess of  $CO_2$  gas was employed. In order to influence the level of reduction of the hydrosilylation reaction, 2 and 4 equivalents of  $CO_2$  vs. silane were used with catalytic systems C18 and C19, respectively. Under such stoichiometric or quasi-stoichiometric conditions, it was possible to observe the formation of BSA in 40 and 63% yields for C18 and C19, respectively. The importance of the stoichiometry conditions was proven for C18 since a larger ratio of  $CO_2$  gave rise to formoxysilane whereas a larger amount of silane led to methoxysilane.

**2.3.4. Hydrosilylation of  $CO_2$  to formaldehyde without the intermediary of BSA.** While formaldehyde was experimentally shown to be obtained from BSA with further insights from calculations, its generation without the intermediary of BSA remains an open question. Besides its experimental observation early on in less than 4%, there is only one theoretical investigation reporting such generation with the Ir-based catalytic system C14.<sup>67</sup> As depicted in Scheme 16, the cationic  $[Ir]$ -hydride complex was calculated to promote silylum transfer to the  $OSiR_3$  moiety of the formoxysilane intermediate in TS1, ultimately leading to formaldehyde via TS2. However, the same calculation showed that the silylum transfer to the oxygen atom of the carbonyl leading to BSA was favoured explaining why formaldehyde was not observed experimentally during the reaction.

#### 2.4. Bis(silyl)acetal as an intermediate in reductive functionalization of $CO_2$

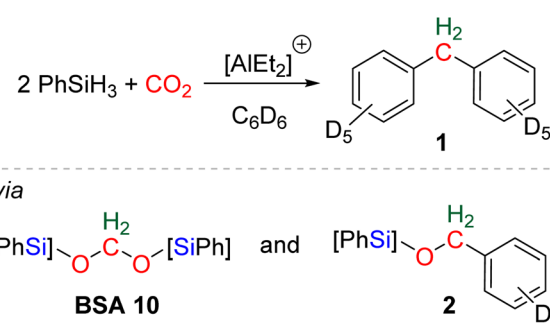
The reductive functionalization of  $CO_2$  refers to the reduction of  $CO_2$  combined with the functionalization of the reduced product with a co-reactant. The term was first employed in the case of the hydrosilylation of  $CO_2$  into formoxysilane, intercepted with amines to afford formamide, formamidine or methylamine derivatives.<sup>20c,74</sup> An early reaction of this type can

be traced back to a report on the preparation of formamide from  $CO_2$  reduction in the presence of amine in 1988.<sup>75</sup> In this case, the reductant was not hydrosilane but dihydrogen. Although unexpected, the first reductive functionalization of  $CO_2$  via the generation of a bis(silyl)acetal (BSA) intermediate was reported in a study devoted to the use of cationic Al-based species for catalysing the hydrosilylation of  $CO_2$  to methane.<sup>76</sup> In the course of the reaction, the formation of deuterated diphenylmethane 1 featuring a bridged-methylene moiety was observed (Scheme 17). Experimental proofs showed that transiently generated BSA reacted with the deuterated solvent via electrophilic catalysis by the cationic Al-based compound to afford compound 1 via compound 2.

Following this preliminary report, subsequent studies reported the use of BSA as a key intermediate for the generation of more complex products in the presence of various co-reactants. Such strategies considerably enlarged the scope of compounds obtained from  $CO_2$  in using BSA as a source of methylene for the formation of C–N, C–C, C–S and C–O bonds.

#### 2.4.1. Reductive functionalization of $CO_2$ via a transient BSA intermediate

**2.4.1.1.  $TBD/PhSiH_3$ : a pioneering reduction system in reductive functionalization. Formation of C–N and C–C bonds.** The first system describing a reductive functionalization of  $CO_2$  with



Scheme 17 First example of reductive functionalization of  $CO_2$  into product 1, involving a BSA intermediate and compound 2.

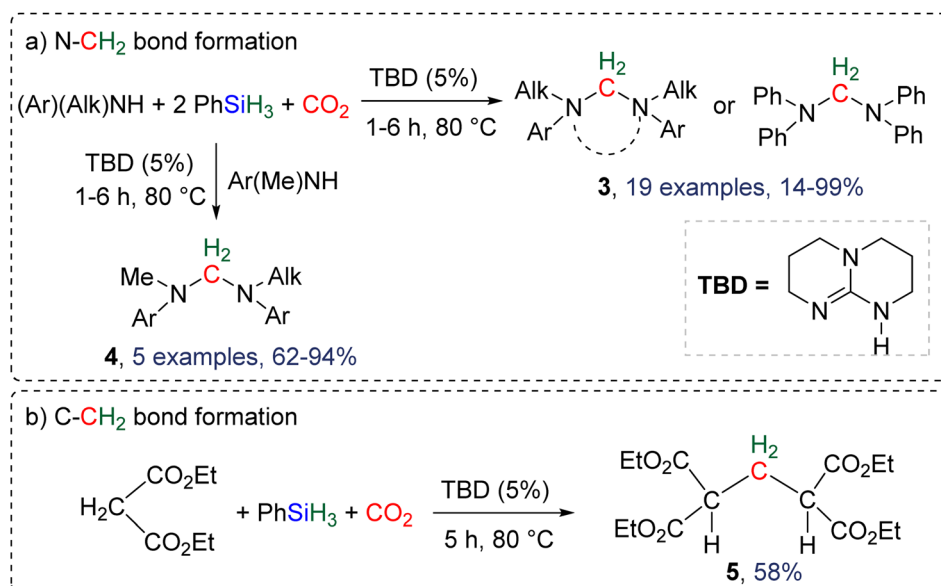


hydrosilane with the intermediary of BSA was reported in 2015 (Scheme 18).<sup>77</sup> It included the use of TBD (1,5,7-triazabicyclo[4.4.0]dec-5-ene) which catalysed the hydrosilylation of  $\text{CO}_2$  with phenylsilane into the corresponding BSA, although it was never directly observed or characterized. Besides TBD, other Lewis basic catalysts including 1,8-diazabicyclo[5.4.0]undec-7-ene (DBU), Verkade's base and NHC (iPr and iBu) were tested to catalyse the reduction step. Slightly lower yields of the final products were obtained. Various co-substrates featuring N–H (Scheme 18a) or C–H functionalities (Scheme 18b) acted as functionalizing agents in intercepting the transiently formed BSA leading to the formation of methylene-bridged “N–CH<sub>2</sub>–N” and “C–CH<sub>2</sub>–C” moieties. In total, 19 cyclic or acyclic symmetrical aminal products **3** were generated selectively with yields ranging from 14 to 99% (larger than 70% in most cases, Scheme 18a). In addition, 5 dissymmetric aminal products **4** were also generated using two different amines with yields ranging from 62 to 94% (Scheme 18a). For the synthesis of these dissymmetric aminal compounds, a key factor was to employ two amines featuring different nucleophilicities, enabling the most nucleophilic amine to first react with BSA, which affords an intermediate aminosilylacetate. Subsequently, the second (less nucleophilic) amine reacts with the aminosilylacetate intermediate yielding the corresponding aminal compound. Replacing the amine co-reactant with 2 equivalents of the nucleophilic malonate compound led to the unique formation of two C–C bonds in 58% yield (compound **5**, Scheme 18b).

**2.4.1.2. Extension of the scope with the TBD/PhSiH<sub>3</sub> reduction system.** The TBD/PhSiH<sub>3</sub> system was proven to be reliable and versatile to insert one or two methylene units in complex structures. To do so, 10–20 mol% of TBD was used at temperatures ranging from 100 to 120 °C and reaction times from 6 to 30 h (Scheme 19). Indolepyrrolidine derivatives were engaged as co-reactants leading to cyclisation reactions with the formation

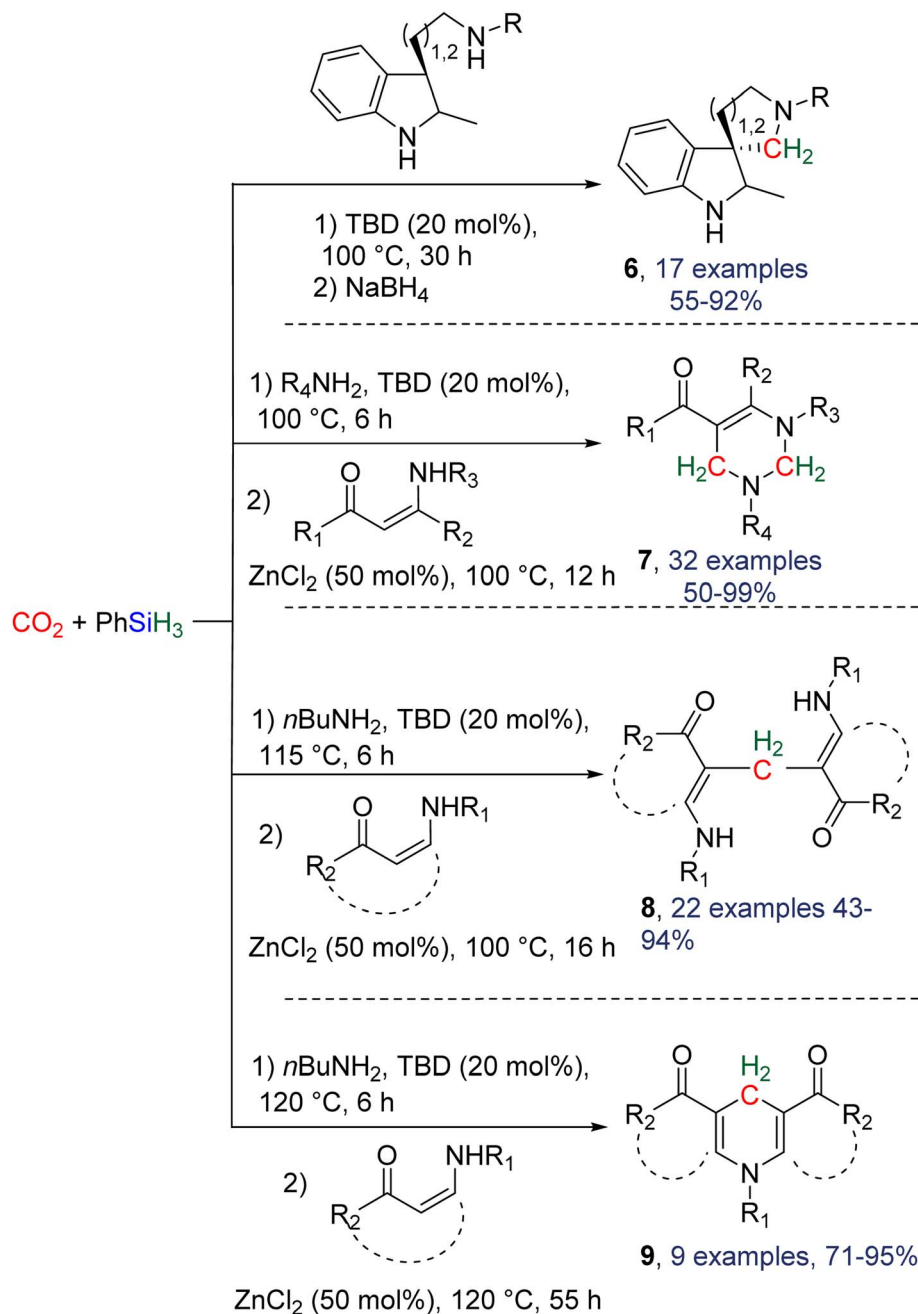
of C–CH<sub>2</sub> and N–CH<sub>2</sub> bonds. A second enantioselective reduction step of the pyrrolidine ring afforded spiro-indolepyrrolidine products **6** (Scheme 19), and 17 different compounds have been obtained in good to very good yields (55–92%).<sup>78</sup> Reductive functionalization with amine was then used to incorporate two methylene units from the hydrosilylation of  $\text{CO}_2$  (Scheme 19, compounds **7**).<sup>73</sup> Key features of these transformations include the use of (i) a primary amine leading to the generation of an imine intermediate and (ii) a Lewis acid-catalysed cyclization reaction with various enaminones. The scope of the reaction was evaluated with 32 identified examples of tetrahydropyrimidine compounds with isolated yields (based on the enaminone) ranging from 50 to 99% (in most cases larger than 80%). The mechanism for the formation of compounds **7** was also investigated by DFT (Scheme 20). TBD was calculated to catalyse the hydrosilylation of  $\text{CO}_2$  into **BSA 10** followed by the liberation of formaldehyde. The imine is then generated from the condensation of the primary amine with formaldehyde (step i). Controlled experiment proved that a stable imine can be formed when a bulky bis(diisopropyl)aniline is used. The enaminone nucleophilically adds to the intermediate imine *via* a Lewis acid/TBD-catalysed reaction (step ii) leading to an aza-diene compound after phenylamine elimination (step iii). The Diels–Alder reaction between the aza-diene intermediate and a second equivalent of *in situ* generated imine finally furnishes the tetrahydropyrimidine **7** (step iv). This elegant strategy employing a primary amine as a first functionalization step transformation was further used to generate enaminones (Scheme 19, compounds **8**, 22 examples, 43–94%) and 1,4-dihydropyridines (Scheme 19, compounds **9**, 9 examples, 71–95%).<sup>79</sup>

**2.4.1.3. Development of new catalysts.** Besides the utilization of TBD as a catalyst, two other catalytic systems were employed for reductive functionalization with hydrosilanes. The



**Scheme 18** First selective reductive functionalization of  $\text{CO}_2$  via the generation of a BSA intermediate leading to the formation of (a) C–N and (b) C–C bonds.





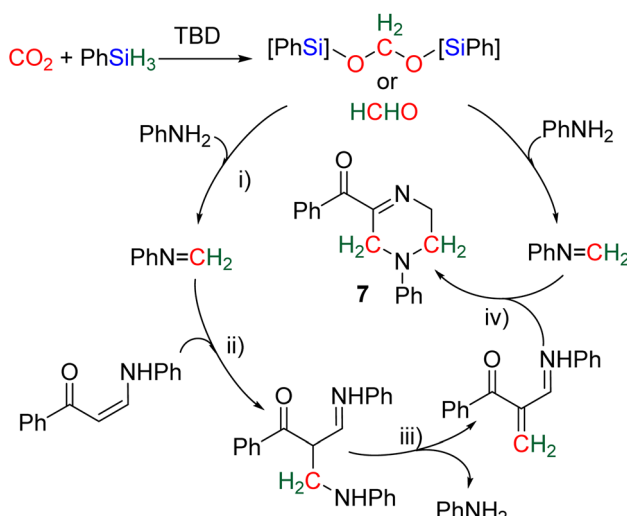
Scheme 19 Extension of the product scope upon reductive functionalization of  $\text{CO}_2$  with hydrosilanes.

combination of  $[\text{CpFe}(\text{CO})_2]_2$  and  $\text{P}(n\text{Bu})_3$  was shown to catalyse the hydrosilylation of  $\text{CO}_2$  with phenylsilane in the presence of tryptamine derivatives to afford a variety of tetrahydro- $\beta$ -carbolines and other nitrogen-containing heterocycles **10** after 36 h at 60 °C (Scheme 21).<sup>80</sup> In total, 19 heterocycles were obtained in yields ranging from 50 to 94%. The  $[\text{CpFe}(\text{CO})_2]_2/\text{P}(n\text{Bu})_3$  system is proposed to catalyse the hydrosilylation of  $\text{CO}_2$  into BSA which is then involved in a Pictet–Spengler-type cyclization. Other Fe-based precursors did not afford any conversion, while diphenylsilane or other tertiary phosphine afforded the expected compounds although in lower yields. Another report described the use of a phosphorus ylide to intercept the

reduction intermediate *via* a Wittig reaction (Scheme 21, compounds **11**).<sup>81</sup>

If the first tests were conducted with the TBD/PhSiH<sub>3</sub> system in acetonitrile, optimization conditions revealed the beneficial role of an inorganic base and notably of sodium *tert*-butoxide ( $\text{NaOtBu}$ ) in DMF in catalysing the hydrosilylation of  $\text{CO}_2$  with PMHS (polymethylhydrosiloxane) – a waste of the silicone industry. This process led to the synthesis of 20 olefins in yields ranging from 30 to 85%. Ionic liquids<sup>24</sup> and covalent organic frameworks<sup>83</sup> were also employed as catalysts in a similar synthesis of aminal by  $\text{CO}_2$  reductive functionalization.





Scheme 20 Proposed mechanism for the synthesis of tetrahydropyrimidine 7.

**2.4.2. Reductive functionalization of CO<sub>2</sub> via an isolated BSA intermediate (BSA 3).** In contrast to the previous examples in which BSA was not isolated or observed, BSA 3 could be isolated before being involved in subsequent transformations.<sup>29a</sup> Such a process avoids compatibility issues between the reduction and the functionalization steps since they are performed independently. Using the Mg-based catalytic system C17, BSA 3, featuring triphenylsilyl groups, was isolated in high yield on a 3 g scale (95% yield, Table 2). As presented in Section 2.1.3, BSA 3 was found to quantitatively release formaldehyde either in DMSO at 100 °C, in the presence of CsF at room temperature or under acidic conditions (H<sub>2</sub>SO<sub>4</sub>) at room

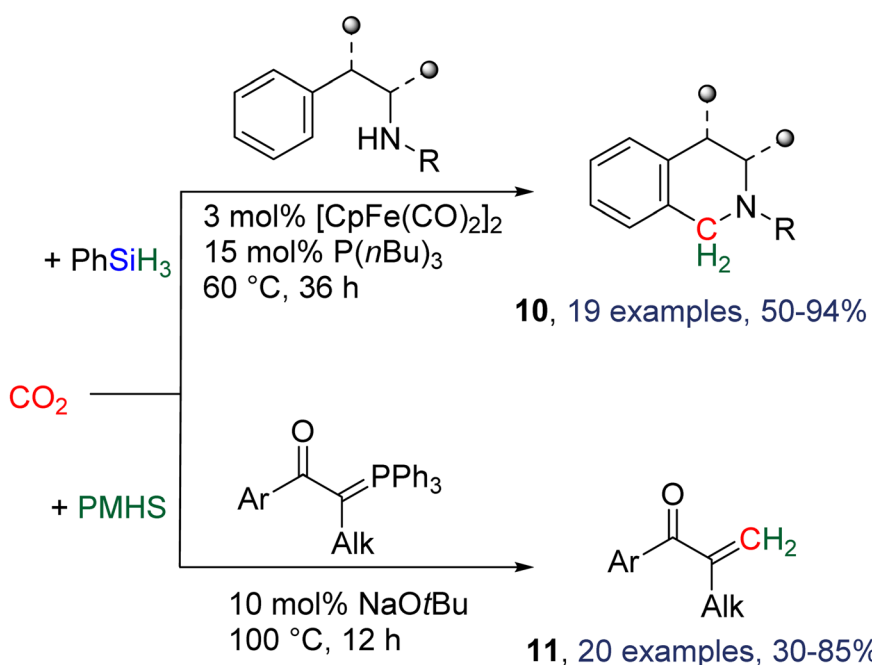
temperature (Scheme 6). Under these conditions, BSA 3 was then engaged in further transformations (Scheme 22).

In the presence of diol or di-thiol substrates under acidic conditions, the cyclic compounds 12 were generated in good yields forming CH<sub>2</sub>—O (69% yield) and CH<sub>2</sub>—S bonds (51% yield), respectively. The reaction with hydrazine proved to be efficient to generate a CH<sub>2</sub>—N bond (compound 13, 62% yield), while reactions with molecules comprising primary amine and thiol or secondary amine function led to benzimidazole and benzothiazole compounds 14 (95 and 57% yields), respectively. Finally, the reaction with ammonia afforded hexamethylene tetra-amine 15 in 77% yield. In addition, C—C bonds were also generated (i) with malonate leading to 5,5-dimethylcyclohexane-1,3-dione compound 16 (89% yield), (ii) through a Wittig reaction leading to the acrylate compounds 17 (80 and 87% yields) and finally (iii) through a Pictet-Spengler-type cyclization reaction leading to compound 18 (82% yield). It must be noted that <sup>13</sup>C-labelled BSA 3 could also be efficiently generated and isolated from the catalytic hydrosilylation of <sup>13</sup>CO<sub>2</sub> and was used as a dry source of <sup>13</sup>C-labeled HCHO.

**2.4.3. Conclusion on the reductive functionalization of CO<sub>2</sub>.** Reductive functionalization of CO<sub>2</sub> with hydrosilanes led to the synthesis of a very broad range of various products in which the intermediate BSA was used as a methylene source to form C—N, C—O, C—S and even C—C bonds. In these reactions, BSA is generated either transiently when PhSiH<sub>3</sub> is the reductant – although not observed – or isolated when Ph<sub>3</sub>SiH is the reductant.

## 2.5. Conclusion and perspectives

In conclusion, the four-electron reduction of CO<sub>2</sub> with hydrosilane is noteworthy for several reasons. Firstly, it distinguishes itself with a considerable number and variety of selective



Scheme 21 New catalysts for reductive functionalization with hydrosilanes.



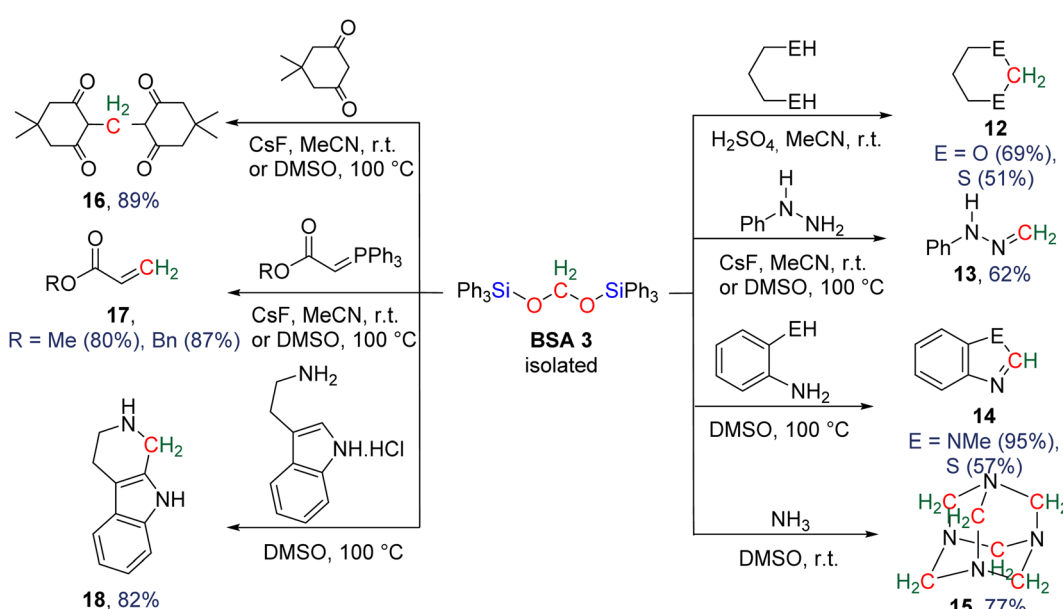
catalytic systems (**C1–24**), primarily based on the combination of transition metal-based complexes and  $\text{B}(\text{C}_6\text{F}_5)_3$ . Comprehensive experimental and theoretical studies have revealed five distinct activation modes, elucidating the 2 to 4 electron reduction stage. Despite the highest reported TON of 3400 and TOF of  $10.4 \text{ h}^{-1}$ , there is room for further enhancements. Secondly, it stands out due to the diverse array of characterized and isolated bis(silyl)acetal (BSA) compounds, with a current total of 11 reported. These isolated BSAs were predominantly obtained from tertiary silanes, demonstrating high selectivity (79 to 99% yields) under mild conditions. Finally, the process is notable for numerous transformations involving BSA in reductive functionalization, ranging from simple condensation to multi-step reactions with co-reactants. Interestingly, when primary silanes were employed, BSA formation was never observed, likely due to its high reactivity. In contrast, tertiary silanes led to the isolation of BSA before engaging in subsequent functionalization through formaldehyde release.

Perspectives in the field of  $4\text{e}^-$   $\text{CO}_2$  hydrosilylation could involve rationalizing the stability of the generated bis(silyl) acetal (BSA) based on the choice of hydrosilane. Generating BSAs with intermediate stability holds particular interest, offering potential for expanding the reactivity scope of BSA compounds. A significant breakthrough would be utilizing BSAs as a  $\text{C}_n$  source for producing high-value added products, an area yet to be explored compared to their borylated counterparts discussed in the next section. However, the primary challenge remains the treatment of the siloxane by-product produced during  $\text{CO}_2$  hydrosilylation, currently considered as waste. Exploring potential uses for these siloxane moieties or designing a regeneration system for the sustainable recycling of hydrosilane presents a promising avenue for further research.

### 3. Hydroboration

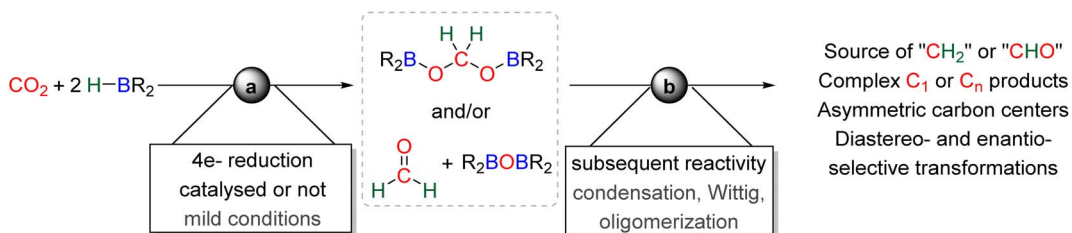
In the realm of hydroelementation reactions, hydroboration holds an important and specific place. Since the discovery of hydroboration of olefins,<sup>84</sup> this reaction has been largely developed for the reduction of unsaturated bonds.<sup>8b,85</sup> Beyond reduction, the formal addition of B–H bonds is used as a privileged access to organoboron compounds which are then used as reagents in coupling reactions.<sup>86</sup> Hydroboration of  $\text{CO}_2$  involves the addition of a B–H bond to the C=O bond, transferring the hydride to the carbon atom and forming a B–O bond. It is favoured both kinetically and thermodynamically by the polarity of the B–H bond (E. N. of H = 2.2, B = 2.0) and the strength of the formed B–O bond ( $\text{BDE}(\text{B–O}) > 500 \text{ kJ mol}^{-1}$ ),<sup>87</sup> respectively. As a consequence,  $\text{CO}_2$  hydroboration reactions, like  $\text{CO}_2$  hydrosilylation ones, operate under much milder conditions – usually room temperature and 1 atm of  $\text{CO}_2$  – than  $\text{CO}_2$  hydrogenation.<sup>8a</sup> However, it is noticeable that the catalytic systems used for the hydroboration or the hydrosilylation of  $\text{CO}_2$  are different in most cases.

The first catalytic hydroboration of  $\text{CO}_2$  was reported in 2010 with a Ni-based catalytic system and was shown to afford the  $6\text{e}^-$  reduction product, methoxyborane, readily hydrolysed to methanol.<sup>88</sup> While the  $2\text{e}^-$  reduction product – formoxyborane – was observed, no  $4\text{e}^-$  reduction product was detected, although formaldehyde was proposed as an elusive intermediate.<sup>88,89</sup> The Ni-based pincer system used as the catalyst remains one of the most efficient catalyst of  $\text{CO}_2$  hydroboration into methoxyborane with TOF and TON of 495 and  $495 \text{ h}^{-1}$ , respectively. It is worth noticing that an earlier report described the use of borane in the reduction of  $\text{CO}_2$ . However, it was not a hydroboration reaction, but the reduction of  $\text{CO}_2$  into CO by  $\text{B}_2\text{pin}_2$  and a (NHC)Cu-based catalyst.<sup>19b</sup> It was only in 2012 and 2014 that



Scheme 22 Products obtained from the functionalization of HCHO released from BSA 3.



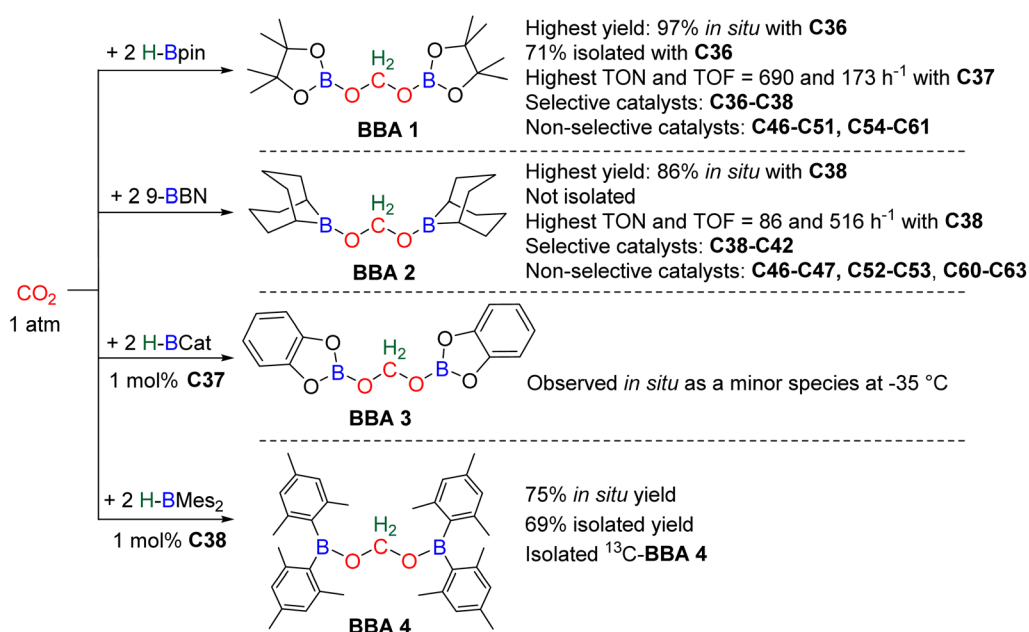
Scheme 23 General scheme for Section 3:  $\text{CO}_2$  hydroboration.

bis(boryl)acetal (BBA)<sup>90</sup> and formaldehyde<sup>91</sup> were respectively characterized from the hydroboration of  $\text{CO}_2$ , although not in a selective manner. Later on, the efficient and selective generation of BBA derivatives was reported using different hydroboranes as reductants. These transformations (Scheme 23, step a) will be presented in the first part 3.1 and the mechanism will be discussed in part 3.2. Finally, the use of these 4e<sup>-</sup> reduced products as reactants in further transformations (Scheme 23, step b) will be described in part 3.3 and a general conclusion will be drawn in part 3.4.

### 3.1. Hydroboration of $\text{CO}_2$ into bis(boryl)acetals (BBAs) and formaldehyde

In total, 7 BBA derivatives have been synthesized by the hydroboration of  $\text{CO}_2$ .<sup>92</sup> **BBA 1–4** were obtained from the hydroboration of  $\text{CO}_2$  (Scheme 24) catalysed by compounds **C36–C45** (selective catalysts, Fig. 4) and **C46–C63** (unselective catalysts, Fig. 4). **BBA 5–7** were obtained in the absence of a catalytic system (Scheme 25). **BBA 2** and **4** were shown to be key intermediates leading to formaldehyde in high yields. These transformations are described hereafter.

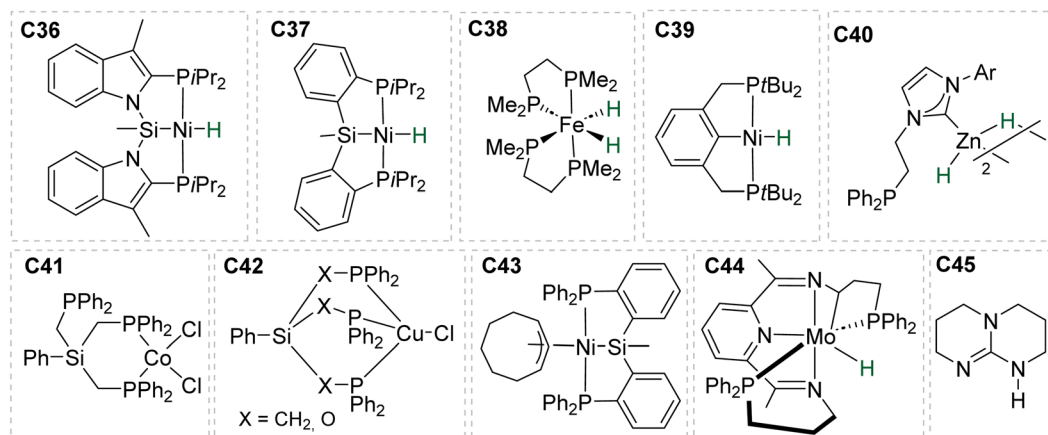
**3.1.1. Catalytic hydroboration of  $\text{CO}_2$  into BBA 1–4 catalysed by C36–C63.** **BBA 1**, featuring pinacolboryl moieties (Scheme 24), was the first BBA reported in the literature in 2012. It was characterized *in situ* as a minor product with Ru-based catalysts **C46–C47** bearing a tricyclohexylphosphine ( $\text{PCy}_3$ ) ligand.<sup>90</sup> Its selective generation was reported with **C38** albeit with a low yield of 30%.<sup>93</sup> It was only in 2017 that the use of 0.2% of the Ni hydride catalyst **C36** led to its selective generation at room temperature, with high *in situ* yields of 84% and 97% after reaction times of 1 h and 4 h, respectively.<sup>94</sup> Such high selectivity enabled the isolation of **BBA 1** by precipitation in 71% yield. This currently remains the only example in which **BBA 1** was isolated. Under optimized reaction conditions, benzene was the solvent of choice. While cyclohexane gave a similar result, the use of THF induced a net decrease (30% yield). **C43**<sup>95</sup> (15 min at room temperature with 2% of the Ni-based precatalyst) and **C44**<sup>96</sup> (2 h at 90 °C with 1% of the Mo-based catalyst) were shown to afford **BBA 1** as the major product. It must be noted that **BBA 1** was observed as a minor product in hydroboration reactions catalysed by compounds **C46–C47**,<sup>90</sup> **C48–C50**,<sup>94,97</sup> **C51**,<sup>98</sup> and **C54–C61**.<sup>99,100</sup>



Scheme 24 Catalytic generation of BBA 1–4 with C36–C63 catalysts.



## a) Selective catalysts (BBA as major product)



## b) Other catalysts (BBA as minor product)

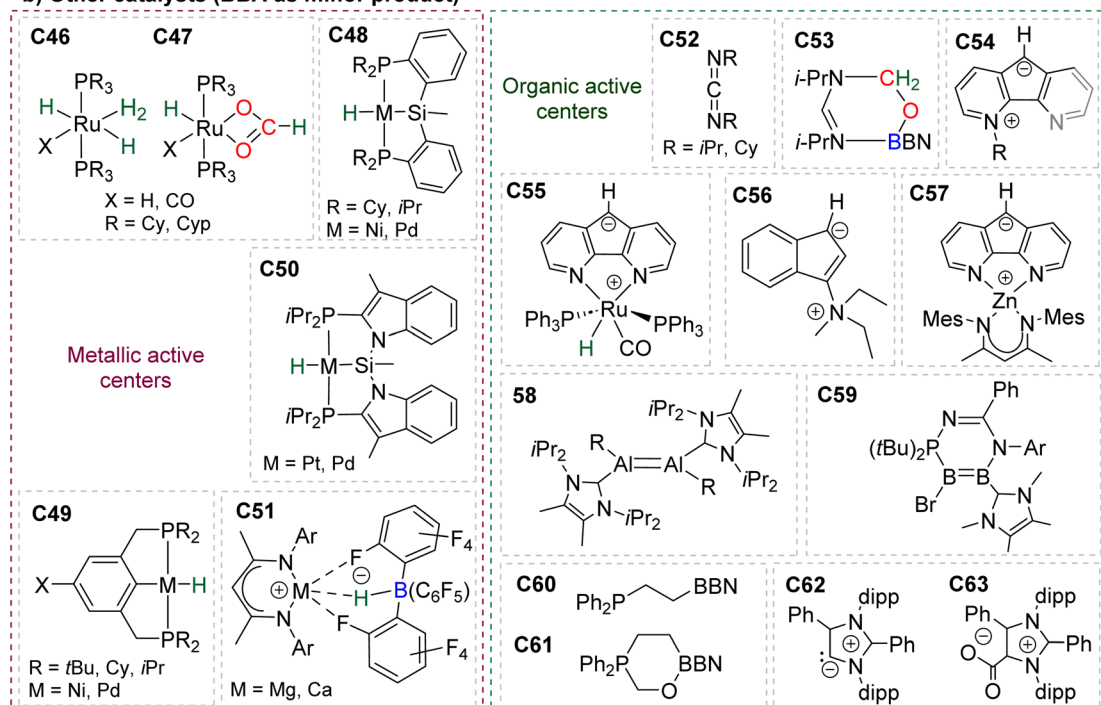


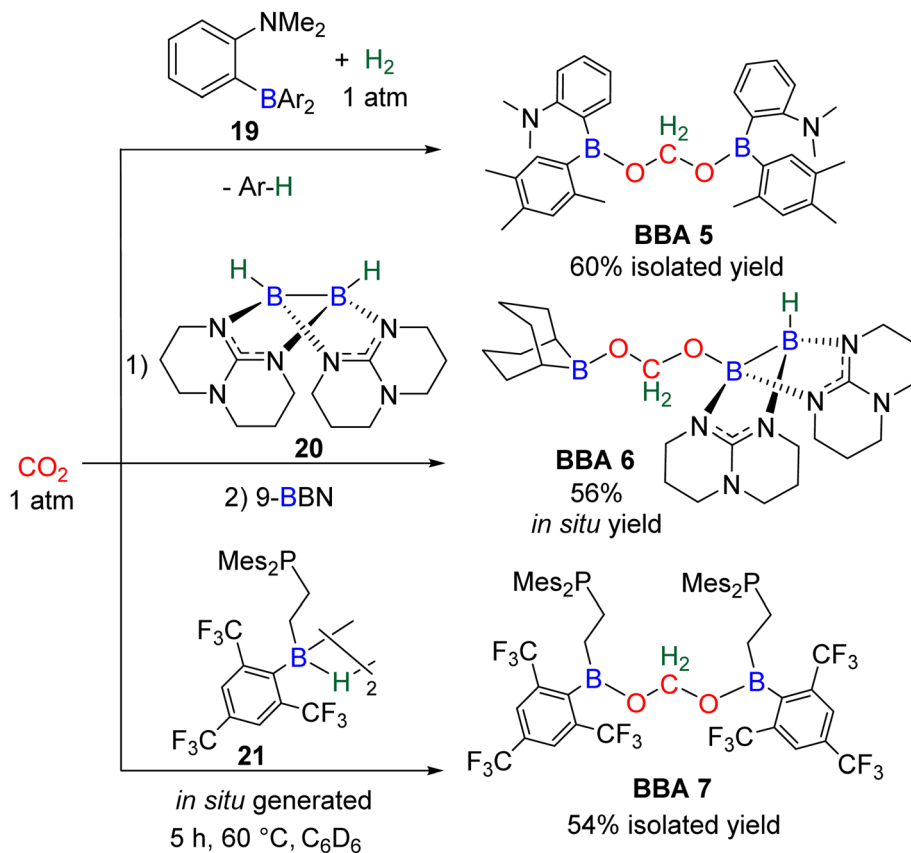
Fig. 4 Catalysts C36–C63 for the generation of BBA 1–7 and formaldehyde: (a) selective catalysts C36–C45 and (b) unselective catalysts C46–C63.

**BBA 2** was reported for the first time in 2014 in  $\text{CO}_2$  hydroboration catalysed by the nitrogen-based Lewis base TBD (C45).<sup>101</sup> This study focused on the reduction of  $\text{CO}_2$  to the methoxyborane compound with various metal-free catalysts and hydroboranes. Using 9-BBN and 2.5 mol% of catalyst C45, **BBA 2** was detected as the major intermediate after 1 h (85% ratio) before decaying, leading to the final methoxyborane compound. The selective generation of **BBA 2** and yield quantification (instead of ratio) were then described with C37–C39.

In 2015, the well-defined iron dihydride bis-diphosphine catalyst C38 was used at room temperature and under 1 atm of  $\text{CO}_2$  to afford **BBA 2** in 85% yield (TOF =  $109 \text{ h}^{-1}$ ) with a catalyst loading of 1 mol%.<sup>93</sup> The importance of the THF

solvent was identified since such selectivity was not observed with benzene or toluene. Moreover, a high TOF of  $516 \text{ h}^{-1}$  was measured upon increasing the temperature to 60 °C with the generation of **BBA 2** in 86% yield in only 10 min. In 2016, the well-defined [Co]- and [Cu]-precatalysts C41 and C42 were shown to generate **BBA 2** as the major product after 24 h at room temperature and 60 °C, respectively.<sup>102</sup> Beyond these selective systems, catalysts C46–C47,<sup>90</sup> C52–C53,<sup>103</sup> C60–C61<sup>104</sup> and C62–C63<sup>105</sup> were also reported to catalyze the generation of **BBA 2** as a minor product under mild conditions. **BBA 3** has only been partially characterized once as a minor compound, despite numerous studies using HBCat for  $\text{CO}_2$  hydroboration. This is in marked contrast with the selective generation of **BBA 1** and





Scheme 25 Catalyst free generation of BBA 5–7.

**BBA 2**, and might be explained by the ability of HBCat to readily reduce  $\text{CO}_2$  to the methoxyborane stage (*vide infra* in mechanistic consideration).

In this context, **BBA 3** was characterized *in situ* as a minor intermediate, during methoxyborane preparation with catalyst **C37**.<sup>97</sup> Following the reaction, a minor signal was observed by  $^1\text{H}$  NMR in the characteristic area of acetals. Its broadness suggested the reversible formation of **BBA 3**. This assumption was confirmed by its sharpening at  $-35\text{ }^\circ\text{C}$  leading to the first characterization of the acetal moiety of **BBA 3**. When  $^{13}\text{CO}_2$  was used, this acetal signal appeared as a doublet, which finally disappeared upon further reduction to the methoxyborane product. **BBA 4** was obtained from the  $\text{CO}_2$  hydroboration with  $\text{HBMe}_2$  catalysed by the iron hydride catalyst **C38** with an *in situ* yield of 75%.<sup>30</sup> This BBA exhibits higher stability as compared to **BBA 1–3**, as shown by an isolated yield of 69% and its characterization by X-ray diffraction analysis.<sup>30</sup> Moreover, **BBA 4** featuring a  $^{13}\text{C}$ -labelled methylene fragment was also isolated in similar yield from  $^{13}\text{CO}_2$  hydroboration. The stability of **BBA 4** was used to perform enzymatic transformations (*vide infra*). It is noteworthy that catalyst **C38** is able to catalyse the selective generation of three BBA derivatives, namely, **BBA 1**, **2** and **4**.

The performances of catalysts **C36–C42** for the selective generation of **BBA 1–2** and **BBA 4** are reported in Table 3. The performances of catalysts **C43–C45** are not indicated because

only the ratio between the detected products were measured and not the quantitative yields. The performances of catalysts **C46–C63** are not given since **BBA 1–3** were only observed as minor compounds. Among the seven selective catalytic systems (**C36–C42**), one can notice that all of them are transition metal (TM)-based catalysts and five based on 3d-TM (**C36–C39**, **C41**). The active centre is a metal hydride fragment either present in the initial catalyst or presumably generated *in situ* during the reaction with the hydroborane. The best performances in terms of TON and TOF were obtained with **C37** (487 and  $122\text{ h}^{-1}$ ) and **C38** (85,  $109\text{ h}^{-1}$  at room temperature and 86,  $516\text{ h}^{-1}$  at  $60\text{ }^\circ\text{C}$ ) for the generation of **BBA 1** and **BBA 2**, respectively. The best yields were obtained with catalysts **C36** (97% yield) and **C38** (86% yield) for the generation of **BBA 1** and **2**, respectively. The selectivity is an important factor to be considered when the generated BBA is further engaged in additional reactions (see Section 3.3). If a catalytic system exhibits high TON and TOF but poor selectivity, the presence of other products or of the remaining hydroborane may be detrimental for the subsequent reactions.

**3.1.2. Catalyst-free generation of BBA 5–8.** Currently, three BBA derivatives, **BBA 5–8**, have been obtained without any catalyst (Scheme 25). **BBA 5** features two different aryl substituents on each boryl moiety, *o*- $\text{Me}_2\text{C}_6\text{H}_4$  and *o*- $\text{NMe}_2\text{C}_6\text{H}_4$  groups (Scheme 25). It resulted from the reaction of the ambiphilic ortho amino-borane compound **19** with  $\text{H}_2$  and  $\text{CO}_2$  (72 h,

Table 3 Catalytic performances of the selective formation of BBA 1, 2 and 4 with catalysts C36–C42

BBA	Catalyst	TON	TOF (h <sup>-1</sup> )	Yield <sup>a</sup> (%)	P <sub>CO<sub>2</sub></sub> (atm)	T (°C)	Time <sup>b</sup>	Cat loading (%)	Ref.
1	C36	487	122	97	1	rt	4	0.2	94
	C37	690	173	69	1	rt	4	0.1	97
	C38	6	1.2	30	1	25	5	5	93
	C38	85	109	85	1	rt	47 min	1	93
		86	516	86	1	60	10 min	1	
	C39	32	2	64	1	rt	16	1	97
	C40	15	3.8	75	1	rt	4	5	106
	C41	25	1	38	1	60	24	1.5	102
4	C38	75	75	75	1	25	1	1	30
				69 <sup>c</sup>					

<sup>a</sup> *In situ* yield unless otherwise stated. <sup>b</sup> Hour unless otherwise stated. <sup>c</sup> Isolated yield.

room temperature). **BBA 5** was isolated in 60% yield as a monocrystal suitable for the first X-ray diffraction analysis of a BBA. DFT investigations suggested that H<sub>2</sub> led to the proto-deborylation of compound **19** giving rise to a monohydroborane compound (not observed) which would formally doubly add to CO<sub>2</sub> and generate **BBA 5**. **BBA 6** is a dissymmetric BBA featuring one diboryl and one BBN moieties (Scheme 25).<sup>107</sup> It is the only dissymmetric BBA reported to date and was obtained in two consecutive steps. Compound **20**, so-called diborane (4), was proposed to be nucleophilic enough to readily transfer a hydride to CO<sub>2</sub> affording a formoxyborane intermediate, which was characterized *in situ* in a mixture of compounds in 70% yield. In a second step, 9-BBN reduced the formoxy fragment to afford **BBA 6** within 5 h with an *in situ* NMR yield of 80% (56% overall yield). **BBA 7** features boryl units bearing two different substituents at the boron atom, a perfluoroaryl group (1,3,5-tris(trifluoromethyl)phenyl) and an alkyl phosphine group (2-dimesitylphosphino-ethyl, Scheme 25).<sup>108</sup> It was readily synthesized in 5 h at 60 °C and isolated in 54% yield from the *in situ* generated phosphino-hydroborane dimer **21**. **BBA 7** was characterized by XRD analysis.

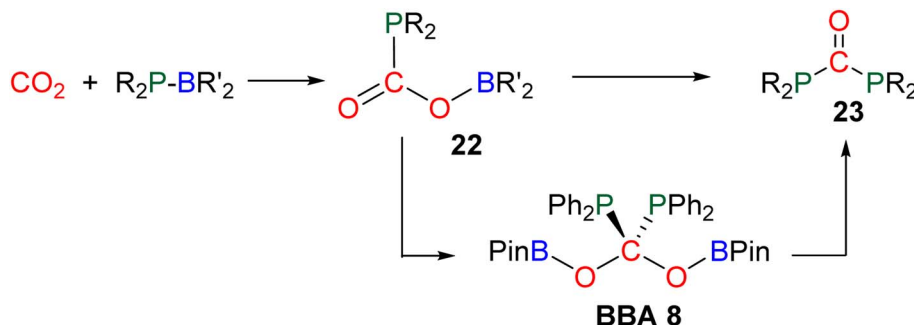
**3.1.3. Summary of the generation of BBA 1–7.** In total, seven BBA derivatives resulting from CO<sub>2</sub> hydroboration have

been characterized so far in the literature since the first report in 2012. **BBA 1–4** were obtained using commercially available pinacolborane (HBPin), 9-borabicyclo[3.3.1]nonane (9-BBN) and catecholborane (HBCat) and the non-commercially available dimesitylborane (HBMes<sub>2</sub>), respectively (Scheme 24). It is worth mentioning that the commercially available hydroborane BH<sub>3</sub> led to the reduction of CO<sub>2</sub> to the methoxyborane stage.<sup>104,109</sup> To our knowledge, detection of a corresponding BBA was never reported. NMR analysis was used as a key tool to characterize these species that are often difficult to isolate. The methylene moiety was indeed easily characterized by <sup>1</sup>H and <sup>13</sup>C NMR in a narrow range of chemical shifts: 4.90 < δ<sup>1</sup>H < 5.72 and 81.9 < δ<sup>13</sup>C < 91.3 (Table 4). Moreover, <sup>13</sup>C-labelled control experiments with <sup>13</sup>CO<sub>2</sub> allowed confirmation of the origin of the carbon atom in the product. Boron chemical shift is not characteristic of BBA since the boron atom substituents have a strong impact. They also influence the stability of BBA as observed in the case of BSA derivatives. This general feature is illustrated in BBA compounds by (i) the rather ease of generating **BBA 1** and **2** as opposed to **BBA 3**, (ii) the stability of **BBA 4**, **5** and **7** which could be isolated and crystallized while **BBA 2** was never isolated and (iii) the possibility to generate BBA in the absence of a catalyst in the cases of **BBA 5–7**.

Table 4 Selected NMR chemical shifts for BBA 1–7

BBA	Isolated	XRD	Solvent	δ <sup>13</sup> C(CH <sub>2</sub> )	δ <sup>1</sup> H(CH <sub>2</sub> )	δ <sup>11</sup> B	Ref.
1	Yes	No	C <sub>6</sub> D <sub>6</sub>	85.7	5.51	22.8	94
				85.4	5.49 <sup>1</sup> J <sub>HC</sub> = 167.2 Hz	—	90
2	No	No	THF- <i>d</i> <sub>8</sub>	87.0	5.54 <sup>1</sup> J <sub>HC</sub> = 165.2 Hz	58.6 (ref. 100c)	93
3	No	No	C <sub>6</sub> D <sub>6</sub>	81.9	5.27	n.d	97
4	Yes	Yes	THF- <i>d</i> <sub>8</sub>	89.6	5.49	48.5	30
5	Yes	Yes	C <sub>6</sub> D <sub>6</sub>	90.9	5.72	46.1	110
6	No	No	CD <sub>2</sub> Cl <sub>2</sub>	91.3	5.20 6.8 55.5	−5.4 51.0	107 32
7	Yes	Yes	C <sub>6</sub> D <sub>6</sub>	88.5	4.90		



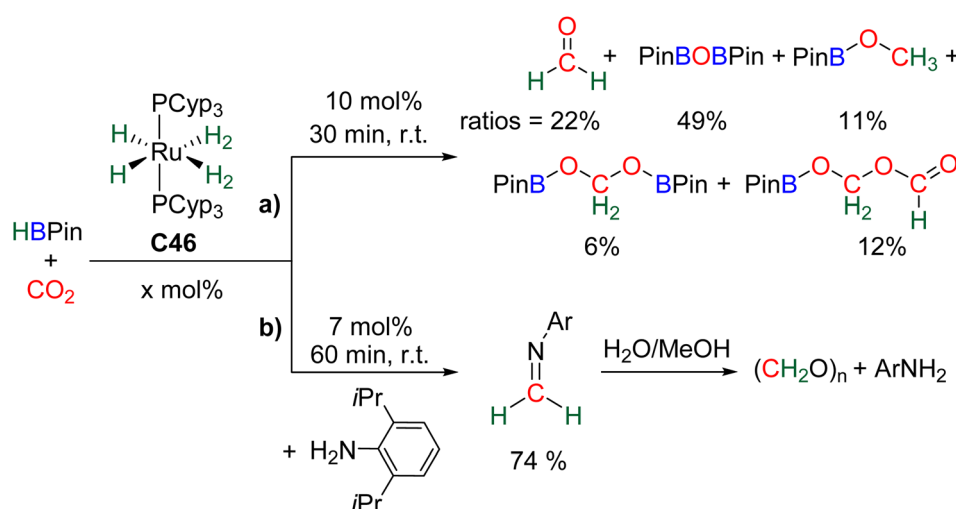
Scheme 26 Synthesis of BBA 8 by the phosphoborylation of  $\text{CO}_2$ .

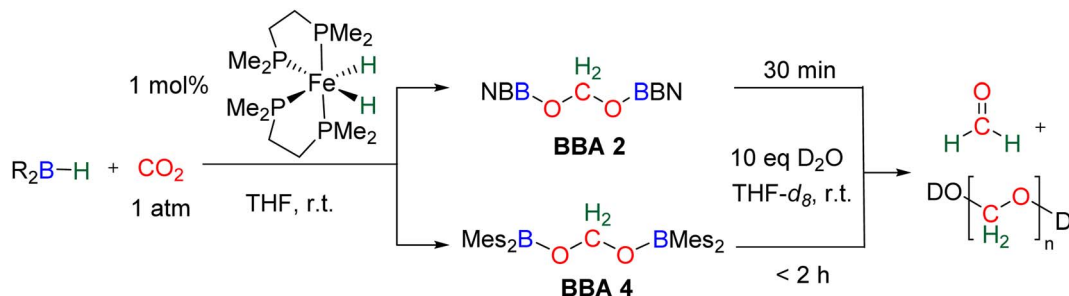
**3.1.4. Miscellaneous BBA 8.** BBA 8 is an additional bis(boryl)acetal that is not presented with the other BBAs because it does not result from a double hydroboration of  $\text{CO}_2$  but rather from formal double phosphoborylation (Scheme 26).<sup>111</sup> This compound features a central acetal core that is substituted by two diphenylphosphino substituents. The reactivity of a series of phosphinoborane compounds ( $\text{R}_2\text{PBR}_2$ ) toward  $\text{CO}_2$  led to a single insertion (compound 22) and then ultimately to the formation of diphosphaurea compound 23. BBA 8 was shown experimentally, with support from theoretical calculation, to be an intermediate and was synthesized and crystallized enabling its XRD analysis at low temperature. However, its instability precluded any further characterization in solution.

**3.1.5. Hydroboration of  $\text{CO}_2$  into formaldehyde.** The direct observation of free formaldehyde from the hydroboration reaction has been described only once, in 2014, with the ruthenium catalyst C46 featuring two tricyclopentylphosphine (PCyp<sub>3</sub>) ligands and HBpin as the reductant (Scheme 27a).<sup>91</sup> Under optimized conditions, HBpin was consumed in 30 min at room temperature with 10 mol% catalyst loading. Formaldehyde was observed as the major reduction product (ratio of 22%) along with other borylated products including BBA 1 and

methoxyborane ( $\text{CH}_3\text{OBPin}$ ). Labelling experiments using <sup>13</sup> $\text{CO}_2$  confirmed the generation of free formaldehyde with its characteristic resonances in <sup>1</sup>H and <sup>13</sup>C NMR spectra (8.74 and 193.0 ppm, respectively in  $\text{C}_6\text{D}_6$ ). In order to drive the selectivity toward formaldehyde, 2,6-bis(diisopropyl)aniline was added in the reaction mixture before  $\text{CO}_2$  pressurization. The related imine resulting from the condensation reaction between formaldehyde and the aniline was generated after 1 h at room temperature in 74% and 85% yields based on  $\text{CO}_2$  and aniline, respectively (Scheme 27b). Upon hydrolysis of the generated imine, a formalin solution was obtained.

Observation of formaldehyde from  $\text{CO}_2$  hydroboration was also mentioned in two other studies.<sup>95,112</sup> In both cases, it appears to result from the evolution of BBA 1. Using the selective formation of BBA as a tool to access formaldehyde was further developed recently. BBA 2 and BBA 4 were selectively generated with catalyst C38, and subsequently hydrolysed with 10 equivalents of  $\text{D}_2\text{O}$ . This led to their complete hydrolysis into formaldehyde at room temperature within 30 min and less than 2 h for BBA 2 and BBA 4, respectively (Scheme 28). The generated formaldehyde was then further transformed in organo-<sup>29b</sup> or enzymatic<sup>30</sup>-catalyzed reactions (see Section 3.3). It is remarkable that BBA 2 and BBA 4 were stable enough to be

Scheme 27 Hydroboration of  $\text{CO}_2$  into formaldehyde: (a) generation and (b) selective trapping of  $\text{HCHO}$ .



Scheme 28 Generation of formaldehyde from BBA 2 and BBA 4 hydrolysis.

generated selectively – and even isolated in the case of **BBA 4** – and yet efficiently released formaldehyde under mild hydrolytic conditions.

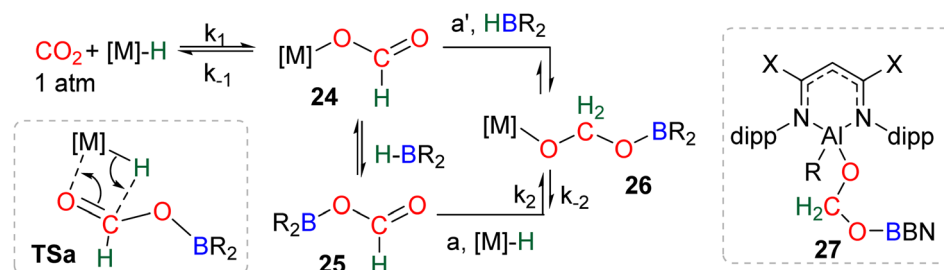
### 3.2. Mechanistic considerations

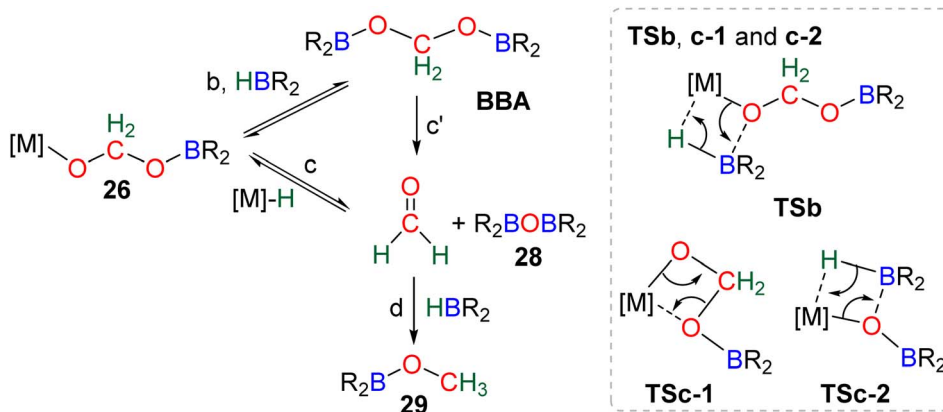
This section is dedicated to mechanistic considerations for the formation of bis(boryl)acetal (BBA) or formaldehyde. It is divided into three parts: (i) metal-hydride catalysis (**C36–C44**, **C46–C51**), (ii) organic catalysis (**C45**, **C52–C63**) and (iii) uncatalyzed generation of **BBA 5–7**.

**3.2.1. Metal hydride catalysis.** The catalysts **C36–C44** and **C46–C51** feature a metal hydride moiety or are believed to generate such a function upon reaction with the hydroborane (**C41–C43**). This hydride is proposed to be the key species of the catalytic process leading to BBA. As shown in Scheme 29, the elementary steps accounting for the  $2e^-$  reduction of  $\text{CO}_2$  are the insertion of  $\text{CO}_2$  into the M–H bond leading to the formate complex **24**, followed by a  $\sigma$ -bond metathesis with the hydroborane leading to formoxyborane **25**. We will not describe further this  $2e^-$  reduction of  $\text{CO}_2$  since it was reviewed elsewhere.<sup>8</sup> Our discussion will rather concentrate on the ensuing reduction step leading to BBA and formaldehyde. At present, theoretical<sup>89,113</sup> and experimental<sup>90,91,97,112,114</sup> studies are converging on the central role of metal boryl acetal compound **26**, which is proposed to result from the reaction of **25** with M–H (step a, Scheme 29). The corresponding transition state (**TSa**, Scheme 29) is characterized by a hydride attack on the electrophilic carbon atom of **25**, as proposed by several DFT calculations on Ni,<sup>89,115</sup> Ru,<sup>113</sup> Fe,<sup>113a</sup> Os<sup>113a</sup> and Mn<sup>116</sup> systems. The concomitant M–O interaction is often calculated to occur but does not seem mandatory. The likely involvement of

a formoxyborane species **25** as an intermediate to the  $4e^-$  and  $6e^-$  stages was experimentally asserted when a formoxyborane featuring a pinacolboryl moiety was shown to give similar rate and product distribution to that in  $\text{CO}_2$  hydroboration with catalyst **C46**.<sup>112</sup>

Numerous experimental proofs demonstrated that formate complex **24** obtained from  $\text{CO}_2$  insertion into M–H bond could be used in hydroboration reactions.<sup>8a,90,91</sup> However, although the metal boryl acetal species **26** has been calculated to be central for the  $4e^-$  reduction of  $\text{CO}_2$ , identification and or isolation of these species are still lacking. The aluminum compound **27** is the only metal boryl acetal compound characterized without ambiguity (Scheme 29).<sup>114</sup> It was obtained from the subsequent reaction of the corresponding  $[\text{Al}]$ –H with  $\text{CO}_2$  and then with 9-BBN and **27** was fully analysed by NMR and X-ray diffraction (XRD) studies. It is noticeable that only 9-BBN gave access to this metal boryl acetal structure. Analogous structures could indeed neither be observed with HBpin because of the lack of reactivity nor with HBCat or  $\text{BH}_3$  because of subsequent reduction processes. It is also important to notice that like boron, aluminum is a group 13 element and that despite mimicking important steps of  $\text{CO}_2$  hydroboration, neither the starting Al hydride complex nor complex **27** catalyses the  $\text{CO}_2$  hydroboration reaction because the initial Al–H species is not regenerated under the reaction conditions. Step a' (Scheme 29) is an alternative step to generate **26** from the direct hydroboration of the formate complex **24**. To the best of our knowledge, it has not been reported in DFT investigations but we believe that it should not be discarded *ipso facto*. Compound **26** is a key intermediate because it serves as a bifurcation point either toward BBA (Scheme 30, step b) or

Scheme 29 Calculated elementary steps (a and a') leading to the generation of the elusive intermediate **26** and structure of the only metal boryl acetal (**27**) so far characterized.



Scheme 30 Calculated elementary steps (b, c, c', d) and transition states (TSb, TSc-1 and TSc-2) from metallic boryl acetal.

formaldehyde (Scheme 30, step c). BBA is formed from the hydroboration of the metallic acetal intermediate **26**. **TSb** represents the type of transition state calculated to account for this step. It formally corresponds to an M–O metathesis. Step c illustrates the route leading to formaldehyde and the boryl ether **28** which eventually leads to the  $6\text{e}^-$  reduction hydroboration product **29** through step d. This last step was experimentally identified with the Ru–H complex **C46** that was shown to catalyse the hydroboration of formaldehyde into methoxyborane with HBpin. The first transition state **TSc-1** does not involve  $\text{HBR}_2$  and is simply a rearrangement of the metal boryl acetal **26**. The aliphatic chain rearranges to enable the interaction of the second oxygen atom with the metal centre. This reorganization weakens the M–O bond of the first oxygen atom and the O– $\text{CH}_2$  bond of the second oxygen atom. This leads to the release of formaldehyde and the formation of an M– $\text{OBR}_2$  intermediate which is subsequently hydroborated to regenerate the metal hydride and affords the ether compound **28** *via* **TSc-2**.

The factors influencing the selectivity have been explored in a thorough study involving the use of various hydride pincers of Ni- and Pd-based catalysts and three different hydroboranes, namely, HBpin, HBCat and 9-BBN.<sup>97</sup> The origin of the selectivity between the  $2\text{e}^-$  and  $4\text{e}^-$  reduction products was proposed to be dependent on the relative rate of reaction between the metal hydride fragment ( $\text{M}-\text{H}$ ) and either (i)  $\text{CO}_2$  to afford the formoxyborane **25** ( $k_1$ ) or (ii) the formoxyborane intermediate **25** to afford the metal boryl acetal **26** ( $k_2$ ) (Scheme 29). It was indeed shown that a lower pressure of  $\text{CO}_2$  led to a higher selectivity toward the  $4\text{e}^-$  reduction product presumably by disfavouring  $k_1$ . It was also proposed that  $k_2$  could be favoured by (i) increasing the concentration of the hydroborane, (ii) decreasing the steric hindrance of the boryl unit, (iii) increasing its electrophilicity and (iv) using a Lewis acid to co-activate the formoxyborane.

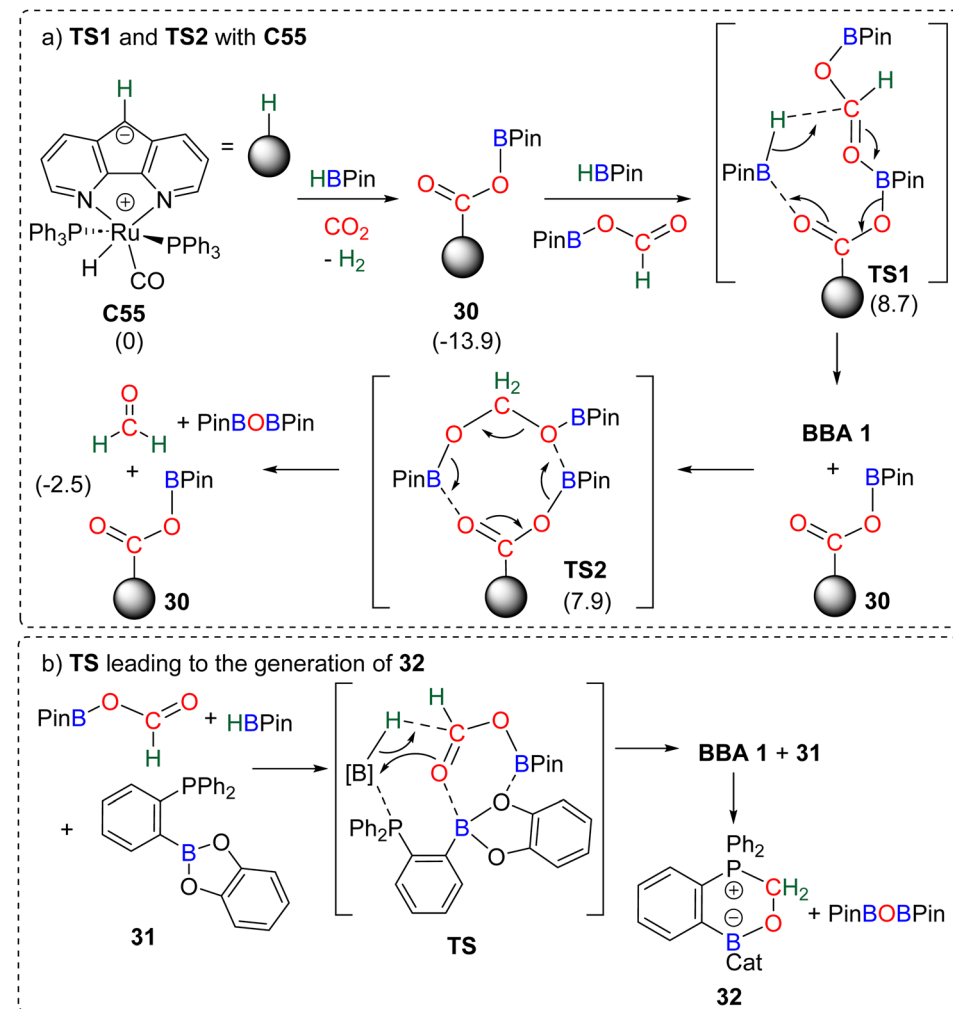
The origin of the selectivity between the  $4\text{e}^-$  and the  $6\text{e}^-$  reduction products appears to be the preference between the formation of BBA and the formation of formaldehyde, since the latter readily leads to further reduction. However, the factors influencing the preference toward BBA or formaldehyde remain to be disclosed. In addition, the formation of BBA was shown to

be reversible which eventually led to the final generation of the more stable methoxyborane in various systems.<sup>90,97</sup> This feature explains the key role that the boryl moieties may play in the kinetic and/or thermodynamic stabilization of the corresponding BBA. Step c' is an alternative path generating formaldehyde directly from BBA (Scheme 30). Such evolution has not been proposed as a plausible path for M–H catalysis but for organic catalysis (*vide infra*).<sup>96,98</sup> The direct generation of a methoxyborane compound **29** from the metal boryl acetal **26** has not been identified so far.

**3.2.2. Organic catalysis.** As shown in the first section, compounds **C45** (TBD) and **C52–63** are able to catalyse the hydroboration of  $\text{CO}_2$  without any metal centre. The metal ions in compounds **C55** and **C57** are not believed to be the active catalytic centres. The suggested mechanism with **C55** and **C57** indeed follows a similar pathway to that with **C54** and **C56**, as it involves the anionic carbon moiety as the active catalytic centre. This was based on the theoretical investigations conducted on the Ru-based system **C55** and is depicted in Scheme 31(a).<sup>82,117</sup>

The carbanion located on the backbone of the ligand of the complex was found to react both with HBPin and  $\text{CO}_2$  to produce the catalytic species **30**. Compound **30** was proposed to activate the formoxyborane intermediate **25** and HBPin concomitantly through **TS1** to afford **BBA 1**. The regenerated catalyst **30** could then be involved in the transformation of **BBA 1** into formaldehyde *via* an 8-membered-ring (**TS2**). In this reaction, formaldehyde was not experimentally observed but was proposed to be a transient intermediate *en route* to the observed methoxyborane structure. The ambiphilic phosphine borane **31** was shown to catalyse  $\text{CO}_2$  hydroboration into methoxyborane with different hydroboranes (HBCat, HBPin, 9-BBN and  $\text{BH}_3$ ) (Scheme 31b).<sup>118</sup> Although no free formaldehyde nor BBA was observed, a pathway, similar on various aspects to the previous one (Scheme 31a), was proposed. Theoretical investigations notably concluded on the co-activation of HBPin and formoxyborane (**TS**, Scheme 31b) to afford **BBA 1**. **BBA 1** then evolves to formaldehyde which ultimately reacts with compound **31** to form the formaldehyde adduct **32**. Interestingly, labelling experiments proved that the formaldehyde moiety of compound **32** was not reduced further to afford the





Scheme 31 Calculated elementary steps for the  $4\text{e}^-$  reduction mechanism of  $\text{CO}_2$  with (a) **C55** (energies indicated in parenthesis are  $\Delta G$  values in  $\text{kcal mol}^{-1}$ ) and (b) compound **31**.

methoxyborane.<sup>109a</sup> Instead, the adduct **32** acts as a more effective catalyst in the hydroboration of  $\text{CO}_2$  into methoxyborane with the various boranes tested. This feature is responsible for an observed induction period, which was also noticed (i) in the  $\text{CO}_2$  hydroboration reactions with catalyst **C52** leading to the generation of **C53**,<sup>103,119</sup> (ii) in the hydroboration of  $\text{CO}_2$  with  $\text{PtBu}_3$  in which a formaldehyde derived intermediate (compound **36**, Scheme 33) was also observed,<sup>120</sup> and (iii) when using catalyst **C60** leading to **C61** which was proven to be a more active catalyst.<sup>104</sup> The similar pathway identified in these two studies implies (i) the reduction of  $\text{CO}_2$  into formoxyborane as the  $2\text{e}^-$  reduction intermediates are observed with metal

hydride catalysts and (ii) the subsequent generation of BBA (Scheme 32, step a) and then formaldehyde (Scheme 32, step b) before further reduction to the  $6\text{e}^-$  reduction product.<sup>121</sup> This latter feature stands in contrast with the metal hydride systems in which BBA and formaldehyde are not generated along the same pathway (Scheme 30). This common pathway remains to be confirmed by further studies on additional organo-catalysed systems. Generalizing such a mechanism remains highly hypothetical because of (i) the very small number of reported theoretical investigations, (ii) the large variety of organic catalysts **C45** and **C52–C63** and (iii) the difficulty to study very reactive intermediates experimentally. A general trend is the



Scheme 32 Elementary steps a and b for the reduction of formoxyborane **25** to methoxyborane **29** calculated with compound **32**.

ability of these main group organic catalysts to co-activate several substrates and/or intermediates ( $\text{CO}_2$ , hydroborane, formoxyborane). This feature highlights the powerful synergy observed between moderately reactive centres (moderate Lewis acid and Lewis base fragments) for the transformation of very stable molecules such as carbon dioxide.

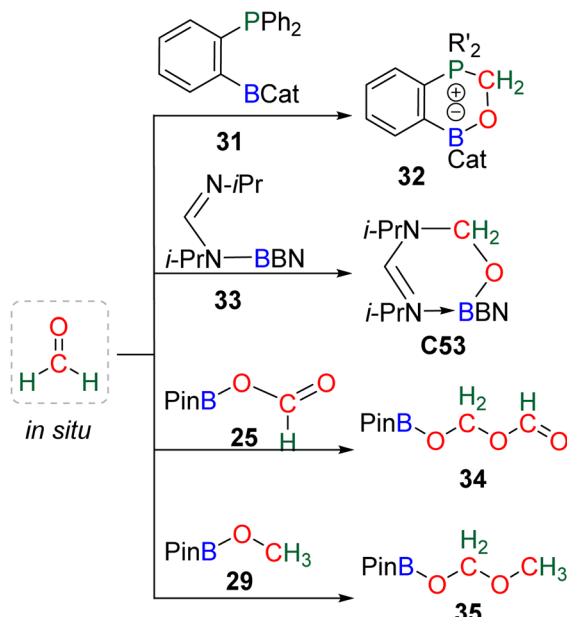
**3.2.3. Uncatalyzed hydroboration for the generation of BBA 5–7.** No DFT investigations have been performed to rationalize the catalyst-free generation of **BBA 5–7**. At first glance, the presence of a pendent N- or P-based Lewis base on the boryl unit in all three cases is a striking feature. Based on the ability of main group organic compounds to catalyse  $\text{CO}_2$  hydroboration, one could assume that the pendent Lewis base plays a role either in the intramolecular B–H activation or in an intermolecular  $\text{CO}_2$  anchoring/activation.<sup>43</sup> Another role could lie in the stabilization of the formed BBA, even though no interaction of the pendent Lewis base was detected in the XRD analyses of **BBA 4, 5 and 7**. Finally, the uncatalyzed addition of the hydroborane **21** to  $\text{CO}_2$  affording **BBA 7** is surprising if one considers the hydride transfer as being the first elementary step for such transformation. Indeed, the presence of a perfluoroaryl substituent on the boron atom certainly decreases the hydricity of the B–H bond.<sup>122</sup> With this reactive trend in mind, one would assume that the B–H bond hydricity in compound **21** is lower than the one in  $\text{HBPin}$ ,  $\text{HBCat}$  and  $\text{9-BBN}$  which were proved unreactive toward  $\text{CO}_2$  in the absence of a catalyst. That the empty p orbital at the boron atom might be at play in the first elementary step is worth considering at least in the latter case.

### 3.3. Use of formaldehyde and bis(boryl)acetal as $\text{C}_1$ and $\text{C}_n$ sources

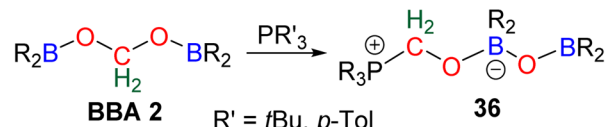
The known high reactivity of formaldehyde was first evidenced in four side reactions involving  $\text{CO}_2$  reduction. In these reactions, *in situ* generated formaldehyde reacted with other products or catalysts present in solution (Scheme 33a).

The formation of compounds **32**<sup>109a,118</sup> and **C53**<sup>103</sup> was postulated from calculation to arise from the reaction between transiently generated formaldehyde and the ambiphilic compounds **31** and **33**, respectively. Compounds **34**<sup>90,112,123</sup> and **35**<sup>91</sup> were shown experimentally to arise from the reaction of formaldehyde with **25** and **29**, respectively, which was confirmed by labelling experiments. BBA compounds were also shown to readily react under mild conditions. We believe that the characterization of compound **36** was the first observation of such BBA reactivity (Scheme 33b).<sup>120</sup> Although the authors did not elaborate on the mechanism of its formation, we propose that **36** could be formed from the reaction of **BBA 2** with the phosphine used as the catalyst, on the basis of a similar reaction later observed between **BBA 2** and an NHC leading to compound **48** (Scheme 37) analogous to compound **36**. These examples showed that BBA intermediates or formaldehyde is prone to react. Such “undesired” yet attractive reactivities may pave the way to more controlled transformations. Along this idea, we present hereafter different examples using BBA or formaldehyde in subsequent reactions either (i) as a  $\text{C}_1$  source for the formation of  $\text{C}-\text{O}$ ,  $\text{C}-\text{N}$ ,  $\text{C}-\text{P}$  and  $\text{C}-\text{C}$  bonds, or (ii) as a  $\text{C}_n$

### a) Side reactions with *in situ* generated $\text{HCHO}$



### b) Side reaction with **BBA 2**

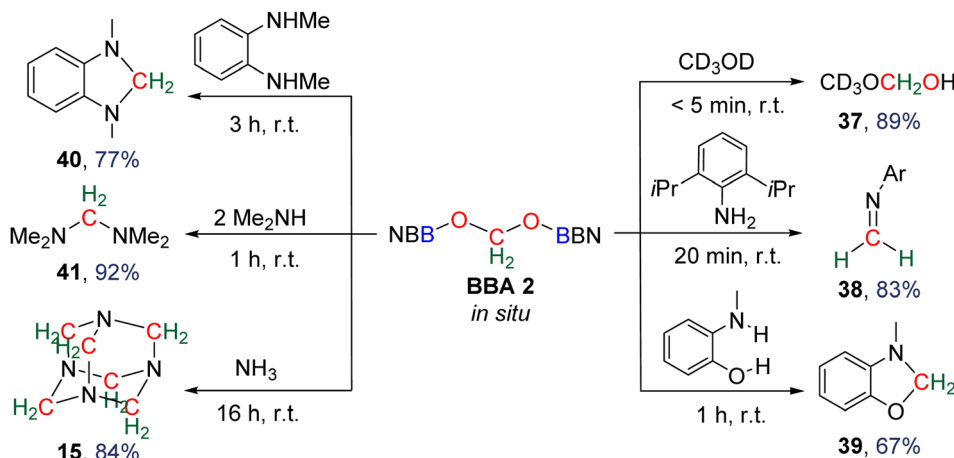


Scheme 33 Side reactions obtained with *in situ* generated  $\text{HCHO}$  (a) and **BBA 2** (b).

source in oligomerization reactions leading to the formation of carbon chains and the synthesis of chiral carbon centres.

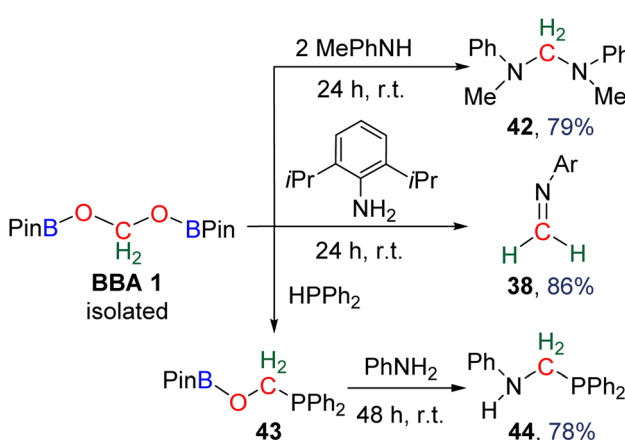
**3.3.1. BBA as a  $\text{C}_1$  source in the formation of  $\text{H}_2\text{C}-\text{O}$ ,  $\text{H}_2\text{C}-\text{N}$  and  $\text{H}_2\text{C}-\text{P}$  bonds.** **BBA 2** was the first BBA involved in reductive functionalization.<sup>93,124</sup> Although **BBA 2** has never been isolated so far, its selective and efficient generation in 85% yield after 47 min at room temperature from  $^{12}\text{CO}_2$  and  $^{13}\text{CO}_2$  hydroboration enabled probing of its reactivity toward various E–H substrates ( $\text{E} = \text{RO}$  or  $\text{R}_2\text{N}$ , Scheme 34).<sup>93</sup> Its reaction with methanol and (diisopropyl)aniline led to the characterization of the hemiacetal compound **37** (89% yield, <5 min) and imine **38** (83% yield, 20 min), respectively. These short reaction times and high yields were the first evidence that **BBA 2** could indeed be used as a formaldehyde surrogate leading to the transfer of a methylene fragment for the formation of  $\text{H}_2\text{C}-\text{O}$  and  $\text{H}_2\text{C}=\text{N}$  bonds. The reactivity was further extended to the generation of the hemiaminal **39** (67% yield, 1 h) and both cyclic and acyclic aminal compounds **40** (77% yield, 3 h) and **41** (84% yield, 1 h), respectively. Finally, the reaction with ammonia afforded the cage compound hexamethylenetetramine **15** in 84% yield after 16 h. In the latter example, it is remarkable that the six fully deoxygenated carbon atoms are issued from **BBA 2** and thus from  $\text{CO}_2$ . **BBA 1** was also used as a source of methylene in



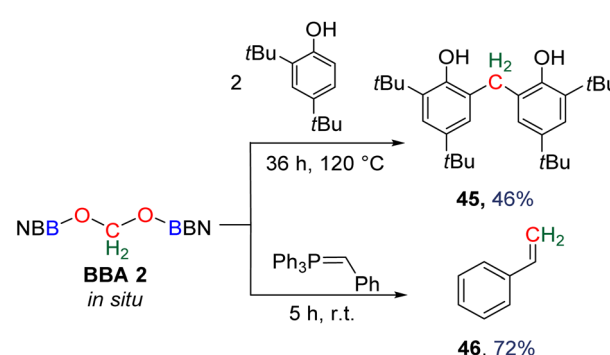
Scheme 34 Formation of  $\text{CH}_2\text{-N}$ ,  $\text{CH}_2=\text{N}$  and  $\text{CH}_2\text{-O}$  bonds from BBA 2: generation of compounds 15, 37–41.

reductive functionalization reactions (Scheme 35).<sup>94</sup> Being selectively generated (71% isolated yield), its reactivity was explored first with (diisopropyl)aniline giving rise to the corresponding imine 38 (86% yield, 24 h). It is interesting to note that similar yields were obtained starting from both **BBA 1** and **BBA 2** (*i.e.*, 83% and 86% yields, respectively) but with longer reaction time with **BBA 1** (24 h) than with **BBA 2** (20 min). The reaction with phenylmethylamine afforded the aminal 42 (79% yield, 24 h). Finally, the reaction with diphenylphosphine gave rise to a single product assigned to compound 43. Subsequent reaction with phenylamine led to the isolation of compound 44 (78% yield, 48 h) featuring for the first time a C-P bond.

**3.3.2.  $\text{CO}_2$  as a  $\text{C}_1$  source in the formation of C-C bonds.** The formation of C-C bonds from  $\text{CO}_2$  reduction is of high interest, yet challenging. Such a process was first described with the condensation reaction between **BBA 2** and 2 equivalents of a substituted phenol derivative, leading to the generation of the methylene-bridged compound 45 (46% yield, 36 h, 120 °C, Scheme 36). **BBA 2** was also used in a Wittig reaction, producing styrene 46 (72% yield, 5 h, room temperature). These two examples showed that the formation of C-C and C=C bonds could be successfully achieved from  $\text{CO}_2$ .<sup>93</sup>

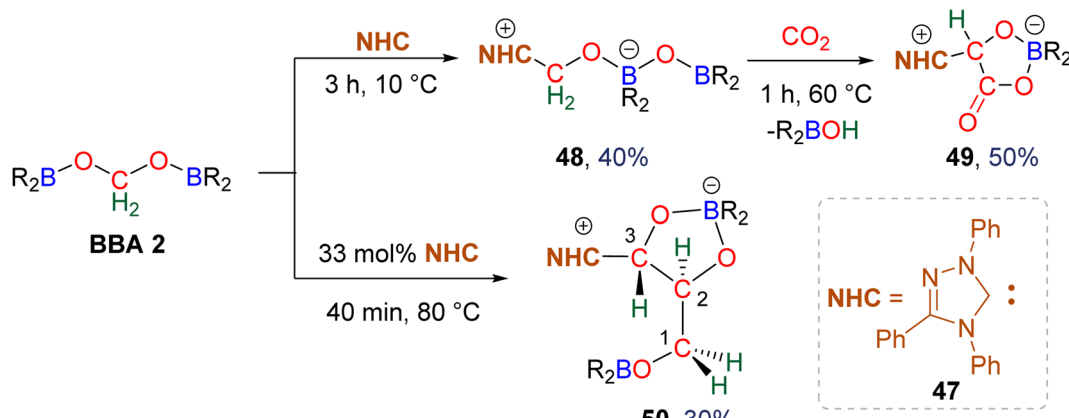
Scheme 35 Generation of  $\text{CH}_2\text{-N}$  and  $\text{CH}_2\text{-P}$  bonds from BBA 1.

**3.3.3. BBA as a  $\text{C}_n$  source: oligomerization of BBA and formaldehyde.** The conversion of  $\text{CO}_2$  into  $\text{C}_n$  compounds by the construction of a carbon chain is an appealing process because of the higher complexity and diversity of the  $\text{C}_n$  products as compared to the  $\text{C}_1$  products. However, this reaction is highly challenging in terms of conditions, selectivity and scope of products.<sup>3b,21a-c</sup> In particular, no asymmetric carbon atom was generated from  $\text{CO}_2$ . So far, the  $4\text{e}^-$  reduction of  $\text{CO}_2$  by hydrogenation, hydrosilylation and hydroboration aimed at employing  $\text{CO}_2$  exclusively as a  $\text{C}_1$  source. While the difficulties encountered in controlling the  $4\text{e}^-$  reduction processes may have been the main reason for this, the long-known possibilities of oligomerizing formaldehyde – the so-called formose reaction – were strongly calling for using  $\text{CO}_2$   $4\text{e}^-$  reduction products as a  $\text{C}_n$  source.<sup>125</sup> This was first accomplished upon reacting **BBA 2**, generated *in situ* from  $\text{CO}_2$  hydroboration, with N-heterocyclic carbene (NHC, Scheme 37).<sup>32</sup> Ender's NHC carbene 47 is a classical organo-catalyst able to catalyse the formation of C-C bonds of carbonyl compounds and notably the oligomerization of formaldehyde.<sup>126</sup> Its stoichiometric reactivity with **BBA 2** was first probed, leading to the formation and isolation of compound 48 (40% yield, 3 h, 10 °C) (Scheme 37). This reaction resulted from the formal isomerization of **BBA 2** triggered by the addition of the NHC on the electrophilic methylene moiety of



Scheme 36 Generation of C-C and C=C bonds from BBA 2.



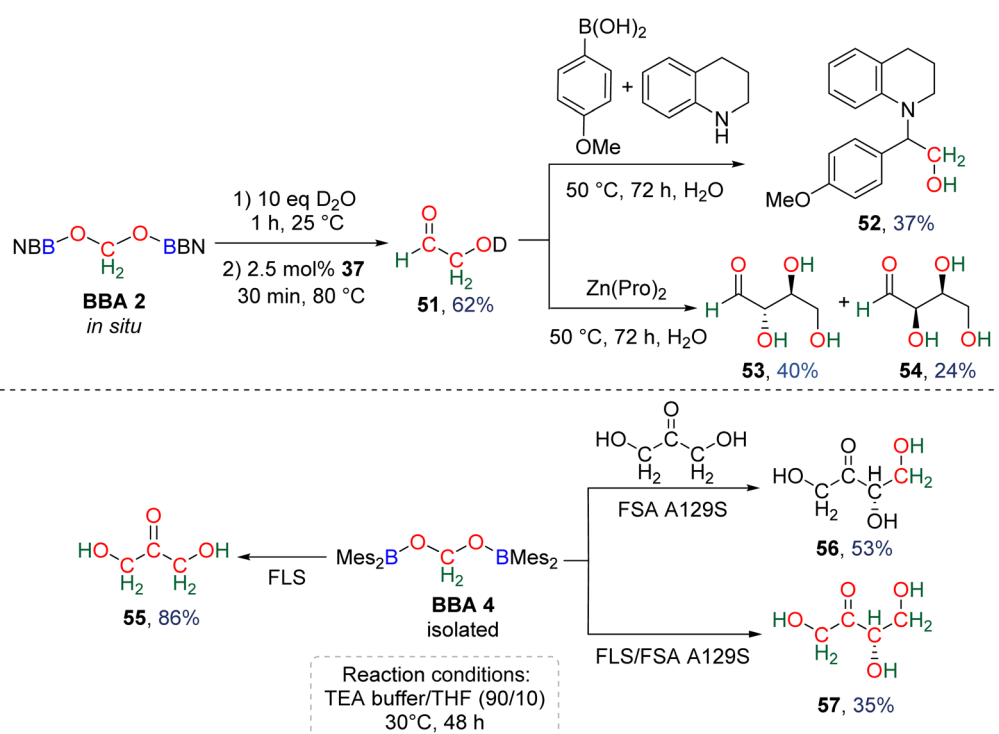


Scheme 37 Homocoupling of BBA 2 resulting in the formation of compounds 49 and 50.

**BBA 2** *via* an SN<sub>2</sub> type mechanism, as proposed by DFT investigations.<sup>32</sup> This reaction illustrated that a Lewis base can promote the migration of an O- $\text{BR}_2$  fragment onto the other Lewis acid moiety of a BBA molecule, which is reminiscent of the generation of compound 36 from the reaction of **BBA 2** with tertiary phosphines (Scheme 33b). The intermediate **48** was shown to further react with CO<sub>2</sub> to form compound **49** (50% yield, 1 h, 60 °C), which was notably characterized by X-ray diffraction analysis. This compound was obtained from the loss of a borinic acid moiety (R<sub>2</sub>BOH), possibly generating a transient original O-borylated Breslow intermediate which was then able to trap a CO<sub>2</sub> molecule in a bifunctional manner.<sup>127</sup>

Compound **49** features a new C-C bond between two carbon atoms arising from two CO<sub>2</sub> molecules. In this reaction, the new

C-C bond was formed thanks to the nucleophilic character of the carbon atom linked to the NHC. This Umpolung process – classical of organocatalyzed C-C bond formation with such a carbene – was further used to generate compound **50** from the homocoupling of three **BBA 2** molecules in the presence of 33 mol% of NHC, generating a chain of three carbon atoms (C<sup>1</sup>, C<sup>2</sup>, C<sup>3</sup>) arising from three CO<sub>2</sub> molecules. It must be pointed out that two of the three carbon atoms (C<sup>2</sup>, C<sup>3</sup>) of the chain are asymmetric carbons and were generated with a high diastereoecontrol, thanks to the presence of the boryl moiety. DFT investigations were conducted to get insights on the elementary steps accounting for these transformations,<sup>32</sup> which stand as the first reported example of the generation of asymmetric carbon centres from CO<sub>2</sub>. In the process leading to **50**, it should



Scheme 38 Chemo- and enzyme-catalysed oligomerization of BBA 2 and 4.



be noticed that formaldehyde is never released from **BBA 2**. The oligomerization reaction involves BBA without the intermediary of formaldehyde, as shown from the presence of boryl moieties in the final product **50**. The possibility that formaldehyde could be released from BBA – in the same vein as what was explored with **BSA 3** – before its engagement in the oligomerization process, was recently explored with **BBA 2** and **BBA 4** (Scheme 38). Despite its powerful nature, the formose reaction remains a challenging reaction due to the difficulty in controlling both the length of the carbon chain and the chirality of the generated carbohydrates.<sup>26,126,128</sup>

As presented earlier, **BBA 2** was shown to quantitatively release formaldehyde after 1 h at room temperature in the presence of 10 equivalents of D<sub>2</sub>O. Optimization of both the hydrolysis and the formose steps led to the synthesis of the C<sub>2</sub> carbohydrate glycolaldehyde **51** in 62% yield after 30 min at 80 °C using 2.5 mol% of NHC **47** as the catalyst (Scheme 37).<sup>29b</sup> Glycolaldehyde was further engaged in one-pot reactions leading to the formation of compound **52** (37% isolated yield) *via* a Petasis–Borono–Mannich reaction or to the formation of the C<sub>4</sub> carbohydrates erythrose (**53**, 40% yield) and threose (**54**, 24% yield) generated from Zn(pro)-catalysed dimerization reactions (pro = proline).

In a parallel study, **BBA 4** was identified as a promising candidate to conduct enzymatic transformations.<sup>30</sup> Its isolation, in contrast to **BBA 2**, was seen as an important feature toward this aim. If it was stable enough for isolation, **BBA 4** was nonetheless shown to readily release formaldehyde upon hydrolysis under relatively similar conditions to those with **BBA 2**. Enzymatic transformations were then thought about in order to control the length of the generated carbon chain and the chirality of the product. While formaldehyde is usually responsible for enzyme inhibition and even denaturation,<sup>129</sup> D-fructose-6-phosphate aldolase (FSA) and formolase (FLS) were shown to catalyse aldolization and formose transformations of formaldehyde, respectively.<sup>24,130</sup> These enzymes were thus selected to perform the transformation of formaldehyde released from **BBA 4**. The enzymatic transformations were conducted at 30 °C for 48 h in a triethanolamine (TEA) buffered solution (25 mM, pH 7.0 with 1 mM MgSO<sub>4</sub> and 0.1 mM thiamine pyrophosphate (TPP)) with THF. The presence of 10% THF was found optimal to ensure the solubility of **BBA 4**, while limiting the detrimental effect of this organic solvent on FLS and FSA activities (Scheme 38).<sup>30</sup> Under these conditions, **BBA 4** was oligomerized by FLS into dihydroxyacetone (**55**) in 86% yield. **BBA 4** was then reacted with commercial dihydroxyacetone in the presence of the mono-mutant FSA A129S<sup>131</sup> to afford the corresponding C<sub>4</sub> carbohydrate, L-erythrulose (**56**) in 53% yield with a perfect enantiocontrolled aldol reaction. In this case, one carbon atom of the carbon chain arose from **BBA 4**. Following recently reported cascade reactions with formaldehyde,<sup>132</sup> these two enzymes were then combined in a one-pot cascade reaction to achieve the transformation of **BBA 4** into L-erythrulose **57** in 35% yield. All four carbon atoms of the carbohydrate arose from CO<sub>2</sub>, including the chiral one. This reaction corresponds to the first cell-free enantioselective transformation of CO<sub>2</sub>.

### 3.4. Conclusion and perspectives

In conclusion, the 4e<sup>-</sup> hydroboration of CO<sub>2</sub> stands out for several reasons: (i) the uncatalyzed formation of three bis(boryl) acetal (BBA) compounds derived from specific hydroboranes; (ii) the highest reported turnover frequency (TOF) at 516 h<sup>-1</sup> among hydroelementation reactions; (iii) the reactive nature of BBA at room temperature, facilitating condensation reactions or formaldehyde release; (iv) the utilization of BBA as a C<sub>n</sub> source with or without formaldehyde release, wherein the reaction without formaldehyde release results in the formation of an O-borylated C<sub>3</sub> compound; (v) the use of BBA in the pioneering enantioselective generation of a carbon centre from CO<sub>2</sub>.<sup>30–32</sup> This significant breakthrough was achieved through formaldehyde release and subsequent enzymatic cascade reactions.

As perspectives in CO<sub>2</sub> hydroboration, the primary challenge lies in the stoichiometric utilization of hydroborane and thus the stoichiometric amount of borinic acid (R<sub>2</sub>BOH) generated as a co-product following the hydrolysis of BBA compounds. Since there is currently no sustainable process for regenerating hydroborane from this co-product, CO<sub>2</sub> hydroboration is scarcely applicable unless the product synthesized from BBA holds a very high value. For example, carbohydrates, particularly rare and non-natural ones, are of significant interest to the pharmaceutical industry. Their synthesis from CO<sub>2</sub>, especially with isotope labelling, could be an avenue worth exploring for generating chiral complex C<sub>n</sub> products from CO<sub>2</sub>. On the other hand, the prospect of generating O-borylated C<sub>n</sub> products could open new avenues to retain boryl moieties in CO<sub>2</sub> transformation products, instead of treating them as waste after B–O bond hydrolysis. This would allow for further functionalization of the generated compounds. To achieve these objectives, future efforts could focus on exploring a broader variety of hydroboranes with diverse properties. Such a range of hydroboranes could lead to the formation of a diverse array of BBA compounds with varying stability and reactivity, suitable for various applications. Additionally, other CO<sub>2</sub> hydroelementation reactions, beyond hydrosilylation and hydroboration, may provide an even greater variety of acetal compounds with unique properties. Specific CO<sub>2</sub> hydroelementation reactions involving early transition-metal hydride species are discussed in the subsequent section of this review.

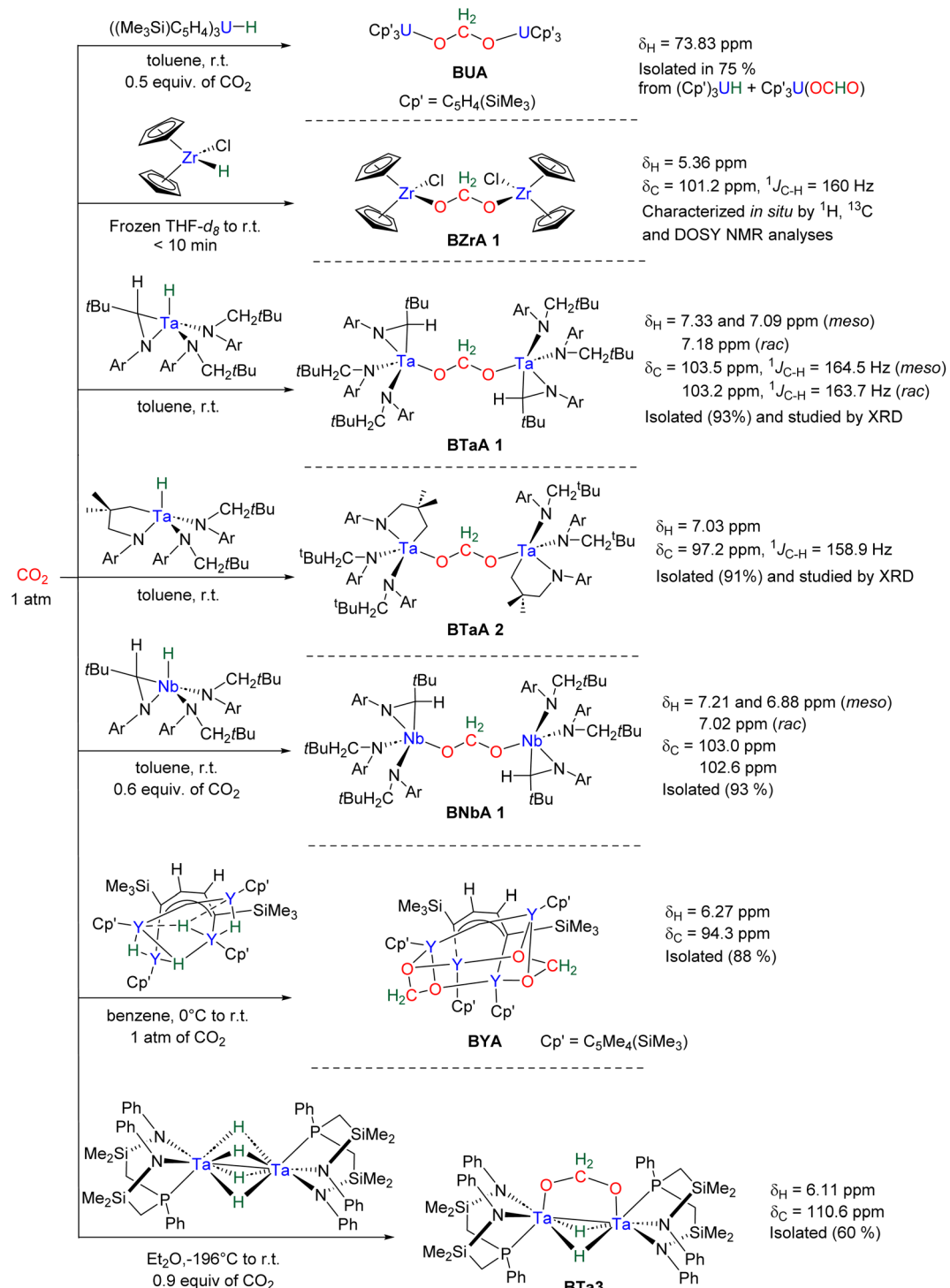
## 4. Other hydroelementation reactions

The CO<sub>2</sub> hydroelementation involving metal hydrides and phosphines has seen limited development. We have compiled these results in this concise standalone section, separated from the broader and more extensive sections.

### 4.1. Hydroelementation with actinide, early TM and rare earth metal hydride species to acetal complexes

Hydride complexes of U, Zr, Ta, Nb and Y were shown to react with CO<sub>2</sub> under mild conditions to afford the bi-metallic acetal or methylene diolate complexes shown in Scheme 39. The reaction of the U(IV) hydride complex (Cp')<sub>3</sub>U(H) (Cp' =

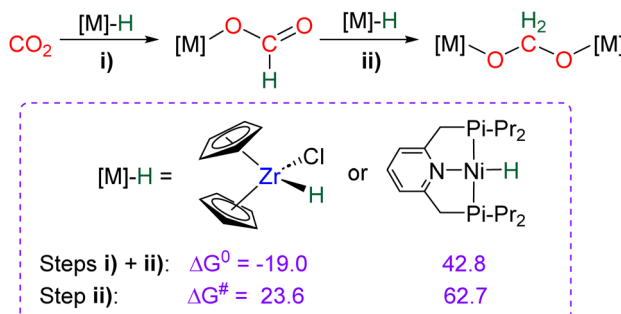




Scheme 39 Generation of BZrA 1, BTaA 1, BTaA 2 and BNbA 1.

$\text{C}_5\text{H}_4(\text{SiMe}_3)$  with 1 atm  $\text{CO}_2$  led to the expected formoxy uranium  $(\text{Cp}')_3\text{U}(\text{OCHO})$ . However, when only 0.5 equiv. of  $\text{CO}_2$  was introduced in an NMR tube, the bis(uranyl)acetal complex (**BUA**) was generated.<sup>131</sup> This complex was also isolated by crystallization from the stoichiometric reaction of  $(\text{Cp}')_3\text{U}(\text{OCHO})$  with  $(\text{Cp}')_3\text{U}(\text{H})$  in 75% yield after 4 h at 70 °C. The methylene fragment was characterized at 73.83 ppm in  ${}^1\text{H}$  NMR

due to the proximity with the paramagnetic uranium centre. The reaction of the Schwartz's reagent,  $\text{Cp}'\text{Zr}(\text{H})\text{Cl}$ , was investigated with  ${}^{13}\text{CO}_2$ .<sup>134</sup> A frozen THF- $d_8$  solution of the Zr complex was prepared and reaction with  ${}^{13}\text{CO}_2$  was investigated at an early stage. After initiating the reaction by a gentle shaking of the frozen solution, the acetal **BZrA 1** could be observed by  ${}^1\text{H}$  NMR analysis for only 10 min. To further characterize the acetal



Scheme 40 DFT investigations for the formation of metallic acetal upon reaction of  $[\text{Ni}]$ -H and  $[\text{Zr}]$ -H hydrides with  $\text{CO}_2$  (free enthalpies in  $\text{kcal mol}^{-1}$ ).

species,  $^1\text{H}$  and  $^{13}\text{C}\{^1\text{H}\}$  NMR analyses were conducted at 235 K.<sup>134b</sup> The methylene signal appeared at  $\delta^1\text{H} = 5.36 \text{ ppm}$  and  $\delta^{13}\text{C} = 101.2 \text{ ppm}$ . Low temperature diffusion ordered NMR spectroscopy (DOSY) confirmed the dimeric nature of **BZrA 1** in solution.<sup>134a</sup> The reduction of  $\text{CO}_2$  was also investigated with Ta-H and Nb-H complexes. The acetal complexes **BTaA 1**, **BTaA 2** and **BNbA 1** were isolated and characterized, notably by XRD in the case of the two former ones (Scheme 39).<sup>135</sup> Two diastereoisomers with diastereotopic methylene protons, the *rac* and *meso* forms, were observed for **BTaA 1** and **BNbA 1**, being the result of a  $C_2$  and  $C_s$  symmetry, respectively. The [Ta]- and [Nb]-based hydride complexes featured a peculiar aziridine-metallacycle which was shown to generate a 5-membered cycle leading to **BTaA 2**. Another Ta acetal complex **BTaA 3** was later reported from the reaction of a dinuclear Ta tetrahydride complex with 0.9 equivalent of  $\text{CO}_2$  at low temperature.<sup>134</sup> The methylene signal was characterized in solution at  $\delta^1\text{H} = 6.11 \text{ ppm}$  and  $\delta^{13}\text{C} = 110.6 \text{ ppm}$  and the complex was structurally characterized by X-ray diffraction analysis. Finally, a tetranuclear yttrium tetrahydride complex was also shown to readily react with 1 atm of  $\text{CO}_2$  to afford **BYA** featuring two methenediolate bridge fragments maintaining the tetranuclear

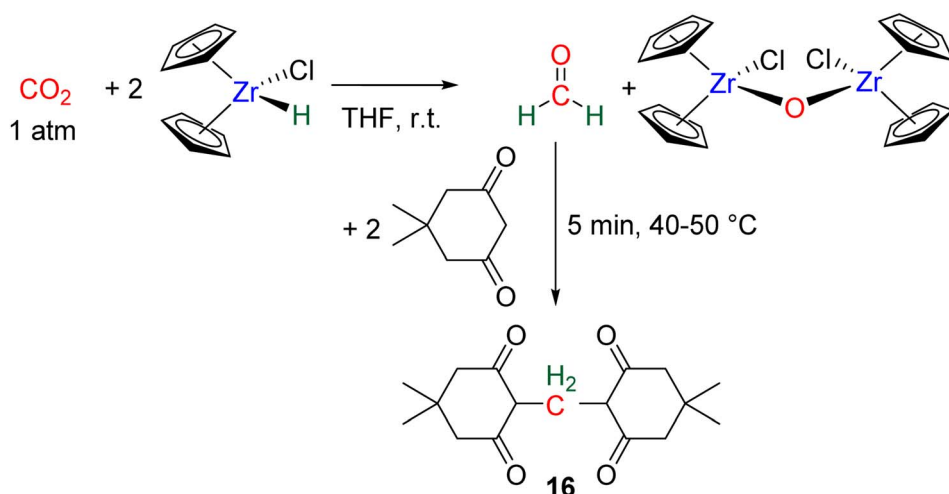
structure. The complex was analysed in the solid state by X-ray diffraction and in solution by NMR ( $\text{CH}_2$  fragment:  $\delta^1\text{H} = 6.27 \text{ ppm}$  and  $\delta^{13}\text{C} = 94.3 \text{ ppm}$ ).<sup>137</sup>

The methylene signal of these acetal products appeared at a lower field in  $^1\text{H}$  NMR ( $6.11 \text{ ppm} < \delta^1\text{H} < 7.33 \text{ ppm}$ ) as compared to BBA, BSA and **BZrA 1** structures while the  $^{13}\text{C}\{^1\text{H}\}$  NMR chemical shifts of the early-TM acetals are in a slightly lower field area as compared to the ones obtained from BBA and BSA derivatives ( $101.2 \text{ ppm} < \delta^{13}\text{C} < 103.5 \text{ ppm}$ ).

DFT investigations<sup>89</sup> were conducted to compare the reactivity of  $\text{CO}_2$  toward the Schwartz's reagent  $[\text{Zr}]$ -H complexes<sup>134</sup> vs.  $[\text{Ni}]$ -H complexes used as catalysts in  $\text{CO}_2$  hydroboration,<sup>88</sup> regarding the formation of the corresponding metallic acetal species (Scheme 40). This study disclosed a rare comparison between the reactivities of early and late TM complexes toward  $\text{CO}_2$ .<sup>138</sup> The formation of the acetal from two equivalents of  $[\text{M}]$ -H and  $\text{CO}_2$  (steps (i) + (ii), Scheme 36) is exergonic with  $\Delta G^0 = -19.0 \text{ kcal mol}^{-1}$  for the Zr complex, while it is endergonic for the Ni analogue by  $+42.8 \text{ kcal mol}^{-1}$ . Replacing the bulky  $^3\text{Bu}$  group of the pincer system on Ni led to a more accessible, yet still endergonic reaction by  $+26.9 \text{ kcal mol}^{-1}$ . The thermodynamic barriers ( $\Delta G^\#$ ) for step (ii) were calculated to equal 23.6 and 62.7  $\text{kcal mol}^{-1}$  for the Zr-H and Ni-H, respectively. These calculations explained why the bis-nickel acetal was never observed in contrast to the Zr analogue.<sup>89</sup>

#### 4.2. Hydroelementation to formaldehyde and reductive functionalization

While the formation of **BZrA 1** is favourable as shown in experiments and upon DFT calculations, it is not stable at room temperature, in contrast to **BTaA 1**, **BTaA 2** and **BNbA 1**. The reaction of group IV elements toward  $\text{CO}_2$  has been studied for a long time, with an early report in the 1970s.<sup>139</sup> Using Schwartz's reagent as the reductant,  $\text{CO}_2$  was readily reduced to formaldehyde at room temperature (Scheme 41).<sup>139a,b</sup> Besides the formation of a  $[\text{ZrOZr}]$  complex, the proof for the formation of formaldehyde was obtained by *in situ* condensation with 5,5-



Scheme 41 Condensation of a cyclohexanedione with formaldehyde generated from  $\text{CO}_2$  hydrozirconation.



dimethylcyclohexane-1,3-dione to afford the corresponding maledone compound **16** which displays a methylene-bridged structure. This study reported the actual first example of reductive  $\text{CO}_2$  functionalization.<sup>139a,140</sup>

### 4.3. Hydrophosphination

$\text{CO}_2$  hydrophosphination was reported to afford the corresponding formate compound.<sup>141</sup> Despite similar electronegativity values for P and H atoms, 1,3,2-diazaphospholene (NHP-H) exhibits zwitterionic properties<sup>142</sup> leading to the  $2\text{e}^-$  reduction of  $\text{CO}_2$  into a phosphorus formate moiety in high yield (93% isolated yield). However, no further reduction to the 4, 6 or  $8\text{e}^-$  reduction levels was evidenced. One can imagine that further structural modification would be necessary to achieve further reduction.

### 4.4. Conclusion

In conclusion, the  $4\text{e}^-$  hydroelementation with early TM presented in this section stands out by the fact that (i) only four examples were reported so far; (ii) formaldehyde is spontaneously released at low temperature from **BzrA 1**; and (iii) the insertion of  $\text{CO}_2$  into the early TM hydride bond is uncatalyzed.

As perspectives, hydroelementation of  $\text{CO}_2$  to the  $4\text{e}^-$  reduction level might offer a wide range of reactivity *via* the modification of the coordination sphere of the metal fragment.

## 5. Hydrogenation

The hydrogenation of  $\text{CO}_2$  into  $\text{HCOOH}$ ,  $\text{HCHO}$ ,  $\text{CH}_3\text{OH}$  and  $\text{CH}_4$  are reactions of utmost importance in the actual momentum of producing green  $\text{H}_2$  from water electrolysis.<sup>13f,15a,16a,143</sup> As opposed to hydroelementation, hydrogenation of  $\text{CO}_2$  is a 100% atom economical reaction making  $\text{CO}_2$  perfectly fitted to store energy and/or to afford key  $\text{C}_1$  building blocks for the chemical industry. As a consequence, these transformations have been intensively investigated but for

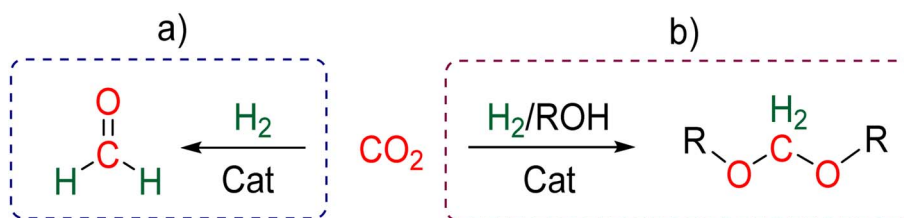
formaldehyde synthesis. There are indeed currently only five catalytic systems, including heterogeneous and homogeneous processes, which have reported the generation and detection of formaldehyde in  $\text{CO}_2$  hydrogenation (Scheme 42a). These systems are presented in Section 5.1. Three of these examples generated formaldehyde as the major product and none disclosed its isolation. Reasons are because of (i) the disfavoured thermodynamic parameters in gas and in liquid phases, (ii) the highly reactive nature of formaldehyde and (iii) its volatility as a gas under atmospheric conditions.

To circumvent such hurdles, the hydrogenation reaction conducted in the presence of alcohol as the solvent and co-reactant led to the stabilization of the  $4\text{e}^-$  reduction stage in the form of acetals (Scheme 42b) as described in Section 5.2, which is in line with the formation of BSA and BBA presented in the previous sections. The specific roles of  $\text{H}_2$  and alcohol are thoroughly explained in the mechanism described in Section 5.2.3.

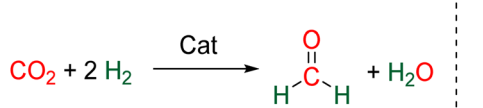
### 5.1. Hydrogenation of $\text{CO}_2$ into formaldehyde

Catalysts **C64–C68** were reported to generate formaldehyde from  $\text{CO}_2$  hydrogenation (Scheme 43). The catalytic conditions and performances are presented in Table 5. It is worth mentioning that the origin of the detected  $\text{HCHO}$  was not confirmed with  $^{13}\text{CO}_2$  labelling experiments in any of these cases.

**C65**,<sup>145</sup> **C67**,<sup>147</sup> and **C68**,<sup>148</sup> gave rise to the generation of formaldehyde as the major product. **C64**,<sup>144</sup> is the only reported molecular homogeneous system and operates in liquid media similarly to **C67** and **C68**, while **C65** and **C66**,<sup>146</sup> operate in the gas phase. Reaction temperatures range between 40 and 200 °C, while the total gas pressure ( $P_{\text{CO}_2} + P_{\text{H}_2}$ ) ranges between 4 and 70 atm. The positive impact of a high  $P_{\text{H}_2}/P_{\text{CO}_2}$  ratio on the selectivity toward  $\text{HCHO}$  formation is a common feature observed for **C64**, **C65** and **C67**. It can also be noticed that both selective systems, **C65** and **C67**, relied on a Pt-based catalyst system. The small number of catalytic systems and their disparities preclude



Scheme 42  $\text{CO}_2$  hydrogenation into  $4\text{e}^-$  reduction products: (a) formaldehyde (Section 5.1) and (b) acetals (Section 5.2).



Cat = **C64–C68**

Homogeneous and heterogeneous systems

$P_{\text{CO}_2} + P_{\text{H}_2} = 4$  to 70 atm

T = 40 to 200 °C

Gas and liquid phases

Scheme 43  $\text{CO}_2$  hydrogenation into formaldehyde catalysed by **C64–C68**.



Table 5 Properties of reported systems for  $\text{CO}_2$  hydrogenation into formaldehyde catalysed by C64–C68

Catalytic systems	$\text{K}[\text{Ru}(\text{EDTA}-\text{H})\text{Cl}] \cdot \text{H}_2\text{O}$		$\text{Pt}-\text{Cu}/\text{SiO}_3$		$\text{Ni}-\text{Co}$ NPs		$\text{Pt}-\text{Ni}$ and $\text{Pt}-\text{Cu}/\text{Al}_2\text{O}_3$		Ru/LDH	
	C64 <sup>144</sup>	C65 <sup>145</sup>	C66 <sup>146</sup>	C67 <sup>147</sup>	C68 <sup>148</sup>	C68 <sup>148</sup>	C68 <sup>148</sup>	C68 <sup>148</sup>	C68 <sup>148</sup>	C68 <sup>148</sup>
Performances	Rate = $2.79 \times 10^{-2} \text{ M h}^{-1}$	5.22 $\times 10^{-3} \text{ M g}_{\text{cat}}^{-1} \text{ h}^{-1}$	$\text{CO}_2$ conv. = 0.24% HCHO ratio = 30%	$0.41 \times 10^{-5} \text{ M g}_{\text{cat}}^{-1} \text{ h}^{-1}$	$0.037 \text{ M g}_{\text{cat}}^{-1} \text{ h}^{-1}$					
$T$ (°C)	40	150	200	25						
$P_{\text{CO}_2}$ (atm)	17	0.3	1	4						
$P_{\text{H}_2}$ (atm)	17	5.7	3	66						
Medium	$\text{H}_2\text{O}$	$\text{CO}_2$ gas	$\text{CH}_3\text{OH}$							
HCHO as the major product?	No	Yes	Yes							

further general considerations. C64–C68 systems are described separately hereafter in a chronological order.

The first report of formaldehyde generation dates back to 1989 with the use of the homogeneous Ru-based catalyst C64.<sup>144</sup> The reaction was performed in water at 40 °C with a total gas pressure ( $P_{\text{CO}_2} + P_{\text{H}_2}$ ) of 34 atm. Under these catalytic conditions,  $\text{CO}_2$  hydrogenation led to the generation of  $\text{HCOOH}$  and  $\text{HCHO}$  which then decomposed into  $\text{CO}$  and  $\text{H}_2\text{O}$ . The generation of  $\text{CO}$  was monitored by GC analysis while formation of  $\text{HCOOH}$  and  $\text{HCHO}$  was followed spectrophotometrically upon reaction with Nash's reagent.<sup>149</sup> Kinetic investigation showed that the decrease of  $P_{\text{CO}_2}$  while keeping  $P_{\text{H}_2}$  constant led to a rate increase in  $\text{HCHO}$  formation. The initial rate of formation of formaldehyde was measured at  $2.79 \times 10^{-2} \text{ M h}^{-1}$  using 1 mmol of catalyst loading with an estimated activation energy of 8.3 kcal mol<sup>-1</sup>. The rate of formation of formaldehyde was found to be lower than its rate of decomposition, explaining the lack of formaldehyde build-up within the system. In addition, the rate of formation of formic acid was always higher than that of formaldehyde explaining the favoured selectivity towards formic acid. In 2001, an impregnated Pt/Cu (ratio = 0.03) on  $\text{SiO}_2$  surface (C65) was shown to afford formaldehyde and methanol with a total gas pressure ( $P_{\text{CO}_2} + P_{\text{H}_2}$ ) of 6 atm in the gas phase.<sup>145</sup> The reaction was monitored by temperature programmed surface reaction spectroscopy indicating an optimum temperature of 150 °C for the formation of formaldehyde. While methanol was favoured at a  $P_{\text{H}_2}/P_{\text{CO}_2}$  ratio of 3, the selectivity was reversed when this ratio was increased to 20. At this ratio, the rate of formation reached  $0.12 \text{ g}_{\text{cat}}^{-1} \text{ h}^{-1}$  for methanol and  $5.22 \times 10^{-3} \text{ g}_{\text{cat}}^{-1} \text{ h}^{-1}$  for formaldehyde, respectively. In the absence of Pt, the analogous Cu-based catalyst afforded only methanol. The importance of Pt in the formation of formaldehyde was attributed to the known ability of Pt to adsorb  $\text{H}_2$ . Indeed, the Pt activation of  $\text{H}_2$  along with a higher pressure of  $\text{H}_2$  was proposed to favour a higher concentration of  $\text{H}_2$  in the proximity of the Cu centres, responsible for shifting the product formation from methanol to formaldehyde. These observations suggest that the formation of formaldehyde and methanol follows two distinct competitive pathways and that the accessibility of activated  $\text{H}_2$  is part of the rate determining step for formaldehyde but not for methanol. In 2015, bimetallic Ni–Co nanoparticles (NPs) (C66) were produced in a bottom-up approach and their ability to catalyse  $\text{CO}_2$  hydrogenation was studied.<sup>144</sup> Their catalytic activity was evaluated after deposition of the Ni–Co NPs on a mesoporous silica support and exposition to a  $\text{CO}_2 : \text{H}_2 : \text{He}$  (6.6 : 20.7 : 14.7) gas mixture at a total pressure of 6 atm. At 200 °C, a low conversion of  $\text{CO}_2$  (0.24%) was observed by GC analysis with 30% selectivity for formaldehyde and 70% selectivity for  $\text{CO}$  generated as the major product. Only a trace amount of formaldehyde was detected upon increasing the temperature to 350 °C. Pt–Ni and Pt–Cu (C67) catalysts selectively afforded formaldehyde in methanol medium at 25 °C and a total gas pressure ( $P_{\text{CO}_2} + P_{\text{H}_2}$ ) of 70 atm.<sup>147</sup> The catalysts were prepared by a wet impregnation method using  $\gamma$ -alumina as the support. The final Pt–Ni and Pt–Cu supported catalysts contained 10 wt% Ni or Cu content and 1 wt% Pt content. Once again, a high  $P_{\text{H}_2}/P_{\text{CO}_2}$  ratio (16) led to the generation of formaldehyde with a molar yield of

$0.9 \times 10^{-4}$  M g<sub>cat</sub><sup>-1</sup> in 22 h corresponding to  $0.41 \times 10^{-5}$  M g<sub>cat</sub><sup>-1</sup> h<sup>-1</sup>. This activity is still lower than the one reported with the C65 catalyst ( $5.22 \times 10^{-3}$  M g<sub>cat</sub><sup>-1</sup> h<sup>-1</sup>).

Compound C68 is a heterogeneous catalyst consisting of highly dispersed Ru on layered double hydroxide (LDH). The use of 0.5 wt% Ru was recently shown to catalyse the hydrogenation of CO<sub>2</sub> ( $P_{CO_2} = 10$  atm,  $P_{H_2} = 10$  atm) into 0.446 M g<sub>cat</sub><sup>-1</sup> of formaldehyde in water as the solvent in 12 h, corresponding to 0.037 M g<sub>cat</sub><sup>-1</sup> h<sup>-1</sup>.<sup>148</sup> The detection and quantification of formaldehyde was performed using the colorimetric method with 3-methyl-2-benzothiazolinone hydrazone (MBTH) and high-performance liquid chromatography (HPLC), respectively. In the same study, dihydrogen was replaced by glycerol as a transfer hydrogenation reagent. In a 0.2 M aqueous glycerol solution, catalytic transfer hydrogenation (CTH) of CO<sub>2</sub> afforded formaldehyde in a slightly better yield at 0.1 and 3 wt% Ru under otherwise the same conditions. It is worth mentioning that in the proposed mechanism, initiation of the reaction *via* the dehydrogenation of glycerol into the C<sub>3</sub> carbohydrate dihydroxyacetone (DHA) or glyceraldehyde is proposed. However, the possibility that glycerol – notably *via* the generation of these carbohydrates – could be a source of formaldehyde prior to the CTH of CO<sub>2</sub> was not investigated.<sup>150</sup>

## 5.2. Hydrogenation of CO<sub>2</sub> into acetals

As presented above, the selective 4e<sup>-</sup> hydrogenation of CO<sub>2</sub> into HCHO is still a widely open challenge. In contrast, the selective 4e<sup>-</sup> hydrogenation of CO<sub>2</sub> into acetal was pioneered rather recently in 2016 and 2017 with homogeneous Ru- and Co-based catalytic systems.<sup>151</sup> The formation of an acetal from CO<sub>2</sub> hydrogenation consists in the addition of alcohol to stop at the 4e<sup>-</sup> reduction stage with the formation of acetal species (Scheme 42b). Mechanistic investigations have shown that formaldehyde is never formed during the process which alternates between reduction (hydrogenation) and functionalization (with the alcohol) steps giving rise to the acetal. The interest in the formation of dialkoxymethane derivatives is dual. First, it provides a selective access to formaldehyde since some of them were found to release HCHO in strong acidic media,<sup>153</sup> although to our knowledge, the proof of concept from CO<sub>2</sub> has never been reported. Second, dialkoxymethane derivatives are compounds of interest as fuel additives to lower the formation of soot because of their high oxygen content and the absence of C–C bonds.<sup>151,153</sup> The catalytic performances of the reported systems, the in-depth optimization of the catalytic conditions, the proposed mechanism and the extent of the scope of alcohols employed are presented hereafter.

**5.2.1. Catalytic systems for CO<sub>2</sub> hydrogenation into dimethoxymethane (DMM).** Currently, 10 catalytic systems (C69–C78) have been reported for the hydrogenation of CO<sub>2</sub> in the presence of methanol as the solvent and co-substrate affording dimethoxymethane (DMM). Their structures are depicted in Fig. 5 and the catalytic conditions and performances are reported in Table 6. It must be noted that in all reported studies, the reactions were monitored by <sup>1</sup>H and <sup>13</sup>C NMR spectroscopy and the products characterized and quantified *in situ*.

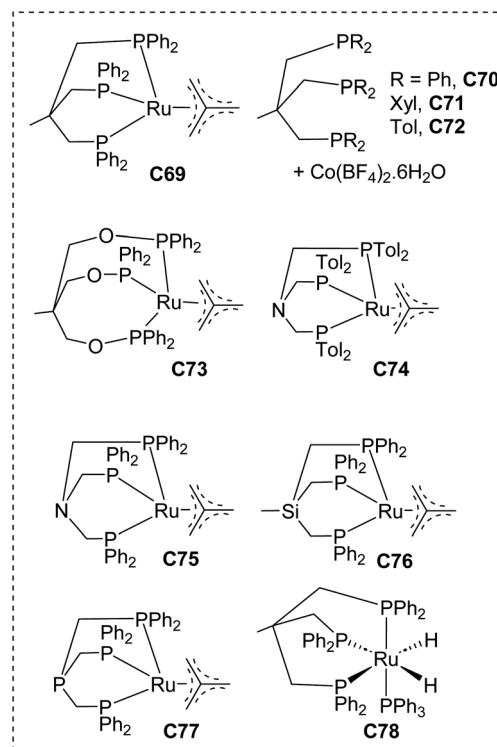


Fig. 5 Catalytic systems C69–C78 leading to the hydrogenation of CO<sub>2</sub> into DMM.

The characteristic methylene signal of DMM was observed at 4.39 ppm in the <sup>1</sup>H NMR analysis in CD<sub>3</sub>OD. With the Ru-based precatalyst C69 featuring a triphosphine ligand (Scheme 44) and a Lewis acid co-catalyst (Al(OTf)<sub>3</sub>), the hydrogenation of CO<sub>2</sub> in methanol was shown to afford the 2e<sup>-</sup> reduction product methoxyformate (MF) and the 4e<sup>-</sup> reduction product dimethoxymethane (DMM) (Scheme 5).<sup>151a</sup> Among the different conditions tested (variation of the Ru-based precatalyst, temperature, pressure, nature of the acid and time), the best TON of 214 was found with C69 under the following conditions:  $P_{CO_2} = 20$  atm,  $P_{H_2} = 60$  atm, 18 h, 80 °C, 2 mL of CH<sub>3</sub>OH, 12.5 µmol of Ru-based precatalyst and 25 µmol of Al(OTf)<sub>3</sub> (Table 6, entry 1). The selectivity toward DMM *vs.* MF was 67%. Following this initial report, catalytic systems C70–C78 were investigated in the same reaction (Fig. 5).

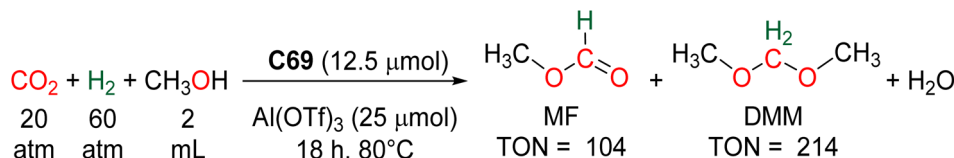
Pre-catalysts C70–C72 are Co-based in contrast to all the other catalysts which are Ru-based.<sup>151b</sup> C70–C72 were found to generate DMM with slightly lower TON of 92 to 157 than C69 (Table 6, entries 2–4 *vs.* entry 1, resp.), with an interesting maximal selectivity of 81% for DMM. Better TONs were observed by replacing Al(OTf)<sub>3</sub> with HN(Tf)<sub>2</sub> as the acid, longer reaction time (22 h) and a higher temperature (100 °C). The impact of the triphosphine ligand was also probed. The use of triphosphine ligands featuring P(Xyl)<sub>2</sub> and P(Tol)<sub>2</sub> moieties increased the TON to 120 and 157 for C71 and C72, respectively. Optimization of the Ru-based system was further explored in detail by another group.<sup>154–156</sup> C73–C75 were tested in a first study.<sup>154</sup> While the phosphinite moieties in C73 gave lower TONs than the other reported catalytic systems (Table 6, entry 5), replacement of the



Table 6 Catalytic conditions and performances of C69–78

Entry	Cat, <i>n</i> (μmol)	Acid, <i>n</i> (μmol)	<i>P</i> <sub>H<sub>2</sub></sub> (atm)	<i>P</i> <sub>CO<sub>2</sub></sub> (atm)	<i>V</i> <sub>CH<sub>3</sub>OH</sub> (mL)	Time (h)	<i>T</i> (°C)	TON	TOF (h <sup>-1</sup> )	Sel <sup>a</sup> (%)	Ref.
1	C69, 12.5	Al(OTf) <sub>3</sub> , 25	60	20	2	18	80	214	12	67	151
2	C70, 15	HN(Tf) <sub>2</sub> , 45	60	20	2	22	100	92	4	74	151b
3	C71, 15	HN(Tf) <sub>2</sub> , 45	60	20	2	22	100	120	5	79	151b
4	C72, 15	HN(Tf) <sub>2</sub> , 45	60	20	2	22	100	157	7	81	151b
5	C73, 1.5	Al(OTf) <sub>3</sub> , 6.25	60	20	0.5	18	80	32	2	28	154
6	C74, 1.5	Al(OTf) <sub>3</sub> , 6.25	60	20	0.5	18	80	221	12	71	154
7	C75, 1.5	Al(OTf) <sub>3</sub> , 6.25	60	20	0.5	18	80	292	16	72	154
8	C75, 1.5	Al(OTf) <sub>3</sub> , 6.25	90	5	0.5	18	90	97	5	92	154
9	C75, 0.38	Al(OTf) <sub>3</sub> , 1.56	90	20	0.5	18	90	786	44	60	154
10	C75, 0.075	Al(OTf) <sub>3</sub> , 3.576	105	12.5	0.55	21	105	2761	131	61	155
11	C75, 0.75	Al(OTf) <sub>3</sub> , 35.76	100	15	0.5	20	100	3874	194	73	155
12	C76, 0.38	Al(OTf) <sub>3</sub> , 3.13	90	20	0.5	18	90	685	38	60	156
13	C77, 0.38	Al(OTf) <sub>3</sub> , 3.13	90	20	0.5	18	90	439	24	46	156
14	C78, 3.1	Al(OTf) <sub>3</sub> , 25	20	100	5	20	100	1176	59	70	157

<sup>a</sup> Selectivity = TON(DMM)/[TON(MF) + TON(DMM)].



Scheme 44 DMM synthesis with C69.

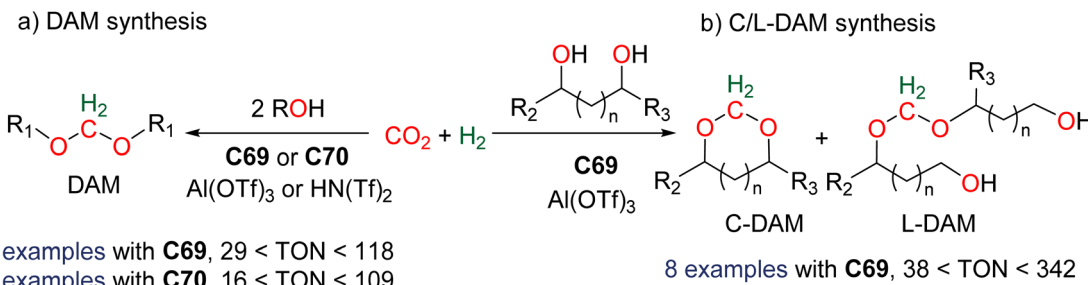
central C atom of the backbone of the ligand by a N atom in C74 and C75 enabled slight increase of the TON to 221 and 292, respectively (Table 6, entries 6 and 7). With C75, the optimization conditions led to a net increase of either the selectivity for DMM to 92% but with a TON of 97 (Table 6, entry 8) or of the TON to 786 but with a selectivity for DMM reduced to 60% (Table 6, entry 9). The quantities of the catalyst and co-catalyst were shown to be the main factor enabling this TON increase. In this optimization study for C75, all possible parameters were carefully optimized individually (univariate optimization) to improve the TON from 214 to 786 (Table 6, entries 1 and 9, resp.) which represents a 367% increase in TON. A subsequent study using a multivariate optimization led to a larger improvement of TON. The pre-catalyst C75 indeed provided TONs of 2761 and 3874 with a 10 fold increase of the scale of the reaction leading to the formation of 2.88 mmol of DMM (Table 6, entries 10 and 11, resp.).<sup>155</sup> This corresponds to a significant improvement of further 493% from the univariate optimization (Table 6, entry 9). These impressive results were made possible mainly by acting on the quantities of the catalyst and co-catalyst. In another report, the replacement of the heteroelement of the backbone by Si or P atoms (C76 and C77, respectively) did not enable any further increase of the catalytic performances or selectivity (Table 6, entries 12 and 13).<sup>156</sup> In order to have a closer look at the active catalyst, dihydride compound C78 was synthesized and tested (Table 6, entry 14).<sup>157</sup> Pre-catalysts C69–77 are indeed sought to generate M–H species which act as the active catalyst in the reaction. This study showed the beneficial aspect of adding tertiary phosphine or phosphite in order to prevent catalyst deactivation by the

formation of a carbonyl ligand from the CO<sub>2</sub> decarbonylation. Overall, optimization strategies presented with catalysts C69–C78 were dedicated to the improvement of TON as the most important parameter. Although interesting selectivities of DMM vs. MM were obtained, the lesser attention to this parameter can be explained by the possibility of hydrogenating MF into DMM in a second step.<sup>154,156</sup> However, the TOF parameter was not optimized. As indicated in Table 6, it ranges between 2 and 194 h<sup>-1</sup>, leaving room for improvement in these systems.

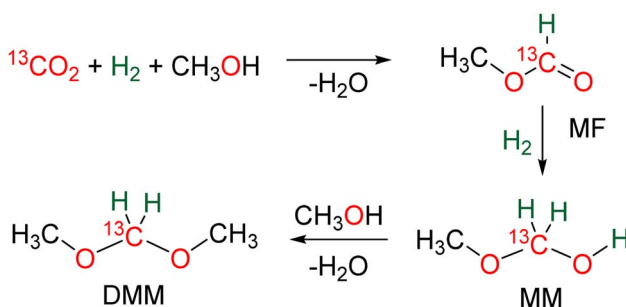
**5.2.2. Extension to other dialkoxymethanes (DAMs).** Other alcohols beside methanol were tested to generate dialkoxy-methane (DAM) compounds. Using C69<sup>151a</sup> and C70 (Fig. 5),<sup>151b</sup> 11 examples were obtained and characterized with TON ranging from 16 to 118 (Scheme 45a). Aliphatic alcohols used included linear chain (containing 2 to 10 carbon atoms), branched (<sup>2</sup>BuOH and <sup>2</sup>iPrOH) and benzyl alcohol. In a subsequent study, the authors used bio-sourced diols to increase the sustainability of the process and the product scope.<sup>158</sup> These diols were shown to afford either a cyclic acetal (C-DAM) or a linear acetal (L-DAM) (Scheme 45b). In total, eight products were characterized and selectivity toward either C-DAM or L-DAM was reached depending on the nature of the diol substrate (*n* = 1–6). A selectivity of 92% was notably observed toward the formation of the C-DAM, 4-methyl-1,3-dioxane, while reversed selectivity of 99% to L-DAM was obtained with the diol featuring a 5-carbon linker.

**5.2.3. Mechanism.** In the initial description of the formation of DMM from CO<sub>2</sub>, the intermediary of methoxymethanol (MM) and methoxymethanol (MM) was demonstrated





Scheme 45 Synthesis of (a) linear DAM with C69 or C70 and (b) cyclic or linear C-DAM or L-DAM, respectively, with C69.



Scheme 46 Proposed mechanism for the formation of DMM.

(Scheme 46).<sup>151a</sup> MF and MM were indeed observed during the reaction and the expected  $^{13}\text{C}$ -labelled products and intermediates were characterized when starting from  $^{13}\text{CO}_2$  and  $^{12}\text{CH}_3\text{OH}$  reactants. In this reaction mechanism, formaldehyde was not an intermediate. One methanol molecule was indeed involved in the first reduction step leading to MF. Compared to formic acid, the methylated analogue MF was hypothesized to “activate” this reduction stage enabling further hydrogenation into MM under rather mild conditions compared to the  $\text{CO}_2$  hydrogenation reaction to methanol in the absence of alcohol. It is reminiscent of pioneering strategies using alcohol<sup>159</sup> or amine<sup>20b,160</sup> to promote the hydrogenation of  $\text{CO}_2$  into methanol under mild conditions in cascade reactions. One additional molecule of methanol is finally reacted with the MM intermediate affording DMM.

Two recent in-depth studies published concomitantly in 2021 proved to be particularly complementary since one is an experimental investigation of the most used  $\text{C75}/\text{Al}(\text{OTf})_3$  catalytic system,<sup>161</sup> while the other is a DFT investigation on the Co-based  $\text{C70}/\text{HN}(\text{Tf})_2$  system.<sup>153b</sup> It is noteworthy that these studies confirmed the elementary steps proposed initially in 2016. The  $\text{C75}/\text{Al}(\text{OTf})_3$  catalytic system was investigated by *in situ* infrared (IR) spectroscopy at three relevant temperatures: 333 K, 353 K and 373 K enabling the determination of rate constants and activation parameters for the three steps:  $\text{CO}_2$  to MF, MF to MM and MM to DMM.<sup>161</sup> These key steps were included in a reaction network analysis. The rate determining step (rds) was shown to be the first  $\text{CO}_2$  to MF step with an activation parameters  $\Delta G^\#$  (333 K) of  $119.0 \text{ kJ mol}^{-1}$  and the lowest rate constant of  $1.41 \times 10^{-6} \text{ s}^{-1} \text{ M}^{-2}$  at the same temperature. In accord with the experiment, the competitive

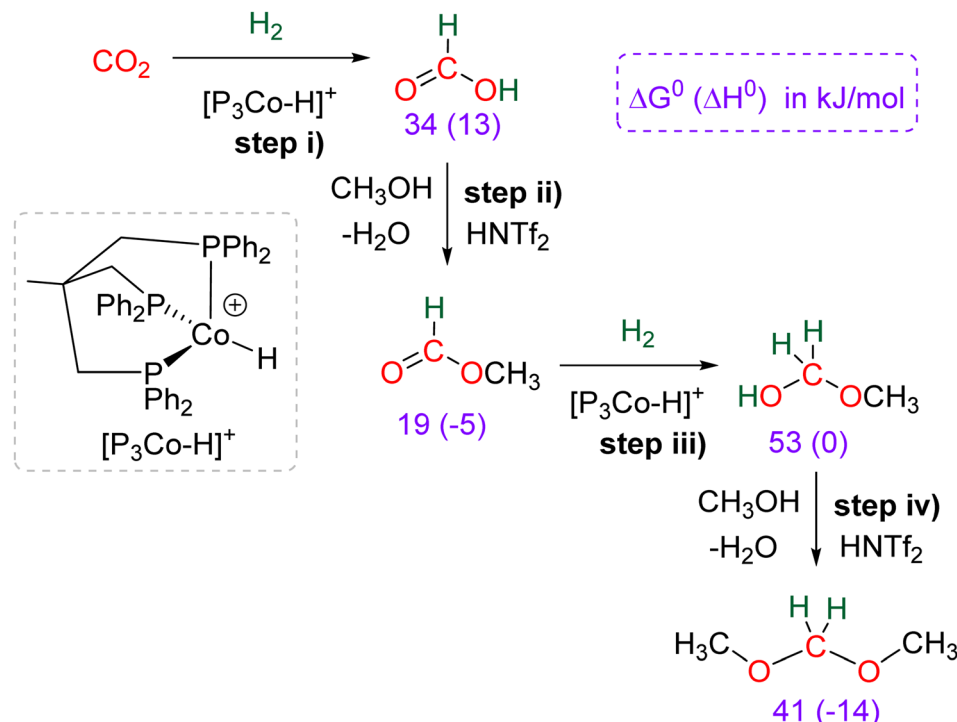
formation of  $\text{CH}_3\text{OH}$  from the hydrogenation of MM was shown to be accessible at higher temperature and the formation of DMM was favoured by the large excess of  $\text{CH}_3\text{OH}$  used as the solvent. Furthermore, this reaction network analysis was also used as a predictive tool to propose new experimental conditions that would favour one product over the other. The positive effect of  $\text{H}_2\text{O}$  removal on the formation of DMM was notably proposed.

The DFT study of the  $\text{C70}/\text{HN}(\text{Tf})_2$  system proposed a detailed kinetic and thermodynamic analysis of each elementary step accounting for the formation of DMM but also for the over-reduction to  $\text{CH}_3\text{OH}$ .<sup>153b</sup> The thermodynamic values  $\Delta G^0$  for the subsequent formation of formic acid, MF, MM and DMM, indicated in Scheme 47, have been calculated to be 34, 19, 53 and  $41 \text{ kJ mol}^{-1}$ , respectively. A major input of this study was to define the exact role of the TM-based catalyst and the acid co-catalyst. The active Co-based species were calculated to be the monohydride cationic Co complex ( $[\text{P}_3\text{Co}-\text{H}]^+$ ) depicted in Scheme 47 (purple box) and was calculated to be the catalyst responsible for the hydrogenation of  $\text{CO}_2$  into formic acid and of MF into MM. The two steps (i) and (iii) have been calculated with  $\Delta G^\#$  of 79 and  $98 \text{ kJ mol}^{-1}$ , respectively. On the other hand, the esterification of formic acid into MM (step ii) and the etherification of MM into DMM (step iv) are catalysed by the acid catalyst  $\text{HN}(\text{Tf})_2$ . It was found that the methylating agent responsible for the etherification of MM to DMM was not directly methanol, but  $\text{CH}_3\text{O-NTf}_2$  *in situ* generated from the reaction of  $\text{CH}_3\text{OH}$  with  $\text{HN}(\text{Tf})_2$ . Nonetheless, the calculated Gibbs free energy barrier from the most stable Co-formate species is  $179 \text{ kJ mol}^{-1}$  for the last step (iv), making it the rate determining step (rds) of the whole process. As in the previous study, the access to DMM via formaldehyde was calculated to be higher in energy and thus discarded. The formation of formaldehyde as an intermediate to DMM was proposed in a related Ru-based system using ethanol instead of methanol, but not with the same level of kinetic or thermodynamic investigations.<sup>162</sup>

### 5.3. Conclusion

In conclusion, the selective  $4\text{e}^-$  reduction of  $\text{CO}_2$  by hydrogenation stands out for several reasons: (i) the development of highly active catalytic systems resulting in the reduction of  $\text{CO}_2$  into acetals, achieving the highest reported turnover number (TON) of 3874 for this reduction stage, following extensive





Scheme 47 Mechanism of formation of DMM based on calculations.

optimization studies; (ii) the synthesis of acetals, which are of interest as fuel additives, in contrast to bis(silyl)acetal (BSA) and bis(boryl)acetal (BBA) compounds that lack known applications. Consequently, a variety of DAM derivatives have been synthesized, utilizing various alcohols, particularly those derived from biomass.

As perspectives, future endeavours could focus on broadening the applicability of DAM, encouraging additional investigations into acetal syntheses *via* CO<sub>2</sub> hydrogenation, and exploring diverse catalytic processes beyond [P<sub>3</sub>Ru] and [P<sub>3</sub>Co] systems.<sup>163</sup> It would be intriguing to explore the potential use of the generated acetal as both C<sub>1</sub> and C<sub>n</sub> sources, similar to what has been described with BSA and BBA. However, the hydrogenation of CO<sub>2</sub> into formaldehyde is still in its early stages, with only three selective systems described so far, operating in gas or liquid phases, involving catalysts C65, C67, and C68. Moreover, no isolation or utilization of the generated formaldehyde has been reported to date. Given its perfect atom efficiency and the reactive nature of formaldehyde, the primary challenge lies in developing an efficient system for hydrogenating CO<sub>2</sub> into formaldehyde, enabling its isolation and/or utilization.

Finally, although the processes of 4e<sup>-</sup> reduction of CO<sub>2</sub> into formaldehyde and into acetal are at very different stages of maturity, it is noteworthy that the stabilization of the 4e<sup>-</sup> reduction stage in the form of acetal parallels the stabilization of monomeric formaldehyde (HCHO) in the form of acetals of various lengths in formalin solution – the common commercial source of formaldehyde for chemical or biochemical transformations.<sup>24–26,128a–130,132,164</sup> It is indeed noticeable that the two examples described in liquid medium for the

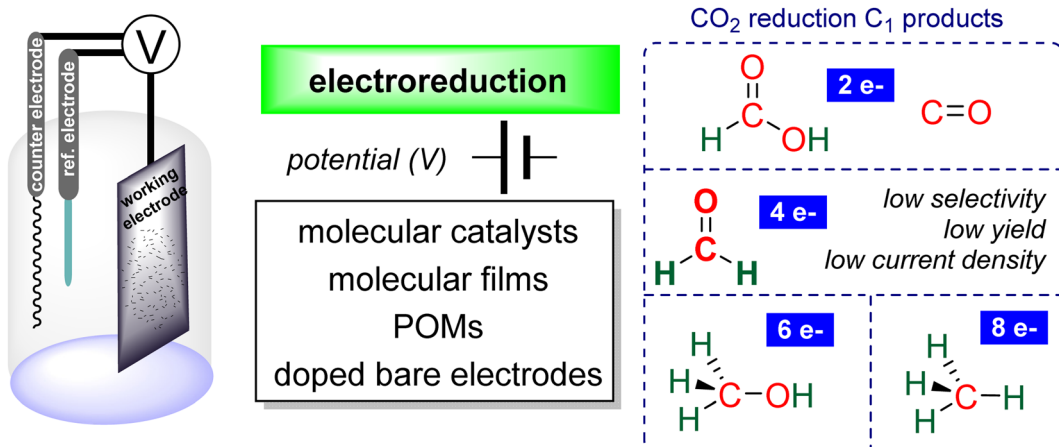
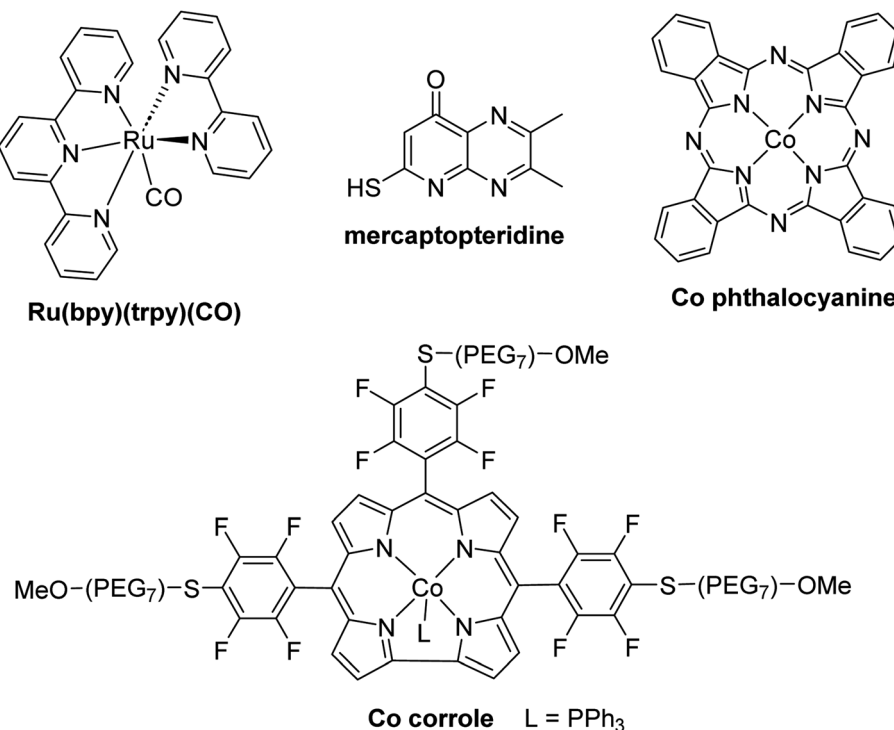
hydrogenation of CO<sub>2</sub> with C64 and C67 were conducted in H<sub>2</sub>O, CH<sub>3</sub>OH or glycerol. Presumably, these solvents stabilize the reactive *in situ* generated monomeric formaldehyde in the form of methanediol or acetal derivatives while avoiding its polymerization as paraformaldehyde.

## 6. Electroreduction

Electrochemical CO<sub>2</sub> reduction reaction (eCO<sub>2</sub>RR) offers a green and sustainable approach for converting this gas into various products, under mild conditions (room temperature and pressure) and both in organic or aqueous media. Regarding C<sub>1</sub> products, while the formation of 2e<sup>-</sup> reduction products has been performed with several catalysts with high selectivity and rate,<sup>10a</sup> the formation of 4, 6 and 8e<sup>-</sup> reduction products has been much more rarely observed (Scheme 48).<sup>165</sup> If methanol and methane have been produced in a few cases, formaldehyde remains an elusive product to date.

### 6.1. Electrocatalytic systems

One of the early examples of CO<sub>2</sub> electrochemical reduction to formaldehyde concerned the use of a Ru based complex with a terpyridine-bipyridine ligand (Fig. 6) which was shown to produce a small amount of HCHO, through the formation of a formyl complex, in a mixture of water and ethanol, at low temperature (−20 °C) upon electrolysis at an Hg pool working electrode ( $E = -1.70$  V vs. Ag/AgCl).<sup>166</sup> A faradaic efficiency (FE) of *ca.* 5% was obtained for HCHO, while methanol and remarkably C–C coupling products were also identified (H(O)CCOOH, HOCH<sub>2</sub>COOH). Unexpectedly, a metal-free organic

Scheme 48 Electrochemical reduction of  $\text{CO}_2$  into  $\text{C}_1$  products.Fig. 6 Examples of molecular catalysts capable of generating formaldehyde from  $\text{CO}_2$  electroreduction.

catalyst, 6,7-dimethyl-4-hydroxy-2-mercaptopteridine (a natural cofactor, Fig. 6) was reported to electrocatalyze  $\text{CO}_2$  reduction to various products, including not only formate, but also methanol and formaldehyde (not quantified).<sup>167</sup> The reaction was conducted in a phosphate buffered solution at a reticulated vitreous carbon electrode ( $E = -0.65$  V vs. Ag/AgCl), and it was suggested that  $\text{CO}_2$  was first reduced to formate, which was subsequently reduced to formaldehyde and methanol (the latter product was obtained with FE 10–23%) *via* a carbamate compound. Recently, a transition metal based polyoxometalate (TOA)<sub>6</sub>[a-SiW<sub>11</sub>O<sub>39</sub>–Co<sub>(1)</sub>] (TOA: tetraoctyl ammonium, 1 = vacant position at the Co atom) was shown to electroreduce  $\text{CO}_2$  under homogeneous

conditions in dichloromethane as the solvent, and a potential of  $-1.5$  V vs.  $\text{Hg}_2\text{Cl}_2/\text{Hg}$  at a Hg electrode.<sup>168</sup> In the presence of an acid as a co-reactant (water and  $\text{H}_2\text{SO}_4$ ), the products were identified as CO, with about 13% FE, and formaldehyde with a maximum efficiency (FE) of *ca.* 25%. The use of an organic and reducible solvent (which is shown to generate HCHO under an Ar atmosphere), limits the development of the process but this example is an interesting case of molecular electrochemical approach for  $\text{CO}_2$ -to-HCHO conversion. Another molecular cobalt complex, a Co corrole (triphenylphosphine 5,10,15-tris(2,3,5,6-tetrafluoro-4-(MeO-PEG(7)thiophenyl)), Fig. 6) modified at the para positions with thiol bound poly(ethylene

glycol) chains terminated by methoxy groups was adsorbed at the carbon paper electrode and then investigated for the eCO<sub>2</sub>RR into methanol and ethanol.<sup>169</sup> In 0.1 M phosphate buffer solutions with 0.1 M NaClO<sub>4</sub> at potentials ranging from  $-0.51$  V to  $-0.8$  V vs. NHE, low formaldehyde efficiencies from 10 to 1%, respectively, were obtained among other liquid phase products (formate, acetate, glyoxal), corresponding to low current densities (from 0.2 to 0.02 mA cm<sup>-2</sup> respectively).

Another strategy was developed upon polymerizing electrode films of metal complexes at the surface of conductive carbon. Cr, Co and Fe bis-terpyridine complexes bearing the vinyl group were used to grow electroactive films upon oxidation, which were further employed as catalysts in aqueous solutions with 0.1 M NaClO<sub>4</sub>.<sup>170</sup> At potentials close to  $-1.1$  V vs. Ag/AgCl, faradaic yields of 28% (Fe), 39% (Co) and 87% (Cr) were reported for formaldehyde, thus showing very high activity for first row transition metals while second and third row transition metals (Ru and Os respectively) gave barely any reactivity, which was assigned to the presence of metal-based redox processes in the former cases compared to ligand-based redox processes in the latter. The CO<sub>2</sub> to CO conversion being now a well-controlled reaction, and CO being a possible intermediate towards formaldehyde production, a parallel approach was developed using CO directly as the reactant and supramolecular catalysts: thin films of Co phthalocyanine and 4,4',4'',4'''-tetracarboxyphthalocyanine made at the carbon fibre were investigated and shown to produce mainly formaldehyde as the CO reduction product with very little methanol, at a potential of  $-0.7$  V vs. SCE (Saturated Calomel Electrode) in sulfuric acid solutions.<sup>171</sup> Recently, it was further shown that CO reduction with a phthalocyanine monomer complex also led to formaldehyde with unambiguous confirmation from labelled studies.<sup>172</sup> These results opened the door to understanding the mechanism of formaldehyde pathway from both CO<sub>2</sub> and CO as reactants, with possibilities of tuning the quantity of formaldehyde being produced and the ratio between HCHO and methanol. It also opens the possibility of setting a cascade approach in which the CO produced from CO<sub>2</sub> reduction could further be used to generate HCHO. A very recent study explored such electro-reduction of CO to HCHO with Co phthalocyanine deposited at a carbon paper electrode. Upon optimization of the pH (12) and of the electrode potential, a partial current density of 0.64 mA cm<sup>-2</sup> (17.5% faradaic efficiency) was achieved for HCHO, with a maximum ratio between HCHO and CH<sub>3</sub>OH of *ca.* 7.5. Mechanistic insights illustrate that the binding of CO to the metal cobalt site is strong enough for further reducing it, while controlling the amount of protons and the electrode potential is key to favouring formaldehyde formation and release at the expense of methanol production.<sup>173</sup> A puzzling discovery was made upon direct electroreduction of CO<sub>2</sub> in various solutions (methanol, water and even sea water) at boron doped diamond (BDD) electrodes without any additional catalyst.<sup>174</sup> These materials have several advantages, including a large potential window, high stability and furthermore the presence of sp<sup>3</sup>-bonded carbon atoms on BDD which are believed to be active sites for triggering chemical transformations. Upon 1 h electrolysis at  $E = -1.7$  V vs. Ag/AgCl, a maximum yield (FE) of 74%

was obtained for formaldehyde, along with formic acid and a very small amount of dihydrogen as a by-product. The formaldehyde was deemed to be formed from the 2e<sup>-</sup> reduction of formic acid initially obtained from CO<sub>2</sub> conversion, while current densities were low, typically in the range of 0.1 to 0.2 mA cm<sup>-2</sup>. Finally, an elegant indirect approach has been proposed with methanol as the solvent. While methanol itself was oxidized to formaldehyde in the anodic compartment, electroreduction of CO<sub>2</sub> at the Sn electrode led to formic acid, which reacted with the solvent to give methyl formate. Finally, the latter was reduced to formaldehyde, with faradaic efficiencies for HCHO from 10 to 50% depending on the electrolyte conditions.<sup>175</sup>

## 6.2. Conclusion and perspectives

In conclusion, the electrochemical reduction of CO<sub>2</sub> to formaldehyde poses a formidable challenge, with only a limited number of examples identified thus far. These cases exhibit low yields, low current density, and, in many instances, uncertainties regarding the origin of the produced formaldehyde. The challenge of obtaining formaldehyde also arises from its susceptibility to further transformation at the electrode into more reduced products, such as methanol. Additionally, the precise catalytic mechanisms involved in these processes remain elusive with only very few mechanistic studies.<sup>173</sup>

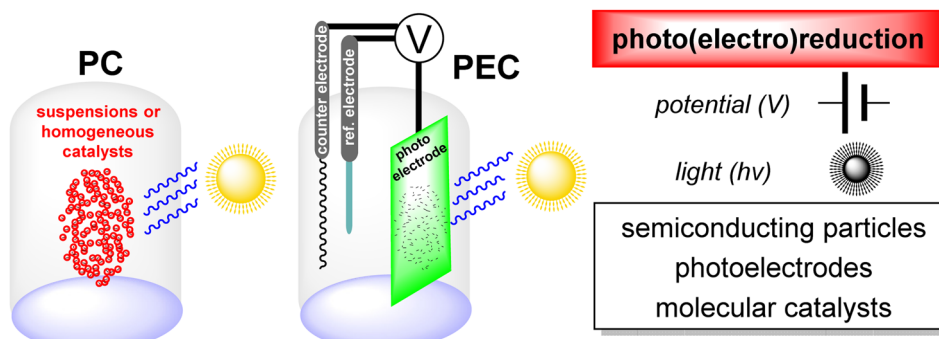
As perspectives, the prospect of *in situ* generating a substantial quantity of formaldehyde under mild conditions across a range of precisely controlled potentials is enticing. This potential development could pave the way for utilizing formaldehyde in subsequent chemical reactions, particularly in coupling reactions. As an early illustrative example, co-reduction scenarios involving CO<sub>2</sub> (or CO) with nitrogen-containing species like nitrite (NO<sub>2</sub><sup>-</sup>)<sup>176</sup> or nitrate (NO<sub>3</sub><sup>-</sup>)<sup>176b,177</sup> could facilitate C–N bond formation, yielding a diverse array of products, including amines and urea. The exploration of these processes, along with related ones, under the controlled conditions afforded by electrochemistry is poised to yield new and stimulating results.

## 7. Photo(electro)reduction

The photochemical (PC) and photoelectrochemical (PEC) reduction of CO<sub>2</sub> (Scheme 49), mostly using semiconducting materials, have been extensively studied in the last four decades.<sup>178</sup> However, if compared to other reduction products such as CO or formate, only a limited number of studies so far reported the formation of formaldehyde as a major product and even less studies report a selective HCHO production, mainly because of its high reactivity.<sup>179</sup> Moreover, very few of these studies conducted proper isotope labelled measurements to confirm the origin of the carbon atom, which constitutes a severe drawback.<sup>180</sup>

A very early report questioned the possible formation of formaldehyde from water and CO<sub>2</sub> as the first stage of the photosynthetic process forming carbohydrates.<sup>181</sup> This study showed that an aqueous solution, free of catalyst, containing carbon dioxide gives formaldehyde when irradiated with



Scheme 49 Photochemical and photoelectrochemical reduction of  $\text{CO}_2$ .

UV-light ( $\lambda = 200$  nm) in a first stage, and that subsequent irradiation with lower energy light ( $\lambda = 290$  nm) induced the polymerization of HCHO to sugars. It also showed that the formation of HCHO can be photocatalyzed under visible light through the use of “coloured basic substances” such as malachite-green or methyl-orange. Remarkably, the role of HCHO in the course of the photochemically induced formation of highly reduced compounds from  $\text{CO}_2$  was thus already questioned a century ago. Later, a pioneer work reported that using suspensions of various semiconductors ( $\text{TiO}_2$ ,  $\text{ZnO}$ ,  $\text{CdS}$ ,  $\text{GaP}$  and  $\text{SiC}$ , Table 7, entries 1–5) in  $\text{CO}_2$ -saturated purified water, the generation of formic acid, formaldehyde and methanol was observed up to the millimolar concentration range after 7 h of visible light illumination (500 W Xe or Hg lamp).<sup>182</sup> Trace of methane was also detected. The reduction products were quantified by gas chromatography although no labelled experiment was conducted to assert the origin of the products. The yield in methanol was observed to increase as the conduction band (CB) of the material was more negative compared to the reduction potential of the  $\text{CO}_2$ -to- $\text{CH}_3\text{OH}$  reaction. A quantum yield of  $ca.$   $5 \times 10^{-4}$  was reported for the formaldehyde production with both  $\text{TiO}_2$  and  $\text{SiC}$  photo-catalysts. Using semiconductor electrodes polarized at  $-1.5$  V vs. SCE,  $\text{CO}_2$  reduction to formic acid, formaldehyde and methanol was also observed with non-illuminated  $\text{TiO}_2$  and illuminated  $\text{GaP}$ . Since this seminal paper, the majority of studies published so far have explored various semiconductors,<sup>198</sup> based on metal and metal oxides, doped or not, eventually in combination with co-catalysts,<sup>3c,199</sup> in the form of suspensions, bulk materials or thin films. Some other examples, albeit quite rare, employed either a fully molecular, a heterogeneous material or even a photo-enzymatic approach.

### 7.1. Suspension of a semiconductor

Aqueous suspensions of semiconducting  $\text{SiTiO}_3$ ,  $\text{WO}_3$  and  $\text{TiO}_2$  under both Hg lamp or natural sunlight were reported to generate a mixture of methanol (a few  $\mu\text{mol}$  per hour) and formaldehyde (a few tens of  $\mu\text{mol}$  per hour) from dissolved carbon dioxide, as quantified by gas chromatography ( $\text{CH}_3\text{OH}$ ) and colorimetric (HCHO) measurements (Table 7, entries 6–8).<sup>183</sup> Traces of methane were also detected. In a follow-up study,<sup>184</sup> aqueous suspensions of strontium titanate ( $\text{SrTiO}_3$ )

treated with various transition metal- $\text{TiO}_2$  deposits, namely Rh, Pt, In and Au, and saturated with  $\text{CO}_2$  were irradiated with a 75 W Hg-lamp or a solar concentrator. When using Ir oxide as an additive (4.55 mol%), formic acid was the main product with a rate of  $ca.$   $1 \mu\text{mol h}^{-1}$ . With Ru oxide (4.55 mol%) as the additive, methanol was the main product. The highest rate for formaldehyde formation was obtained with  $\text{SrTiO}_3$  with 0.5 mole % of lanthanum chromite ( $\text{LaCrO}_3$ ) as an additive (Table 7, entry 9). However, the change in selectivity with the nature of the additive was not discussed. Aqueous suspensions of n-type semiconductors such as bismuth ( $\text{Bi}_2\text{S}_3$ ) and cadmium ( $\text{CdS}$ ) sulphides were reported to generate formic acid and formaldehyde at  $ca.$   $10^{-5}$  M concentration after 1 h under wide spectrum irradiation ( $55 \text{ mW cm}^{-2}$ ) when  $\text{H}_2\text{S}$  was present in the system (Table 7, entries 10 and 11).<sup>185</sup> This was explained by a sequential process producing first formic acid by  $2\text{e}^-/2\text{H}^+$  transfers then formaldehyde by additional electron transfers. The catalysis, which was shown to be proportional to the light intensity, stopped due to the poisoning deposition of elemental sulphur at the surface of the particles. The formation of HCHO as the only  $\text{CO}_2$  reduction product was also observed at a rate up to  $0.25 \mu\text{mol h}^{-1}$  with a  $\text{CO}_2$  saturated aqueous suspension of  $\text{TiO}_2$  at 333 K under 500 W high pressure Xe lamp irradiation (Table 7, entry 12), but the origin of such selectivity is unknown.<sup>186</sup>  $\text{TiO}_2$  doping with 0.1 mol%  $\text{WO}_3$  further increased this rate up to  $0.42 \mu\text{mol h}^{-1}$  (Table 7, entries 13 and 14). The deposition of Rh on  $\text{TiO}_2$  led to the formation of  $\text{HCOOH}$  (major),  $\text{CH}_3\text{OH}$  (secondary) and HCHO (minor) up to a total rate of  $0.67 \mu\text{mol h}^{-1}$  (Table 7, entry 15). The doping of  $\text{TiO}_2$  with Au was more thoroughly studied. At 7 bars and  $80^\circ\text{C}$ , a reactor containing 0.6 g of 0.1–0.5 wt% loading of Au/ $\text{TiO}_2$  composites led to the highest yield of formaldehyde ( $270 \text{ mmol kg}_{\text{cat}}^{-1} \text{ h}^{-1}$ , Table 7, entry 16).<sup>187</sup> Another study reported the use of a gold nanoparticle decorated  $\text{TiO}_2$  photonic crystal as the photocatalyst (Au-PMTNTs).<sup>188</sup> When irradiated with an AM1.5 G source, methane was the main reduction product ( $302 \mu\text{mol g}_{\text{cat}}^{-1} \text{ h}^{-1}$ , 89.3% selectivity), whereas, under the irradiation of a UV-poor white lamp, formaldehyde ( $420 \mu\text{mol g}_{\text{cat}}^{-1} \text{ h}^{-1}$ ) and CO ( $323 \mu\text{mol g}_{\text{cat}}^{-1} \text{ h}^{-1}$ ) were the major products (Table 7, entry 17). This so-called optical control of selectivity was explained by the plasmonic effects of the gold surface involving hot electrons but no discussion was made on the hydrogen atom source.



Table 7 Catalytic performance of photochemical and photoelectrochemical systems for  $\text{CO}_2$  reduction to formaldehyde<sup>a</sup>

Suspensions		Entry	Catalyst	Loading	Conditions	Light source	Products	Yield ( $\mu\text{mol h}^{-1} \text{g}_{\text{cat}}^{-1}$ )	Ref.
Entry	Suspensions								
1	TiO <sub>2</sub>	1		1 g/100 mL	Water	500 W Xe or h.p. Hg arc lamp	HCOOH CH <sub>3</sub> OH	n.d. 3.3	182
2	ZnO	2		1 g/100 mL	Water	500 W Xe or h.p. Hg arc lamp	HCOOH CH <sub>3</sub> OH	15.7 n.d.	182
3	CdS	3		1 g/100 mL	Water	500 W Xe or h.p. Hg arc lamp	HCOOH CH <sub>3</sub> OH	5 17.1	182
4	Gap	4		1 g/100 mL	Water	500 W Xe or h.p. Hg arc lamp	HCOOH CH <sub>3</sub> OH	28.6 n.d.	182
5	SiC	5		1 g/100 mL	Water	500 W Xe or h.p. Hg arc lamp	HCOOH CH <sub>3</sub> OH	15.7 13.3	182
6	SrTiO <sub>3</sub>	4-10	$\text{g L}^{-1}$		Water 67 °C	70 W h.p. Hg lamp (>300 nm)	CH <sub>3</sub> OH	1.79 0.01	183
7	WO <sub>3</sub>	4-10	$\text{g L}^{-1}$		Water 67 °C	70 W h.p. Hg lamp (>300 nm)	CH <sub>3</sub> OH	1.26 0.05	183
8	TiO <sub>2</sub>	4-10	$\text{g L}^{-1}$		Water 34 °C	70 W h.p. Hg lamp (>300 nm)	CH <sub>3</sub> OH	0.51 0.08	183
9	SrTiO <sub>3</sub> + 0.5 mole % LaCrO <sub>3</sub>	1	g/160 mL		Water 60 °C	70 W h.p. Hg lamp CH <sub>3</sub> OH	HCOOH	0.98 0.065	184
10	CdS	0.33	$\text{g L}^{-1}$		Water H <sub>2</sub> S 0.097 M	100 W quartz-iodine lamp (>350 nm)	HCOOH HCHO	0.042 1.22	185
11	Bi <sub>2</sub> S <sub>3</sub>	0.5	$\text{g L}^{-1}$		Water H <sub>2</sub> S 0.097 M	100 W quartz-iodine lamp (>350 nm)	HCOOH HCHO	1.95 1.0	185
12	TiO <sub>2</sub> (MCB)	0.3	g		Water 60 °C	500 W h.p. Xe lamp	HCOOH HCHO	1.58 0.94	186
13	TiO <sub>2</sub> + 0.1 mole % WO <sub>3</sub>	0.3	g		Water 60 °C	500 W h.p. Xe lamp	HCHO	1.98 1.18	186
14	TiO <sub>2</sub> + 2 mole % WO <sub>3</sub>	0.3	g		Water 60 °C	500 W h.p. Xe lamp	HCOOH CH <sub>3</sub> OH	1.4 0.53	186
15	1 mole % Rh/TiO <sub>2</sub>	0.3	g		Water 60 °C	500 W h.p. Xe lamp	HCOOH HCHO	0.69 0.37	186
16	0.1 wt% Au/TiO <sub>2</sub>	0.6	g/1.2 L		Water, Na <sub>2</sub> SO <sub>3</sub> 0.85 g L <sup>-1</sup> 80 °C 7 bar CO <sub>2</sub>	med.-p. Hg lamp (254-364 nm)	HCOOH CH <sub>3</sub> OH HCHO	148 721 270	187

Table 7 (Contd.)

Suspensions							
Entry	Catalyst	Loading	Conditions	Light source	Products	Yield (μmol h <sup>-1</sup> g <sub>cat</sub> <sup>-1</sup> )	Ref.
17	Au/TiO <sub>2</sub> NT photonic crystals	85 μg Au per TiO <sub>2</sub> wafer 0.5 g L <sup>-1</sup>	Water vapor 80 °C 7 bar CO <sub>2</sub> "Wet" (70% humidity)	50 W white-cold LED (>400 nm) 125 W med.-p. Hg lamp (254–364 nm)	CO HCHO H <sub>2</sub> HCOOH	323 420 102 2954 16,537	188 189 190 191 192
18	TiO <sub>2</sub>	0.2 g spread on a Cu plate 100 mg/200 mL	Water Water pH 8.5 Na <sub>2</sub> CO <sub>3</sub>	Real sunlight Pen ray lamp (254 nm) 500 W Xe lamp	CH <sub>3</sub> OH HCHO HCHO	732 1392 19.5	190 191 193
19	TiO <sub>2</sub> /ZrO <sub>2</sub> (ZrO <sub>2</sub> 40 weight%)	0.2 g spread on a Cu plate 100 mg/200 mL	Water Water pH 8.5 Na <sub>2</sub> CO <sub>3</sub>	500 W Xe lamp	C <sub>2</sub> H <sub>5</sub> OH CH <sub>3</sub> CO <sub>2</sub> H HCOOH CO	33.5 101.7 51 15.7	192
20	NaTaO <sub>3</sub> –C (annealed at 650 °C)	0.05 g/50 mL	0.1 N NaOH aq. sln	500 W tungsten-halogen lamp	CH <sub>3</sub> OH	1	193
21	Pd/TiO <sub>2</sub> –Fe <sub>2</sub> O <sub>3</sub>	10 g/100 mL	0.1 N NaOH aq. sln	500 W tungsten-halogen lamp	CH <sub>3</sub> OH	0.5	193
22	CoPc/TiO <sub>2</sub> (1% mass ratio, calcined at 400 °C)	10 g/100 mL	0.8 mM TEOA aq. sln	250 W lamp (>420 nm)	CH <sub>4</sub> HCHO CO	0.8 2.1	194
23	RuL1OH/TiO <sub>2</sub> (0.125 μM Ru complex per g <sub>cat</sub> )	10 mg/10 mL	0.1 M KHCO <sub>3</sub> 10 v vol% TEA aq. sln Water r.t.	300 W Xe lamp (>420 nm) 150 W Hg-lamp	HCHO HCOOH H <sub>2</sub> HCOOH CH <sub>4</sub> HCHO H <sub>2</sub>	11.3 6.9 10.8 68 0.23 0.2 17	195
24	Sn <sub>75</sub> –Cu <sub>25</sub> /C <sub>3</sub> N <sub>4</sub>	1.5 mg/3.5 mL	0.3 g/4 mL	150 W Hg-lamp	HCOOH CH <sub>4</sub> HCHO H <sub>2</sub>	0.23 0.2 0.23	196
25 <sup>b</sup>	K <sub>2</sub> Ti <sub>6</sub> O <sub>13</sub> + 0.3 wt% Pt	0.3 g/4 mL	Water r.t.	150 W Hg-lamp	HCOOH CH <sub>4</sub> HCHO H <sub>2</sub>	0.476 3.04 0.27 20.7	196
26 <sup>b</sup>	Cu/ZnO/K <sub>2</sub> Ti <sub>6</sub> O <sub>13</sub> + 0.3 wt% Pt	0.3 g/4 mL	Water r.t.	Concentrated sunlight	HCHO CH <sub>4</sub> HCHO H <sub>2</sub>	0.57 32.8 0.23	196
27 <sup>b</sup>	K <sub>2</sub> Ti <sub>6</sub> O <sub>13</sub> + 0.3 wt% Pt	0.3 g/4 mL	Water 274 °C	Concentrated sunlight	HCHO CH <sub>4</sub> HCHO H <sub>2</sub>	5.59 27.6 20.7	197
28	TiO <sub>2</sub>	30 mg/20 mL	Aq. sln pH 6.5, NADH 5 mM, [Cp <sup>*</sup> Rh(bpy) <sup>2+</sup> ] <sup>0.25</sup> mM	23 W UV lamps (max 365 nm)	(PB buff.) (HCHO) (NaOH-EDTA buff.)	548	197

Table 7 (Contd.)

Suspensions							
Entry	Catalyst	Loading	Conditions	Light source	Products	Yield (μmol h <sup>-1</sup> g <sub>cat</sub> <sup>-1</sup> )	Ref.
29	TiO <sub>2</sub> coupled to FDH: FADH (ratio 1:03) loaded membrane	30 mg/20 mL	Aq. sln pH 5.5, NADH 5 mM, [Cp*Rh(bpy) (H <sub>2</sub> O) <sup>2+</sup> ] 0.25 mM	23 W UV lamps (max 365 nm)	HCHO (PB buff.) HCHO (NaOH-EDTA buff.)	13.5 345	197

Photoelectrodes							
Entry	Catalyst	Bias (V)	Conditions	Light source	Products	Yield (μmol h <sup>-1</sup> cm <sup>-2</sup> )	Ref.
30	Polyaniline coated p-Si	-1.9 V vs. SCE	0.1 M LiClO <sub>4</sub> aq. sln	Xe lamp (150 mW cm <sup>-2</sup> )	HCOOH	60.5	200
31	p-GaAs	-0.5 V vs. SCE	4 M HCl aq. sln with 0.32 M V(IV)/V(III) couple, 50 °C	150 W tungsten or Xe lamp	HCHO HCOOH CH <sub>3</sub> OH	15 n.d.	201
32	Bifunctional TiO <sub>2</sub> with Ru N719 dye	No bias	2 M NaOH aq. sln pH 10	300 W Xe lamp (cutoff > 420 nm)	HCOOH CH <sub>3</sub> OH HCHO	16.7 35.6 25.8	202
33 <sup>b</sup>	Cu <sub>2</sub> O film on Cu	No bias	0.1 M Na <sub>2</sub> CO <sub>3</sub> /NaHCO <sub>3</sub> aq. sln pH 9.0	125 W h-p. Hg lamp	CH <sub>3</sub> OH	9.5	203
34	040-BiVO <sub>4</sub>  Cu	+0.9 V vs. RHE	0.5 M NaCl aq. sln	300 W Xe lamp with an AM 1.5G filter	HCHO CH <sub>3</sub> OH C <sub>2</sub> H <sub>5</sub> OH HCHO	125 108 <sup>c</sup> n.d. 1.18	204
35	Cu/rGO/PVP/Nafion	+0.68 V vs. RHE	0.1 M NaOH aq. sln	300 W Xe lamp with a KG3 filter			205

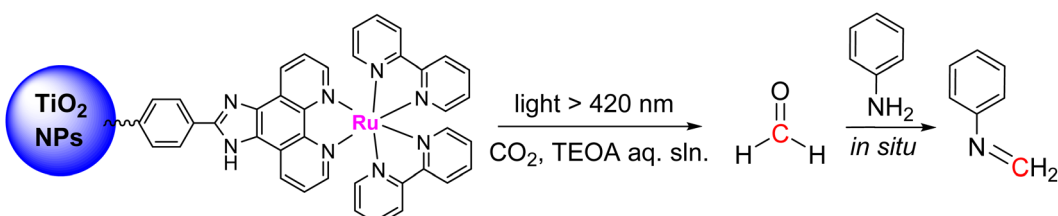
<sup>a</sup> n.d. not determined. <sup>b</sup> Catalyst deposited on a wet paper filter at the bottom of the reaction vessel. <sup>c</sup> In μmol L<sup>-1</sup> h<sup>-1</sup> cm<sup>-2</sup> (reactor volume not specified).

Another example of  $\text{TiO}_2$  based photocatalysis was reported in which sodium sulfite was used as the reducing agent in order to fill in photogenerated holes. Under 7 bars of  $\text{CO}_2$ , at 80 °C and at a  $\text{TiO}_2$  loading of 0.5 g<sup>-1</sup> in basic (pH 14) aqueous solutions, the formation of  $\text{H}_2$  (102  $\mu\text{mol h}^{-1} \text{g}_{\text{cat}}^{-1}$ ), formaldehyde (16 537  $\mu\text{mol h}^{-1} \text{g}_{\text{cat}}^{-1}$ ) and formic acid (2954  $\mu\text{mol h}^{-1} \text{g}_{\text{cat}}^{-1}$ ) were measured depending on experimental conditions (time and pH) under UV irradiation from a medium pressure Hg vapor 125 W lamp introduced into the photoreactor (Table 7, entry 18).<sup>189</sup> The higher formation rate for formaldehyde was observed at the beginning of the reaction (few hours), which was explained by a branched mechanism, with on one hand a  $\text{CO}_2$ -to-formic acid reduction later generating gaseous products (only detected after several hours of irradiation once the hole scavenger is consumed), and on the other hand the direct reduction of carbonates into  $\text{HCHO}$ . Composites made of nanometre-sized  $\text{TiO}_2$  particles and micrometre-sized zirconium oxide ( $\text{ZrO}_2$ ) particles have been reported to generate high yields of formaldehyde and methanol (maximum 300  $\mu\text{mol g}_{\text{cat}}^{-1}$  total after only 300 s) under real solar light illumination (Table 7, entry 19).<sup>190</sup> For that, the composite was scattered on a copper plate and allowed to humidify in a fridge to form a thin layer of water on the composite surface. The assembly was then placed in a gas-barrier plastic bag (allowing  $\text{CO}_2$  diffusion only) containing ambient air and then was illuminated with solar light. It was proposed that reduction products originated from the reduction of bicarbonate ions resulting from the dissolution of  $\text{CO}_2$  contained (from ambient air) in the thin layer of water. A highly crystalline carbon-doped  $\text{NaTaO}_3$  perovskite was also reported to reduce  $\text{CO}_2$  to formaldehyde in neutral aqueous solutions at room temperature and under 254 nm irradiation (4.4 mW cm<sup>-2</sup>), at the optimal rate of 39  $\mu\text{mol g}_{\text{cat}}^{-1}$  after 2 h (Table 7, entry 20).<sup>191</sup> This rate, determined through complexometric measurements, was shown to be dependent on the annealing temperature used to prepare the material as well as the carbon content since the undoped material showed very low formaldehyde yield. Three hematite-based materials, namely  $\text{Fe}_2\text{O}_3$ ,  $\text{TiO}_2\text{-Fe}_2\text{O}_3$  and  $\text{Pd/TiO}_2\text{-Fe}_2\text{O}_3$  were suspended as nanoparticles in an aqueous sodium carbonate solution (pH 8.5) and illuminated with a 500 W xenon lamp. After 2 hours, the highest rate for formaldehyde was obtained with  $\text{Pd/TiO}_2\text{-Fe}_2\text{O}_3$  (1338  $\mu\text{mol L}^{-1} \text{g}_{\text{cat}}^{-1}$ , Table 7, entry 21), when compared with the simple  $\text{Fe}_2\text{O}_3$  (878  $\mu\text{mol L}^{-1} \text{g}_{\text{cat}}^{-1}$ ) and  $\text{TiO}_2\text{-Fe}_2\text{O}_3$  (399  $\mu\text{mol L}^{-1} \text{g}_{\text{cat}}^{-1}$ ) and was explained by the hydrogenation of formic acid with hydrogen atoms on the photocatalyst surface.<sup>192</sup> An example of a system combining a semiconducting material and

a molecule consisted of cobalt phthalocyanine loaded  $\text{TiO}_2$  nanoparticles ( $\text{CoPc/TiO}_2$ ) of *ca.* 11 nm diameter prepared by a sol-gel method and dispersed in alkaline (NaOH) aqueous solutions under a  $\text{CO}_2$  atmosphere.<sup>193</sup> When irradiated with a tungsten-halogen 500 W lamp, a mixture of products containing  $\text{CO}$ ,  $\text{HCOOH}$ ,  $\text{CH}_3\text{OH}$ ,  $\text{CH}_4$  and  $\text{HCHO}$  was produced at a maximum yield of 407  $\mu\text{mol g}_{\text{cat}}^{-1}$  after 20 h under optimized conditions ( $\text{CoPc/TiO}_2$  mass ratio, calcination temperature), the latter accounting for *ca.* 50  $\mu\text{mol g}_{\text{cat}}^{-1}$  (Table 7, entry 22). The  $\text{CO}_2$  reduction to formaldehyde utilizing a heteroleptic ruthenium metal complex covalently linked to  $\text{TiO}_2$  nanoparticles was also reported to occur in aqueous medium at pH 7 under visible light ( $\lambda > 420$  nm) illumination.<sup>194</sup> When the hybrid catalyst was dispersed in neutral water, in the presence of TEOA (triethanolamine) as a sacrificial donor agent, the formation of formaldehyde as the major product (maximum TON of 720 after 5 h, corresponding to a formation rate of 18  $\mu\text{mol h}^{-1} \text{g}_{\text{cat}}^{-1}$ , Table 7, entry 23) was observed in the liquid phase as determined by HPLC, with  $\text{CO}$  and  $\text{CH}_4$  as minor (TON 136 and 64, respectively), gaseous, products. Moreover, recyclability tests showed that the loss of activity was limited to 10–15% after the sixth cycle, due to some material loss during washing steps. In addition, this system used the *in situ* generated formaldehyde in a condensation reaction with amine, generating new  $\text{H}_2\text{C-N}$  bonds (Scheme 50). To the best of our knowledge, this represents the only example of reductive functionalization of  $\text{CO}_2$  *via* formaldehyde in (photo)electroreduction systems.

Very recently,<sup>195</sup> a single-atom catalyst with dual-atom sites (DAS) composed of neighbouring  $\text{Sn}(\text{II})$  and  $\text{Cu}(\text{I})$  centres embedded in a  $\text{C}_3\text{N}_4$  framework was reported to generate  $\text{HCHO}$  from  $\text{CO}_2$  with a selectivity of 61% and a productivity of 259.1  $\mu\text{mol g}^{-1}$  (Table 7, entry 24) after 24 h irradiation. The catalyst was dispersed in a  $\text{CO}_2$ -saturated 0.1 M aqueous  $\text{KHCO}_3$  containing 10 vol% triethylamine (TEA) as the sacrificial electron donor and was irradiated using a 300 W Xe lamp equipped with a 420 nm cut-off filter. The best productivity was obtained with the  $\text{Sn}_{75}\text{-Cu}_{25}/\text{C}_3\text{N}_4$  composition, and the production of  $\text{HCHO}$  from  $\text{CO}_2$ , asserted by <sup>13</sup>C labelled experiments and FTIR and NMR characterization, was attributed to the  $2\text{e}^-$  reduction of  $\text{HCHO}$  through the synergistic action of the two metals.

An original strategy was also tested with a Pt-loaded potassium hexatitanate ( $\text{Pt-K}_2\text{Ti}_6\text{O}_{13}$ ) photocatalyst (0.3 mg) deposited on a filter at the bottom of a flask containing 4 mL of water under a  $\text{CO}_2$  atmosphere.<sup>196</sup> Upon illumination with a 150 W Hg-lamp, formaldehyde was detected as a secondary reduction product ( $\text{H}_2$  as the main one) by GC at a rate of 0.48  $\mu\text{mol h}^{-1}$



Scheme 50 Visible light reduction of  $\text{CO}_2$  into formaldehyde followed by *in situ* condensation with an amine.<sup>194</sup>



$g_{\text{cat}}^{-1}$ , together with  $\text{CH}_4$  and  $\text{HCOOH}$  (Table 7, entry 25). When combined with a  $\text{Cu}/\text{ZnO}$  catalyst, the resulting composite produced  $\text{HCHO}$  as the secondary product ( $\text{H}_2$  – major) at a rate of  $0.57 \mu\text{mol h}^{-1} \text{g}_{\text{cat}}^{-1}$  along with  $\text{CH}_4$  and  $\text{HCOOH}$  (Table 7, entries 26 and 27).

Finally, semiconductors can also be associated with an enzymatic process. For example, a very recent study reported the immobilization of two kinds of dehydrogenases, namely formate dehydrogenase (FDH) and formaldehyde dehydrogenase (FADH) (see Section 8 for more details on these enzymes), on the surface of polyethylene hollow fibre membranes, coupled with UV induced,  $\text{TiO}_2$ -based photocatalytic coenzyme regeneration.<sup>197</sup> In this system, the excitation of  $\text{TiO}_2$  causes charge separation and electrons are transferred to the  $\text{NAD}^+$  formed during the enzymatic cascade  $\text{CO}_2$  reduction, for coenzyme NADH regeneration, using EDTA as the electron donor and pentamethylcyclopentadienyl rhodium bipyridine ( $[\text{Cp}^*\text{Rh}(\text{bpy})(\text{H}_2\text{O})]^{2+}$ ) as the redox mediator. In the absence of an enzyme,  $\text{HCHO}$  was formed at a maximum rate of  $0.207 \text{ mM}$  (with  $\text{H}_2\text{O}$  as the electron donor) and  $4.11 \text{ mM}$  (with EDTA as the electron donor), at pH 6.5 and after 5 h UV irradiation (365 nm max). With the photo-enzyme assembly, the best results were obtained at pH 5.5 with EDTA as the electron donor, reaching  $2.59 \text{ mM}$  of formaldehyde after 5 h of reaction (Table 7, entries 28 and 29). The production of  $\text{HCHO}$  proceeded for 48 h with limited loss of activity.

## 7.2. Photoelectrodes

A p-type Si photoelectrode was coated with a polyaniline film of *ca.* 50 nm thickness upon electro polymerization. Under illumination with a Xe lamp ( $150 \text{ mW cm}^{-2}$ ) at a bias potential of  $-1.9 \text{ V vs. SCE}$ , the photocathode immersed in a  $\text{CO}_2$ -saturated  $0.1 \text{ M LiClO}_4$  aqueous solution generated several micromoles of formic acid and formaldehyde as determined by a colorimetric method (Table 7, entry 30).<sup>200</sup> The bare photoelectrode did not show any activity towards  $\text{CO}_2$  reduction. The total faradaic yield reached 20 to 28% even though no methane or methanol could be detected by gas chromatography. In the presence of the  $\text{V}(\text{II})-\text{V}(\text{III})$  chloride redox couple presumably acting as an electron relay, a p-type GaAs photoelectrode was reported to generate formic acid, formaldehyde and methanol in low yields (from 1 to 3% faradaic yields) in an acidic ( $4 \text{ M HCl}$ ) aqueous solution under visible light illumination (tungsten–halogen lamp,  $980 \text{ mW cm}^{-2}$ ) at a bias potential of  $-0.5 \text{ V vs. SCE}$  and at  $50^\circ\text{C}$  (Table 7, entry 31).<sup>201</sup>

The sequential formation of formic acid (detected by HPLC), formaldehyde (UV-Vis) and methanol (GC) was reported with a bifunctionalized  $\text{TiO}_2$  film under visible-light irradiation (300 W Xe lamp with a cut-off filter) in acetonitrile solution containing DMPIMI electrolyte and the iodide/triiodide couple as a redox mediator.<sup>202</sup> The film was separated into two zones, a sensitized area containing a ruthenium complex (N719) as the dye and a catalytic area composed of a pure  $\text{TiO}_2$  zone. Under illumination, electrons generated in the sensitized zone migrate to the catalytic one through  $\text{TiO}_2$  particles. This film was used as the reduction half-cell in a H-type reactor with Pt as the anode

material, in order to prevent re-oxidation of  $\text{CO}_2$  reduction products. Formic acid was generated first, then formaldehyde and methanol, with a respective yield of *ca.*  $0.05 \text{ mmol cm}^{-2}$  after 5 h (Table 7, entry 32). This yield was enhanced when an external voltage was applied between the reference electrode and the anode thus enabling the regeneration of the redox mediator and consequently of the dye. The effect of the bias potential and the pH on the product distribution was studied with a PEC assembly composed of the  $\text{Cu}/\text{Cu}_2\text{O}$  electrode irradiated with a 125 W high pressure mercury lamp.<sup>203</sup> In  $0.1 \text{ M Na}_2\text{CO}_3/\text{NaHCO}_3$  electrolyte (pH 9.0) saturated with  $\text{CO}_2$ , a high rate for  $\text{HCHO}$  was observed at 0 V bias (Table 7, entry 33), whereas methanol was the main product at  $+0.2 \text{ V}$  bias. At the positive potential bias, some  $\text{HCHO}$  was also observed at pH 8 to 11 as a minor product.

A PEC assembly consisting of a (040)-facet engineered  $\text{BiVO}_4$  plate as the photoanode (040-BVO) and a Cu plate immersed in  $\text{NaCl}$  electrolyte as the cathode has been reported to generate various  $\text{C}_1$  products from  $\text{CO}_2$  when illuminated with solar light under an external bias potential.<sup>204</sup> Depending on the applied potential, the selectivity could be tuned towards a specific product, with a general trend showing that at low potentials, kinetically favourable products are dominant, whereas at high potentials, thermodynamically stable products are dominant. Formaldehyde is produced with 85% faradaic efficiency at an applied potential of  $0.90 \text{ V vs. RHE}$ , corresponding to a yield of  $143 \mu\text{M h}^{-1}$  (Table 7, entry 34). Very recently, it has been shown that a system combining calcium and iron co-doped  $\text{TiO}_2$  films as the photoanode and multilayered Cu based dark electrode as the cathode was able to selectively generate formaldehyde and/or acetaldehyde at the cathode surface by tuning the anode bias potential.<sup>205</sup> Both electrodes were immersed in a  $0.1 \text{ NaOH}$  aqueous electrolyte saturated with  $\text{CO}_2$ , and formaldehyde was detected as the only product with a reduced graphene oxide (rGO) coated copper electrode (Table 7, entry 35). The highest yield was  $470 \mu\text{M cm}^{-2}$  after 8 h (25% faradaic efficiency) under solar simulated irradiation with an applied bias of  $0.68 \text{ V vs. RHE}$ . It is important to note that in the last example  $^{13}\text{C}$  labelled experiments were conducted to confirm the origin of the products.

## 7.3. Solid material approaches

Some studies were also conducted with catalytic solid materials. Two Mo-based heterogeneous catalysts, namely a mixed-valence polyoxomolybdate cluster and composite consisting of a molybdenum keplerate cluster embedded in reduced graphene oxide (RGO), were shown to reduce  $\text{CO}_2$  and oxidize water at the same time, generating sub-mmol amounts of formic acid as the main product and formaldehyde as the secondary product, as quantified by HPLC.<sup>206</sup> Experiments were conducted in pure water with no sensitizer and light irradiation was set at  $373 \text{ nm}$  ( $19 \text{ mW cm}^{-2}$ ). The turnover number and frequency for formic acid (not calculated for formaldehyde) were claimed to reach *ca.*  $10^6$  and *ca.*  $6 \times 10^2 \text{ s}^{-1}$ , respectively. This study shows the possibility of using cheap metal oxides such as oxometallates as catalytic materials for both  $\text{CO}_2$  reduction and water oxidation.

#### 7.4. Molecular approaches

To the best of our knowledge, only two studies employing a fully molecular approach have been reported. A homogeneous system employing pyridine as a catalyst in aqueous solution in the presence of Ru(phen)<sub>3</sub> photosensitizer, ascorbic acid as an electron donor and KCl as an electrostatic stabilizing agent reported the formation, under 470 nm monochromatic illumination, of formate (NMR quantified) as the main product with methanol (GC-MS) as the minor product and traces of formaldehyde detected by NMR.<sup>207</sup> Two ruthenium(II) polypyridyl complexes covalently modified with a pendant pyridyl function have also been shown to be active towards CO<sub>2</sub> reduction under both electrochemical and photochemical conditions in a DMF:water mixture. In the presence of TEA (triethylamine) as a sacrificial donor agent and under 470 nm irradiation, the formation of formate (main product), formaldehyde and methanol (minor) was observed after 1 h irradiation albeit with a very low TON of 16, 7 and 1, respectively.<sup>208</sup> The rapid loss of activity was attributed to ligand photolabilization leading to complex degradation. In neither of these examples has the mechanism been elucidated.

#### 7.5. Conclusion and perspectives

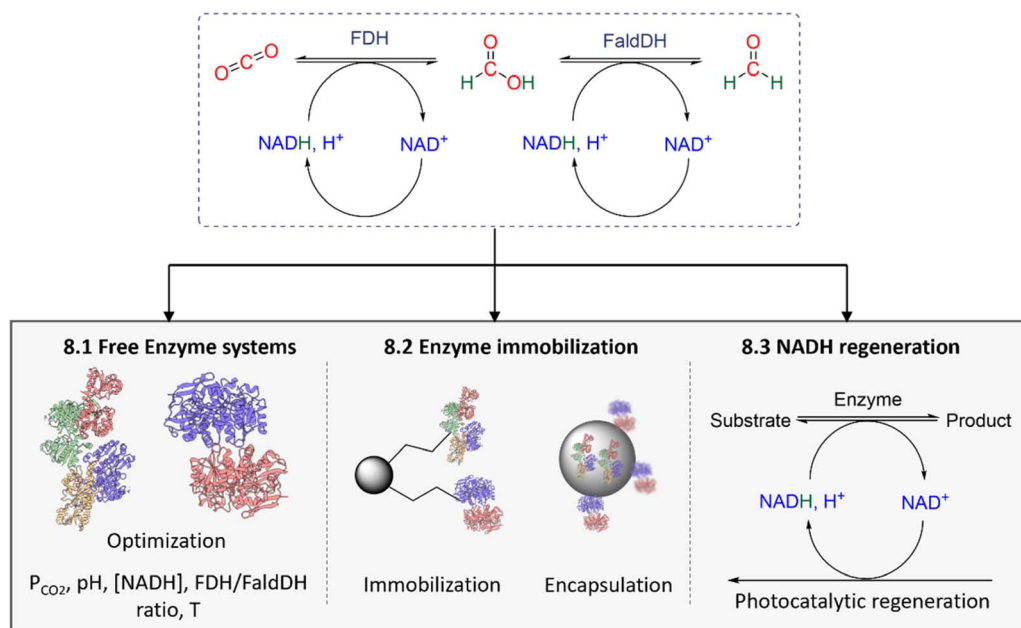
In conclusion, achieving the selective conversion of CO<sub>2</sub> into formaldehyde (HCHO) using light as the primary, if not the sole, energy source is far from realized, as outlined in Table 7 with key examples. The predominant outcome in the majority of studies involves a product mixture, lacking control over selectivity, with low yields and demonstrating limited mechanistic understanding. The inherent high reactivity of HCHO poses a clear challenge to its detection. Therefore, improvements in analytical detection methodologies are imperative. The use of

visible (solar) light still remains scarce, with most systems requiring UV light.

As perspectives, functionalized materials, in particular associating a photoactive material and molecular tuneable unit, open new possibilities to finely control the local environment of the catalytic site and thus to favour the formaldehyde pathway.

### 8. Enzyme-catalysed CO<sub>2</sub> reduction into formaldehyde

Biological fixation of CO<sub>2</sub> occurs through six major pathways including the Calvin–Benson–Bassham (CBB) cycle which represents the most common pathway.<sup>209</sup> Interestingly, the transformation of CO<sub>2</sub> into carbohydrates in the CBB cycle was initially hypothesized to occur *via* a formaldehyde pathway.<sup>181,210</sup> However, it was later demonstrated that the CBB cycle does not involve the intermediate formation of formaldehyde, but the CO<sub>2</sub> fixation to form a carboxylate which is then further reduced in subsequent steps.<sup>211</sup> It is only with isolated enzymes that HCHO and CH<sub>3</sub>OH were obtained from CO<sub>2</sub>. The dehydrogenases, formate dehydrogenases (FDHs, EC 1.2.1.2),<sup>212</sup> formaldehyde dehydrogenase (FaldDH, EC 1.2.1.46)<sup>211</sup> and alcohol dehydrogenase (ADH, EC 1.1.1.1)<sup>213</sup> are able to catalyse the reduction of CO<sub>2</sub>, HCOOH and HCHO into HCOOH, HCHO and CH<sub>3</sub>OH, respectively.<sup>11b,214</sup> Although most of the reports focused on the selective generation of formate, notably because of its implication as an intermediate in the Wood–Ljungdah pathway in acetogens<sup>215</sup> or methanol,<sup>216</sup> only a handful of studies focused on the selective generation of formaldehyde. The two-step enzyme cascade combining formate dehydrogenase (FDH) and formaldehyde dehydrogenase (FaldDH) is currently the only reported process (Scheme 51) for the enzymatic conversion of CO<sub>2</sub> into HCHO. Both enzymes are commercially available and



Scheme 51 Enzymatic sequential generation of formate and formaldehyde with FDH (formate dehydrogenase) and FaldDH (formaldehyde dehydrogenase).



Table 8 Conditions and performances of bio-cascade systems for  $\text{CO}_2$  reduction into formaldehyde<sup>a</sup>

Entry	Immobilization	Substrate	P or [C]	NADH regeneration	Time (h)	HCHO generation (mmol L <sup>-1</sup> )	Ref.
1	Free enzymes	$\text{KHCO}_3$	100 mM	No	72	0.060	217
2	Free enzymes	$\text{CO}_{2(g)}$	0.5 MPa	No	12	0.901	218
3	HDMMC-based system	$\text{CO}_{2(g)}$	0.3 MPa	No	8	0.022	219
4	$\text{TiO}_2$ -NPs	$\text{CO}_{2(g)}$	0.3 MPa	No	4	—	220
5	NPSCs	$\text{CO}_{2(g)}$	0.3 MPa	No	4	0.125	221
6	MCF-MP	$\text{KHCO}_3$	200 mM	No	—	0.037	222
7	3% TCPP@ZIF-8	$\text{NaHCO}_3$	10 $\mu\text{M}$	Yes	8	0.008	223
8	PE-HFMs	$\text{CO}_{2(g)}$	3 mL min <sup>-1</sup>	Yes	4	0.034	197

<sup>a</sup> HDMMCs = hybrid double membrane microcapsules, NPs = nanoparticles, NPSCs = nanoparticle-stabilized capsules, MCF-MP = siliceous mesostructured cellular foams functionalized with mercaptopropyl groups, TCPP = 5,10,15,20-tetrakis(4-carboxyphenyl)porphyrin, ZIF = zeolite-like imidazole framework material, PE-HFMs = polyethylene hollow fibre membranes.

have similar pH and temperature optima. Each step of the cascade is endowed with a  $2\text{e}^-$  reduction of  $\text{CO}_2$  and requires one equivalent of NADH (nicotinamide adenine dinucleotide hydride) as a co-factor, serving as the reductant. Two molecules of NADH are thus oxidized into the corresponding  $\text{NAD}^+$  during the biocatalyzed reduction of  $\text{CO}_2$  to formaldehyde.

The main parameters and performances of these selective catalytic systems are summarized in Table 8. The results are described in three sections: (i) optimized reaction conditions with free enzyme systems, (ii) immobilized and compartmentalized enzymes and, finally, (iii) systems coupled to the NADH regeneration process.

### 8.1. Optimization of the reaction conditions with free enzyme systems

Studies have shown that FDH/FaldDH ratio lower than 1 is beneficial for the production of formaldehyde over formate since the formate is a good substrate for the FDH (Table 8, entry 1).<sup>217</sup> In the same vein, an excess of NADH (NADH/ $\text{NAD}^+$  molar ratio  $> 2000$ ) was also found necessary to drive the reaction. Under optimized conditions, 60  $\mu\text{M}$  of formaldehyde was produced from  $\text{KHCO}_3$  instead of  $\text{CO}_2$  in 72 h with 15 g L<sup>-1</sup> of FaldDH and 1 g L<sup>-1</sup> of FDH. The formaldehyde concentration was quantified using a colorimetric test (Nash reagent)<sup>149</sup> as it was found that indirect detection through UV quantification of NADH disappearance could be erroneous due to interaction with  $\text{CO}_2$ . Following this study, the same cascade was explored with gaseous  $\text{CO}_2$  (Table 8, entry 2).<sup>218</sup> Higher amount of FaldDH as compared to FDH was again necessary and the study disclosed the positive impact of a high  $\text{CO}_2$  pressure (from 0.2 to 0.5 MPa) to generate a high amount of formaldehyde. Under optimized conditions, 901  $\mu\text{M}$  of formaldehyde was produced (0.5 MPa of  $\text{CO}_2$ ) after 12 h. A plateau was found at 10–12 h before a net decrease of formaldehyde, tentatively explained by the consumption of formaldehyde *via* the reverse reaction (*i.e.*, oxidation of HCHO into  $\text{CO}_2$ ) and/or the instability of formaldehyde in the reaction medium.

### 8.2. Enzyme immobilization and compartmentalization

Immobilized systems were explored to improve the performances of the FDH/FaldDH cascade with the aim to increase

enzyme stability, activity<sup>224</sup> and reusability compared to the enzymes freely diffusing systems. FDH and FaldDH were immobilized and spatially separated at organic-inorganic hybrid double membrane microcapsules (HDMMCs) (Table 8, entry 3).<sup>219</sup> FDH was encapsulated in the lumen of the HDMMCs while FaldDH was encapsulated in the intermembrane space. The study showed an improved activity with formaldehyde production of 22  $\mu\text{mol}$  compared to the control experiment with free enzymes (9  $\mu\text{mol}$ ). The same group encapsulated FDH in Ti nanoparticles (NPs) while FaldDH was immobilized at the surface of the particles (Table 8, entry 4).<sup>220</sup> The size of the NPs (from 75 to 375 nm) was shown to have a significant impact on the reaction. The best performances were obtained with NP size of 75 nm. The recycling stability of the enzyme-containing NPs was evaluated and displayed a loss of half of the initial performance after 10 cycles. It was improved in a following report describing the preparation of nanoparticle-stabilized capsules (NPSCs) containing FDH entrapped in the capsule and FaldDH conjugated on the capsule surface (Table 8, entry 5).<sup>221</sup> Furthermore, the distance between both enzymes was evaluated using Förster resonance energy transfer (FRET) analysis on the enzyme labelled with carbocyanine dyes (Table 8, entry 6).<sup>222</sup> While no detectable FRET was observed free in the enzyme system with an estimated distance of 40 nm between the two enzymes, co-immobilization of the enzymes in the silica materials displayed an increased transfer efficiency  $>50\%$  with an estimated distance of less than 10 nm. This feature was proposed to be responsible for the enhanced activity in the particles compared to the enzyme free system, due to probability increase of direct substrate transfer between the two enzymes.

### 8.3. NADH regeneration

NADH is a co-factor that is regenerated in biological systems. When implemented *in vitro*, its stoichiometric use negatively impacts the atom-efficiency of any given transformation. The regeneration of NADH from  $\text{NAD}^+$  has thus been the subject of intense investigation with the development of bio-, electro- and photo-regeneration systems.<sup>225</sup> In the case of the FDH/FaldDH cascade reaction transforming  $\text{CO}_2$  into formaldehyde, only two reports described the combination of the cascade with a regeneration process. FDH and FaldDH were co-immobilized in the cavities of the zeolitic imidazolate framework-8 (ZIF-8)



combined with 5,10,15,20-tetrakis(4-carboxyphenyl) porphyrin (TCPP) as a photosensitizer fixed to the surface of the zeolite (Table 8, entry 7).<sup>223</sup> Triethanolamine (TEOA) was used as an electron donor,  $\text{Cp}^*\text{Rh}(\text{bpy})\text{Cl}$  ( $\text{M}$ ,  $\text{Cp}^*$  = pentamethylcyclopentadienyl, bpy = bipyridine) as an electron mediator and water as a proton donor. Under optimum conditions (1 mg  $\text{mL}^{-1}$  3% TCPP@ZIF-8, pH = 8.0) the NADH regeneration reached 75% yield after 3 h under visible-light exposure. Combining this regeneration system with FDH/FaldDH (2 : 1 ratio) afforded the conversion of 10  $\mu\text{M}$  of  $\text{NaHCO}_3$  into 7.74  $\mu\text{M}$  of formaldehyde (conversion rate 77%) after 8 h under visible-light exposure. The use of titanium dioxide ( $\text{TiO}_2$ ) in a photo-catalytic system<sup>182</sup> was also probed with immobilized FDH/FaldDH on the surface of polyethylene (PE) hollow fibre membranes (HFM) (Table 8, entry 8).<sup>197</sup> Despite side reactions due to the known ability of the UV/ $\text{TiO}_2$  system to photoreduce  $\text{CO}_2$  into various products (*e.g.*, CO,  $\text{HCOOH}$ ,  $\text{HCHO}$ ,  $\text{CH}_3\text{OH}$ ,  $\text{CH}_4$ ),<sup>182</sup> NADH regeneration was observed and 34  $\mu\text{M}$  of formaldehyde was generated under the best conditions (ratio FDH : FaldDH = 1 : 0.3,  $\text{CO}_2$  3  $\text{mL min}^{-1}$ ,  $\text{H}_2\text{O}$  as the electron donor, PB buffer, pH 7.0,  $[\text{NADH}] = 1 \text{ mmol L}^{-1}$ , exposure to two 23 W UV lamps at  $\lambda = 365 \text{ nm}$ ).

#### 8.4. Conclusion and perspectives

In conclusion, the enzymatic conversion of  $\text{CO}_2$  into formaldehyde is still at an early stage of development. Only a few reports have highlighted the selective formation of formaldehyde in cascade reactions involving FDH and FaldDH. Strategies for enzyme immobilization were identified to enhance both the reusability and activities of FDH and FaldDH when compared to free enzyme systems.

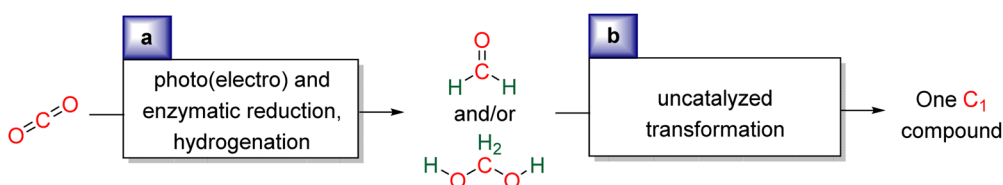
As perspectives, discovering more active and/or robust enzymes from diverse organisms or engineering existing enzymes for improved stability and activity is crucial for advancing current strategies. Additionally, the development of

efficient co-factor regeneration systems is essential to establish an energetically sustainable and cost-effective process. The design of an effective co-immobilized system for enzymes coupled with a co-factor regeneration process remains undisclosed. An attractive approach involves substituting the natural co-factor NADH with a more sustainable electron and proton supplier system, as previously demonstrated in the biocatalyzed generation of formate or methanol from  $\text{CO}_2$ .<sup>11b,213</sup> Similarly, electrochemically driven enzymatic systems represent a promising avenue. Finally, the biocatalyzed four-electron reduction of  $\text{CO}_2$  to formaldehyde has yet to be explored in subsequent transformations. While such processes are enticing, the undefined form taken by the generated formaldehyde and its instability in the enzymatic reaction medium have so far hindered its isolation or utilization in subsequent transformations for the synthesis of more complex products.

## 9. General conclusions

In this comprehensive review, we have examined the reduction of  $\text{CO}_2$  with four electrons, leading to the production of formaldehyde and acetal derivatives through thermal (hydrogenation or hydroelementation reactions), electrochemical, photoelectrochemical, and bio-driven processes. Formaldehyde holds considerable appeal for both energy carrier applications and use as a chemical feedstock. Particularly noteworthy is its versatility for the latter application compared to formic acid, methanol, or methane obtained from the  $\text{CO}_2$  reduction reaction ( $\text{CO}_2\text{RR}$ ). Despite its promising attributes, synthesizing and isolating formaldehyde from the  $\text{CO}_2\text{RR}$  remains significantly more challenging than the aforementioned  $\text{C}_1$  compounds. To date, only a limited number of systems have been reported to generate formaldehyde from  $\text{CO}_2$  as the major product, and in many cases, conclusive evidence regarding the origin of formaldehyde is lacking. The most notable performances of these systems are summarized in Table 9.

**Table 9** Best catalytic performances of the different reduction systems reported for the generation of formaldehyde from electro-, photo-electrochemical, enzymatic and hydrogenation processes and further use as a  $\text{C}_1$  source in subsequent transformations



Reduction system	Hydrogenation	Electroreduction	Photoelectroreduction
Yield	0.037 M $\text{g}_{\text{cat}}^{-1} \text{h}^{-1}$		400–500 $\mu\text{mol h}^{-1} \text{g}_{\text{cat}}^{-1}$ (1 bar $\text{CO}_2$ ) 16 500 $\mu\text{mol h}^{-1} \text{g}_{\text{cat}}^{-1}$ (7 bars $\text{CO}_2$ )
TON	—	$10^4$	
Selectivity (%)	—	90	60–70
Faradaic efficiency (%)	n.a	85–90	NA
Current density ( $\text{mA cm}^{-2}$ )	n.a	0.1–0.2	NA
$\text{C}_1$ source	✗	✗	$\text{CH}_2-\text{N}$
$\text{C}_n$ source	✗	✗	✗
Asymmetric C center	✗	✗	✗



Table 10 Best catalytic performances of the different reduction systems reported for the generation of acetal compounds and further use of the acetals as  $C_1$  and/or  $C_n$  sources in subsequent transformations

Reduction system	Hydrogenation	Hydrosilylation	Hydroboration	Hydrozirconation
TON	3874	3400	690	—
TOF ( $h^{-1}$ )	194	10.4	516	—
Yield (%)	—	99	97	—
Scale	2.88 mmol	4.70 mmol	0.55 mmol	—
$C_1$ source	✗	CH <sub>2</sub> -N, -O, -S, -C	CH <sub>2</sub> -N, -O, -P, -C	CH <sub>2</sub> -C
$C_n$ source	✗	✗	C <sub>2</sub> , C <sub>3</sub> , C <sub>4</sub>	✗
Asymmetric C center	✗	✗	Diastereo- and enantio-selective transformations	✗

In hydrogenation reactions, the highest reported yield of formaldehyde (HCHO) was  $0.037 \text{ M g}_{\text{cat}}^{-1} \text{ h}^{-1}$  achieved with a Ru-based heterogeneous catalyst in an aqueous medium.<sup>148</sup> Another notable instance involved electroreduction, where a film of electropolymerized chromium vinylterpyridine complex exhibited 90% faradaic efficiency (FE) and a turnover number (TON) of  $10^4$ .<sup>170</sup> In photoelectroreduction, optimal performances were observed at  $16\,500 \mu\text{mol h}^{-1} \text{ g}_{\text{cat}}^{-1}$  under 7 bars of CO<sub>2</sub> and 80 °C with a TiO<sub>2</sub> catalyst, achieving 70% selectivity.<sup>189</sup> Remarkably, in all these systems, the generated formaldehyde was utilized only once as a substrate in a cascade reaction to form a C–N bond, leaving significant untapped potential in this area for future exploration.<sup>194</sup> Further investigations are thus imperative, both for fundamental understanding and catalyst development, and it is crucial to gather solid evidence regarding the origin of the generated formaldehyde in each case. In addition to the challenge of generating formaldehyde, detecting and isolating it proves to be a formidable task due to its reactive nature.

On the other hand, the reduction of CO<sub>2</sub> into acetal products has seen successful developments in thermic processes, specifically in (i) the hydrogenation of CO<sub>2</sub> in the presence of alcohol and (ii) hydroelementation reactions involving hydrosilanes, hydroboranes, and early transition metal hydride species. In contrast to the synthesis of formaldehyde, numerous acetal compounds were selectively and efficiently generated, and eventually isolated. Notably, the formation of acetals from the CO<sub>2</sub>RR currently stands as the sole pathway to formaldehyde, enabling its consistent use not only as a  $C_1$  source but also as a  $C_n$  source. Bis(silyl)acetal (BSA) and bis(boryl)acetal (BBA) were indeed shown to release formaldehyde, which was then employed in subsequent  $C_1$  and  $C_n$  transformations. It was also demonstrated that these acetals could serve as a formaldehyde surrogate without releasing formaldehyde. The primary drawback of the acetal approach is its lack of atom efficiency. While the regeneration of hydroborane or hydrosilane in a sustainable reduction process would be an ideal solution, the formation of high value-added compounds *via*

complex transformations may compensate for this issue to some extent. Table 10 compiles the highest reported performances (TON, TOF, yield, selectivity) in each of the reductive processes leading to acetal compounds. While the chemistry of formaldehyde is well-established and developed, the acetal compounds obtained from the four-electron reduction of CO<sub>2</sub> are, for the most part, novel molecules, and their reactivities are still under investigation. Pioneering studies on their reactivity have led to the utilization of several BSA, BBA, and **BZrA 1** as a  $C_1$  source in multicomponent reactions. This facilitated the incorporation of one carbon atom from CO<sub>2</sub> into very diverse molecules in the form of methylene. Table 10 also summarizes the types of C–E bonds (E = N, O, S, P) formed from BSA, BBA, and **BZrA 1**. Moreover, two BBA compounds (**BBA 2** and **4**) were employed as a  $C_n$  source, generating C<sub>2</sub>, C<sub>3</sub>, and C<sub>4</sub> carbohydrates. In the case of the latter two, asymmetric carbon centres were even generated in a diastereo- and enantioselective manner, respectively. Formaldehyde was directly observed only once in 4% yield with hydrosilanes and only once among a mixture of other products with hydroboranes. The intermediary of acetals (**BSA 3**, **BBA 2** and **4**, **BZrA 1**) was essential for the selective generation of formaldehyde, as it was quantitatively released either spontaneously, from hydrolysis, or from CsF activation depending on the acetal properties.

To conclude, the  $4e^-$  reduction of CO<sub>2</sub> is a two-face journey. On one hand, the generation of acetal compounds witnessed important advances both to control this challenging reduction stage and to use it in subsequent complex transformations but at the expense of low atom-efficiency. On the other hand, the generation of formaldehyde from hydrogenation or photo(electro) reduction is more sustainable, but still in its infancy compared to other  $C_1$  reduction compounds such as CO or methanol.

We believe that intertwined processes from the different fields involved in the CO<sub>2</sub>RR (single *vs.* cascade processes, coupling between electro- and organo-catalysis) may be instrumental in addressing the challenging and sustainability issues associated with the  $4e^-$  reduction of CO<sub>2</sub>.



## Data availability

Correspondence and requests should be addressed to julien.bonin@sorbonne-universite.fr, sebastien.bontemps@lcc-toulouse.fr or marc.robert@sorbonne-universite.fr.

## Author contributions

S. B. conceptualized the review. S. B., S. D., J. B. and M. R. wrote and edited the review.

## Conflicts of interest

The authors declare no competing financial interest.

## Acknowledgements

Partial financial support to M. R. from the Institut Universitaire de France (IUF) is warmly thanked. S. D. thanks Région Midi-Pyrénées and Université Fédérale de Toulouse for a doctoral fellowship. S. B. thanks the CNRS for financial and technical support.

## References

- 1 (a) H. Arakawa, M. Aresta, J. N. Armor, M. A. Barteau, E. J. Beckman, A. T. Bell, J. E. Bercaw, C. Creutz, E. Dinjus, D. A. Dixon, K. Domen, D. L. DuBois, J. Eckert, E. Fujita, D. H. Gibson, W. A. Goddard, D. W. Goodman, J. Keller, G. J. Kubas, H. H. Kung, J. E. Lyons, L. E. Manzer, T. J. Marks, K. Morokuma, K. M. Nicholas, R. Periana, L. Que, J. Rostrup-Nielson, W. M. H. Sachtler, L. D. Schmidt, A. Sen, G. A. Somorjai, P. C. Stair, B. R. Stults and W. Tumas, Catalysis Research of Relevance to Carbon Management: Progress, Challenges, and Opportunities, *Chem. Rev.*, 2001, **101**, 953–996; (b) E. Fujita, Photochemical carbon dioxide reduction with metal complexes, *Coord. Chem. Rev.*, 1999, **185–186**, 373–384; (c) W. Leitner, The coordination chemistry of carbon dioxide and its relevance for catalysis: A critical study, *Coord. Chem. Rev.*, 1996, **155**, 247; (d) D. H. Gibson, The organometallic chemistry of carbon dioxide, *Chem. Rev.*, 1996, **96**, 2063–2095; (e) P. Braunstein, D. Matt and D. Nobel, Reactions of carbon dioxide with carbon–carbon bond formation catalyzed by transition-metal complexes, *Chem. Rev.*, 1988, **88**, 747–764; (f) D. B. Dell'Amico, F. Calderazzo, L. Labella, F. Marchetti and G. Pampaloni, Converting Carbon Dioxide into Carbamato Derivatives, *Chem. Rev.*, 2003, **103**, 3857–3898.
- 2 (a) A. Goeppert, M. Czaun, J.-P. Jones, G. K. Surya Prakash and G. A. Olah, Recycling of carbon dioxide to methanol and derived products – closing the loop, *Chem. Soc. Rev.*, 2014, **43**, 7995–8048; (b) M. Aresta, A. Dibenedetto and A. Angelini, Catalysis for the Valorization of Exhaust Carbon: from CO<sub>2</sub> to Chemicals, Materials, and Fuels. Technological Use of CO<sub>2</sub>, *Chem. Rev.*, 2014, **114**, 1709–1742; (c) C. Costentin, M. Robert and J.-M. Saveant, Catalysis of the electrochemical reduction of carbon dioxide, *Chem. Soc. Rev.*, 2013, **42**, 2423–2436; (d) A. M. Appel, J. E. Bercaw, A. B. Bocarsly, H. Dobbek, D. L. DuBois, M. Dupuis, J. G. Ferry, E. Fujita, R. Hille, P. J. A. Kenis, C. A. Kerfeld, R. H. Morris, C. H. F. Peden, A. R. Portis, S. W. Ragsdale, T. B. Rauchfuss, J. N. H. Reek, L. C. Seefeldt, R. K. Thauer and G. L. Waldrop, Frontiers, Opportunities, and Challenges in Biochemical and Chemical Catalysis of CO<sub>2</sub> Fixation, *Chem. Rev.*, 2013, **113**, 6621–6658; (e) G. Centi and S. Perathoner, Opportunities and prospects in the chemical recycling of carbon dioxide to fuels, *Catal. Today*, 2009, **148**, 191–205; (f) E. E. Benson, C. P. Kubiak, A. J. Sathrum and J. M. Smieja, Electrocatalytic and homogeneous approaches to conversion of CO<sub>2</sub> to liquid fuels, *Chem. Soc. Rev.*, 2009, **38**, 89–99; (g) T. Sakakura, J.-C. Choi and H. Yasuda, Transformation of Carbon Dioxide, *Chem. Rev.*, 2007, **107**, 2365–2387; (h) M. Aresta and A. Dibenedetto, Utilisation of CO<sub>2</sub> as a chemical feedstock: opportunities and challenges, *Dalton Trans.*, 2007, 2975–2992; (i) M. Aresta, in *Activation of small molecules*, ed. W. B. Tolman, Wiley, Weinheim, Germany, 2006, pp. 1–42; (j) M. D. Burkart, N. Hazari, C. L. Tway and E. L. Zeitler, Opportunities and Challenges for Catalysis in Carbon Dioxide Utilization, *ACS Catal.*, 2019, **9**, 7937–7956.
- 3 (a) A. Modak, P. Bhanja, S. Dutta, B. Chowdhury and A. Bhaumik, Catalytic reduction of CO<sub>2</sub> into fuels and fine chemicals, *Green Chem.*, 2020, **22**, 4002–4033; (b) F. Marques Mota and D. H. Kim, From CO<sub>2</sub> methanation to ambitious long-chain hydrocarbons: alternative fuels paving the path to sustainability, *Chem. Soc. Rev.*, 2019, **48**, 205–259; (c) X. Li, J. Yu, M. Jaroniec and X. Chen, Cocatalysts for Selective Photoreduction of CO<sub>2</sub> into Solar Fuels, *Chem. Rev.*, 2019, **119**, 3962–4179; (d) K. Sordakis, C. Tang, L. K. Vogt, H. Junge, P. J. Dyson, M. Beller and G. Laurenczy, Homogeneous Catalysis for Sustainable Hydrogen Storage in Formic Acid and Alcohols, *Chem. Rev.*, 2018, **118**, 372–433; (e) S. Remíro-Buenamañana and H. García, Photoassisted CO<sub>2</sub> Conversion to Fuels, *ChemCatChem*, 2018, **11**, 342–356; (f) J. Qiao, Y. Liu, F. Hong and J. Zhang, A review of catalysts for the electroreduction of carbon dioxide to produce low-carbon fuels, *Chem. Soc. Rev.*, 2014, **43**, 631–675; (g) A. J. Morris, G. J. Meyer and E. Fujita, Molecular Approaches to the Photocatalytic Reduction of Carbon Dioxide for Solar Fuels, *Acc. Chem. Res.*, 2009, **42**, 1983–1994.
- 4 (a) F. Della Monica and A. W. Kleij, Mechanistic guidelines in nonreductive conversion of CO<sub>2</sub>: the case of cyclic carbonates, *Catal. Sci. Technol.*, 2020, **10**, 3483–3501; (b) Y. Yang and J.-W. Lee, Toward ideal carbon dioxide functionalization, *Chem. Sci.*, 2019, **10**, 3905–3926; (c) S. Wang and C. Xi, Recent advances in nucleophile-triggered CO<sub>2</sub>-incorporated cyclization leading to heterocycles, *Chem. Soc. Rev.*, 2019, **48**, 382–404; (d) A. Cherubini-Celli, J. Mateos, M. Bonchio, L. Dell'Amico



and X. Companyó, Transition Metal-Free CO<sub>2</sub> Fixation into New Carbon–Carbon Bonds, *ChemSusChem*, 2018, **11**, 3056–3070; (e) J. Luo and I. Larrosa, C–H Carboxylation of Aromatic Compounds through CO<sub>2</sub> Fixation, *ChemSusChem*, 2017, **10**, 3317–3332; (f) T. Janes, Y. Yang and D. Song, Chemical reduction of CO<sub>2</sub> facilitated by C-nucleophiles, *Chem. Commun.*, 2017, **53**, 11390–11398; (g) F.-G. Fontaine, M.-A. Courtemanche, M.-A. Légaré and É. Rochette, Design principles in frustrated Lewis pair catalysis for the functionalization of carbon dioxide and heterocycles, *Coord. Chem. Rev.*, 2017, **334**, 124–135; (h) Y. Li, X. Cui, K. Dong, K. Junge and M. Beller, Utilization of CO<sub>2</sub> as a C<sub>1</sub> Building Block for Catalytic Methylation Reactions, *ACS Catal.*, 2016, 1077–1086, DOI: [10.1021/acscatal.6b02715](https://doi.org/10.1021/acscatal.6b02715); (i) D. Yu, S. P. Teong and Y. Zhang, Transition metal complex catalyzed carboxylation reactions with CO<sub>2</sub>, *Coord. Chem. Rev.*, 2015, **293**–294, 279–291; (j) Q. Liu, L. Wu, R. Jackstell and M. Beller, Using carbon dioxide as a building block in organic synthesis, *Nat. Commun.*, 2015, **6**, 1–15; (k) L. Wu, Q. Liu, R. Jackstell and M. Beller, Carbonylations of Alkenes with CO Surrogates, *Angew. Chem., Int. Ed.*, 2014, **53**, 6310–6320; (l) I. Omae, Recent developments in carbon dioxide utilization for the production of organic chemicals, *Coord. Chem. Rev.*, 2012, **256**, 1384–1405; (m) K. Huang, C.-L. Sun and Z.-J. Shi, Transition-metal-catalyzed C–C bond formation through the fixation of carbon dioxide, *Chem. Soc. Rev.*, 2011, **40**, 2435–2452; (n) M. Cokoja, C. Bruckmeier, B. Rieger, W. A. Herrmann and F. E. Kühn, Transformation of Carbon Dioxide with Homogeneous Transition-Metal Catalysts: A Molecular Solution to a Global Challenge?, *Angew. Chem., Int. Ed.*, 2011, **50**, 8510–8537; (o) S. N. Riduan and Y. Zhang, Recent developments in carbon dioxide utilization under mild conditions, *Dalton Trans.*, 2010, **39**, 3347–3357.

5 (a) G. Garcia-Garcia, M. C. Fernandez, K. Armstrong, S. Woolass and P. Styring, Analytical Review of Life-Cycle Environmental Impacts of Carbon Capture and Utilization Technologies, *ChemSusChem*, 2021, **14**, 995–1015; (b) A. Sternberg, C. M. Jens and A. Bardow, Life cycle assessment of CO<sub>2</sub>-based C<sub>1</sub>-chemicals, *Green Chem.*, 2017, **19**, 2244–2259; (c) J. A. Martens, A. Bogaerts, N. De Kimpe, P. A. Jacobs, G. B. Marin, K. Rabaey, M. Saeys and S. Verhelst, The Chemical Route to a Carbon Dioxide Neutral World, *ChemSusChem*, 2017, **10**, 1039–1055; (d) N. von der Assen, P. Voll, M. Peters and A. Bardow, Life cycle assessment of CO<sub>2</sub> capture and utilization: a tutorial review, *Chem. Soc. Rev.*, 2014, **43**, 7982–7994.

6 R. I. Masel, Z. Liu, H. Yang, J. J. Kaczur, D. Carrillo, S. Ren, D. Salvatore and C. P. Berlinguette, An industrial perspective on catalysts for low-temperature CO<sub>2</sub> electrolysis, *Nat. Nanotechnol.*, 2021, **16**, 118–128.

7 (a) J. Klankermayer, S. Wesselbaum, K. Beydoun and W. Leitner, Selective Catalytic Synthesis Using the Combination of Carbon Dioxide and Hydrogen: Catalytic Chess at the Interface of Energy and Chemistry, *Angew. Chem., Int. Ed.*, 2016, **55**, 7296–7343; (b) W.-H. Wang, Y. Himeda, J. T. Muckerman, G. F. Manbeck and E. Fujita, CO<sub>2</sub> Hydrogenation to Formate and Methanol as an Alternative to Photo- and Electrochemical CO<sub>2</sub> Reduction, *Chem. Rev.*, 2015, **115**, 12936–12973; (c) W. Wang, S. Wang, X. Ma and J. Gong, Recent advances in catalytic hydrogenation of carbon dioxide, *Chem. Soc. Rev.*, 2011, **40**, 3703–3727; (d) P. G. Jessop, F. Joo and C.-C. Tai, Recent advances in the homogeneous hydrogenation of carbon dioxide, *Coord. Chem. Rev.*, 2004, **248**, 2425–2442; (e) T. Schaub, CO<sub>2</sub>-based hydrogen storage: CO<sub>2</sub> hydrogenation to formic acid, formaldehyde and methanol, *Phys. Sci. Rev.*, 2018, **3**, 20170015.

8 (a) S. Bontemps, Boron-Mediated Activation of Carbon Dioxide, *Coord. Chem. Rev.*, 2016, **308**(Part 2), 117–130; (b) C. C. Chong and R. Kinjo, Catalytic Hydroboration of Carbonyl Derivatives, Imines, and Carbon Dioxide, *ACS Catal.*, 2015, **5**, 3238–3259.

9 (a) F. J. Fernández-Alvarez and L. A. Oro, Homogeneous Catalytic Reduction of CO<sub>2</sub> with Silicon-Hydrides, State of the Art, *ChemCatChem*, 2018, **10**, 4783–4796; (b) F. J. Fernandez-Alvarez, A. M. Aitani and L. A. Oro, Homogeneous catalytic reduction of CO<sub>2</sub> with hydrosilanes, *Catal. Sci. Technol.*, 2014, **4**, 611–624.

10 (a) E. Boutin, L. Merakeb, B. Ma, B. Boudy, M. Wang, J. Bonin, E. Anxolabéhère-Mallart and M. Robert, Molecular catalysis of CO<sub>2</sub> reduction: recent advances and perspectives in electrochemical and light-driven processes with selected Fe, Ni and Co aza macrocyclic and polypyridine complexes, *Chem. Soc. Rev.*, 2020, **49**, 5772–5809; (b) S. Fukuzumi, Y.-M. Lee, H. S. Ahn and W. Nam, Mechanisms of catalytic reduction of CO<sub>2</sub> with heme and nonheme metal complexes, *Chem. Sci.*, 2018, **9**, 6017–6034; (c) K. M. Waldie, A. L. Ostericher, M. H. Reineke, A. F. Sasayama and C. P. Kubiak, Hydricity of Transition-Metal Hydrides: Thermodynamic Considerations for CO<sub>2</sub> Reduction, *ACS Catal.*, 2017, **8**, 1313–1324; (d) N. Elgrishi, M. B. Chambers, X. Wang and M. Fontecave, Molecular polypyridine-based metal complexes as catalysts for the reduction of CO<sub>2</sub>, *Chem. Soc. Rev.*, 2017, **46**, 761–796; (e) H. Takeda, C. Cometto, O. Ishitani and M. Robert, Electrons, Photons, Protons and Earth-Abundant Metal Complexes for Molecular Catalysis of CO<sub>2</sub> Reduction, *ACS Catal.*, 2016, **7**, 70–88; (f) A. M. Appel and M. L. Helm, Determining the Overpotential for a Molecular Electrocatalyst, *ACS Catal.*, 2014, **4**, 630–633; (g) Y. Dong, P. Duchesne, A. Mohan, K. K. Ghuman, P. Kant, L. Hurtado, U. Ulmer, J. Y. Y. Loh, A. A. Tountas, L. Wang, A. Jelle, M. Xia, R. Dittmeyer and G. A. Ozin, Shining light on CO<sub>2</sub>: from materials discovery to photocatalyst, photoreactor and process engineering, *Chem. Soc. Rev.*, 2020, **49**, 5648–5663; (h) C. S. Yeung, Photoredox Catalysis as a Strategy for CO<sub>2</sub> Incorporation: Direct Access to Carboxylic Acids from a Renewable Feedstock, *Angew. Chem., Int. Ed.*, 2019, **58**, 5492–5502; (i) L. j. Guo, Y. j. Wang and T. He, Photocatalytic Reduction of CO<sub>2</sub> over Heterostructure Semiconductors into Value-Added Chemicals, *Chem. Rec.*, 2016, **16**, 1918–1933;



(j) X. Chang, T. Wang and J. Gong, CO<sub>2</sub> photo-reduction: insights into CO<sub>2</sub> activation and reaction on surfaces of photocatalysts, *Energy Environ. Sci.*, 2016, **9**, 2177–2196; (k) J. L. White, M. F. Baruch, J. E. Pander III, Y. Hu, I. C. Fortmeyer, J. E. Park, T. Zhang, K. Liao, J. Gu, Y. Yan, T. W. Shaw, E. Abelev and A. B. Bocarsly, Light-Driven Heterogeneous Reduction of Carbon Dioxide: Photocatalysts and Photoelectrodes, *Chem. Rev.*, 2015, **115**, 12888–12935; (l) S. Nitopi, E. Bertheussen, S. B. Scott, X. Liu, A. K. Engstfeld, S. Horch, B. Seger, I. E. L. Stephens, K. Chan, C. Hahn, J. K. Nørskov, T. F. Jaramillo and I. Chorkendorff, Progress and Perspectives of Electrochemical CO<sub>2</sub> Reduction on Copper in Aqueous Electrolyte, *Chem. Rev.*, 2019, **119**, 7610–7672.

11 (a) M. Yuan, M. J. Kummer and S. D. Minteer, Strategies for Bioelectrochemical CO<sub>2</sub> Reduction, *Chem.-Eur. J.*, 2019, **25**, 14258–14266; (b) S. Schlager, A. Dibenedetto, M. Aresta, D. H. Apaydin, L. M. Dumitru, H. Neugebauer and N. S. Sariciftci, Biocatalytic and Bioelectrocatalytic Approaches for the Reduction of Carbon Dioxide using Enzymes, *Energy Technol.*, 2017, **5**, 812–821.

12 (a) K. A. Grice, Carbon dioxide reduction with homogenous early transition metal complexes: Opportunities and challenges for developing CO<sub>2</sub> catalysis, *Coord. Chem. Rev.*, 2017, **336**, 78–95; (b) A. Pinaka and G. C. Vougioukalakis, Using sustainable metals to carry out “green” transformations: Fe- and Cu-catalyzed CO<sub>2</sub> monetization, *Coord. Chem. Rev.*, 2015, **288**, 69–97; (c) L. Zhang and Z. Hou, N-Heterocyclic carbene (NHC)-copper-catalysed transformations of carbon dioxide, *Chem. Sci.*, 2013, **4**, 3395–3403; (d) S. P and S. K. Mandal, From CO<sub>2</sub> activation to catalytic reduction: a metal-free approach, *Chem. Sci.*, 2020, **11**, 10571–10593.

13 (a) K. Liu, P. Cao, W. Chen, C. I. Ezech, Z. Chen, Y. Luo, Q. Liu, H. Zhao, Z. Rui, S. Gao, Z. Yin, X. Sun and X. Yu, Electrocatalysis enabled transformation of earth-abundant water, nitrogen and carbon dioxide for a sustainable future, *Mater. Adv.*, 2022, **3**, 1359–1400; (b) H. Lu, J. Tournet, K. Dastafkan, Y. Liu, Y. H. Ng, S. K. Karuturi, C. Zhao and Z. Yin, Noble-Metal-Free Multicomponent Nanointegration for Sustainable Energy Conversion, *Chem. Rev.*, 2021, **121**, 10271–10366; (c) F. Naseem, P. Lu, J. Zeng, Z. Lu, Y. H. Ng, H. Zhao, Y. Du and Z. Yin, Solid Nanoporosity Governs Catalytic CO<sub>2</sub> and N<sub>2</sub> Reduction, *ACS Nano*, 2020, **14**, 7734–7759; (d) L. Wang, W. Chen, D. Zhang, Y. Du, R. Amal, S. Qiao, J. Wu and Z. Yin, Surface strategies for catalytic CO<sub>2</sub> reduction: from two-dimensional materials to nanoclusters to single atoms, *Chem. Soc. Rev.*, 2019, **48**, 5310–5349; (e) H. Yin, K. Xing, Y. Zhang, D. M. A. S. Dissanayake, Z. Lu, H. Zhao, Z. Zeng, J.-H. Yun, D.-C. Qi and Z. Yin, Periodic nanostructures: preparation, properties and applications, *Chem. Soc. Rev.*, 2021, **50**, 6423–6482; (f) A. Álvarez, A. Bansode, A. Urakawa, A. V. Bavykina, T. A. Wezendonk, M. Makkee, J. Gascon and F. Kapteijn, Challenges in the Greener Production of Formates/Formic Acid, Methanol, and DME by Heterogeneously Catalyzed CO<sub>2</sub> Hydrogenation Processes, *Chem. Rev.*, 2017, **117**, 9804–9838; (g) L. Zhang, Z.-J. Zhao, T. Wang and J. Gong, Nano-designed semiconductors for electro- and photoelectrocatalytic conversion of carbon dioxide, *Chem. Soc. Rev.*, 2018, **47**, 5423–5443; (h) J. Zhong, X. Yang, Z. Wu, B. Liang, Y. Huang and T. Zhang, State of the art and perspectives in heterogeneous catalysis of CO<sub>2</sub> hydrogenation to methanol, *Chem. Soc. Rev.*, 2020, **49**, 1385–1413.

14 (a) S. Liang, L. Huang, Y. Gao, Q. Wang and B. Liu, Electrochemical Reduction of CO<sub>2</sub> to CO over Transition Metal/N-Doped Carbon Catalysts: The Active Sites and Reaction Mechanism, *Adv. Sci.*, 2021, **8**, 2102886; (b) S. Jin, Z. Hao, K. Zhang, Z. Yan and J. Chen, Advances and Challenges for the Electrochemical Reduction of CO<sub>2</sub> to CO: From Fundamentals to Industrialization, *Angew. Chem., Int. Ed.*, 2021, **60**, 20627–20648; (c) R. Küngas, Electrochemical CO<sub>2</sub> Reduction for CO Production: Comparison of Low- and High-Temperature Electrolysis Technologies, *J. Electrochem. Soc.*, 2020, **167**, 044508; (d) F.-Y. Gao, R.-C. Bao, M.-R. Gao and S.-H. Yu, Electrochemical CO<sub>2</sub>-to-CO conversion: electrocatalysts, electrolytes, and electrolyzers, *J. Mater. Chem. A*, 2020, **8**, 15458–15478.

15 (a) R. Sun, Y. Liao, S.-T. Bai, M. Zheng, C. Zhou, T. Zhang and B. F. Sels, Heterogeneous catalysts for CO<sub>2</sub> hydrogenation to formic acid/formate: from nanoscale to single atom, *Energy Environ. Sci.*, 2021, **14**, 1247–1285; (b) P. Duarah, D. Haldar, V. S. K. Yadav and M. K. Purkait, Progress in the electrochemical reduction of CO<sub>2</sub> to formic acid: A review on current trends and future prospects, *J. Environ. Chem. Eng.*, 2021, **9**, 106394; (c) M. F. Philips, G.-J. M. Gruter, M. T. M. Koper and K. J. P. Schouten, Optimizing the Electrochemical Reduction of CO<sub>2</sub> to Formate: A State-of-the-Art Analysis, *ACS Sustain. Chem. Eng.*, 2020, **8**, 15430–15444; (d) P. Ding, H. Zhao, T. Li, Y. Luo, G. Fan, G. Chen, S. Gao, X. Shi, S. Lu and X. Sun, Metal-based electrocatalytic conversion of CO<sub>2</sub> to formic acid/formate, *J. Mater. Chem. A*, 2020, **8**, 21947–21960; (e) W. Leitner, Carbon-Dioxide as a Raw-Material - the Synthesis of Formic-Acid and Its Derivatives from CO<sub>2</sub>, *Angew. Chem., Int. Ed.*, 1995, **34**, 2207–2221.

16 (a) X. Jiang, X. Nie, X. Guo, C. Song and J. G. Chen, Recent Advances in Carbon Dioxide Hydrogenation to Methanol via Heterogeneous Catalysis, *Chem. Rev.*, 2020, **120**, 7984–8034; (b) E. Alberico and M. Nielsen, Towards a methanol economy based on homogeneous catalysis: methanol to H<sub>2</sub> and CO<sub>2</sub> to methanol, *Chem. Commun.*, 2015, **51**, 6714–6725; (c) Y.-N. Li, R. Ma, L.-N. He and Z.-F. Diao, Homogeneous hydrogenation of carbon dioxide to methanol, *Catal. Sci. Technol.*, 2014, **4**, 1498–1512; (d) G. A. Olah, Towards Oil Independence Through Renewable Methanol Chemistry, *Angew. Chem., Int. Ed.*, 2012, **52**, 104–107.

17 (a) S. W. Sheehan, Electrochemical methane production from CO<sub>2</sub> for orbital and interplanetary refueling, *iScience*,



2021, **24**, 102230; (b) C. Vogt, M. Monai, G. J. Kramer and B. M. Weckhuysen, The renaissance of the Sabatier reaction and its applications on Earth and in space, *Nat. Catal.*, 2019, **2**, 188–197; (c) P. Melo Bravo and D. P. Debecker, Combining CO<sub>2</sub> capture and catalytic conversion to methane, *Waste Dispos. Sustain. Energy.*, 2019, **1**, 53–65.

18 S. Bagherzadeh and N. P. Mankad, Catalyst Control of Selectivity in CO<sub>2</sub> Reduction Using a Tunable Heterobimetallic Effect, *J. Am. Chem. Soc.*, 2015, **137**(34), 10898–10901.

19 (a) H. Zhao, Z. Lin and T. B. Marder, Density Functional Theory Studies on the Mechanism of the Reduction of CO<sub>2</sub> to CO Catalyzed by Copper(I) Boryl Complexes, *J. Am. Chem. Soc.*, 2006, **128**, 15637–15643; (b) D. S. Laitar, P. Mueller and J. P. Sadighi, Efficient Homogeneous Catalysis in the Reduction of CO<sub>2</sub> to CO, *J. Am. Chem. Soc.*, 2005, **127**, 17196–17197.

20 (a) Y. Zhang, T. Zhang and S. Das, Catalytic transformation of CO<sub>2</sub> into C<sub>1</sub> chemicals using hydrosilanes as a reducing agent, *Green Chem.*, 2020, **22**, 1800–1820; (b) M. Hull and P. J. Dyson, Pivotal Role of the Basic Character of Organic and Salt Catalysts in C–N Bond Forming Reactions of Amines with CO<sub>2</sub>, *Angew. Chem., Int. Ed.*, 2020, **59**, 1002–1017; (c) A. Tlili, E. Blondiaux, X. Frogneux and T. Cantat, Reductive functionalization of CO<sub>2</sub> with amines: an entry to formamide, formamidine and methylamine derivatives, *Green Chem.*, 2015, **17**, 157–168.

21 (a) T. K. Todorova, M. W. Schreiber and M. Fontecave, Mechanistic Understanding of CO<sub>2</sub> Reduction Reaction (CO<sub>2</sub>RR) Toward Multicarbon Products by Heterogeneous Copper-Based Catalysts, *ACS Catal.*, 2020, **10**, 1754–1768; (b) G. Prieto, Carbon Dioxide Hydrogenation into Higher Hydrocarbons and Oxygenates: Thermodynamic and Kinetic Bounds and Progress with Heterogeneous and Homogeneous Catalysis, *ChemSusChem*, 2017, **10**, 1056–1070; (c) M. D. Porosoff, B. Yan and J. G. Chen, Catalytic reduction of CO<sub>2</sub> by H<sub>2</sub> for synthesis of CO, methanol and hydrocarbons: challenges and opportunities, *Energy Environ. Sci.*, 2016, **9**, 62–73; (d) S. A. Fors and C. A. Malapit, Homogeneous Catalysis for the Conversion of CO<sub>2</sub>, CO, CH<sub>3</sub>OH, and CH<sub>4</sub> to C<sub>2+</sub> Chemicals via C–C Bond Formation, *ACS Catal.*, 2023, **13**, 4231–4249.

22 (a) L. E. Heim, H. Konnerth and M. H. G. Prechtl, Future Perspectives for Formaldehyde: Pathways for Reductive Synthesis and Energy Storage, *Green Chem.*, 2017, **19**, 2347–2355; (b) G. Reuss, W. Disteldorf, A. O. Gamer and A. Hilt, *Formaldehyde in Ullmann's Encyclopedia of Industrial Chemistry*, Wiley, Weinheim, 2003; (c) M. Trincado, H. Grützmacher and M. H. G. Prechtl, CO<sub>2</sub>-based hydrogen storage – Hydrogen generation from formaldehyde/water, *Phys. Sci. Rev.*, 2018, **3**, 20170013.

23 A. W. Franz, H. Kronemayer, D. Pfeiffer, R. D. Pilz, G. Reuss, W. Disteldorf, A. O. Gamer and A. Hilt, in *Ullmann's Encyclopedia of Industrial Chemistry*, 2016, pp. 1–34, DOI: [10.1002/14356007.a11\\_619.pub2](https://doi.org/10.1002/14356007.a11_619.pub2).

24 S. Desmons, R. Fauré and S. Bontemps, Formaldehyde as a Promising C<sub>1</sub> Source: The Instrumental Role of Biocatalysis for Stereocontrolled Reactions, *ACS Catal.*, 2019, **9**, 9575–9588.

25 S. Meninno and A. Lattanzi, Asymmetric Aldol Reaction with Formaldehyde: a Challenging Process, *Chem. Rec.*, 2016, **16**, 2016–2030.

26 (a) I. Zafar and N. Senad, The Formose Reaction: A Tool to Produce Synthetic Carbohydrates Within a Regenerative Life Support System, *Curr. Org. Chem.*, 2012, **16**, 769–788; (b) I. V. Delidovich, A. N. Simonov, O. P. Taran and V. N. Parmon, Catalytic Formation of Monosaccharides: From the Formose Reaction towards Selective Synthesis, *ChemSusChem*, 2014, **7**, 1833–1846.

27 T. Nash, The colorimetric estimation of formaldehyde by means of the Hantzsch reaction, *Biochem. J.*, 1953, **55**, 416–421.

28 T. Chatterjee, E. Boutin and M. Robert, Manifesto for the routine use of NMR for the liquid product analysis of aqueous CO<sub>2</sub> reduction: from comprehensive chemical shift data to formaldehyde quantification in water, *Dalton Trans.*, 2020, **49**, 4257–4265.

29 (a) M. Rauch, Z. Strater and G. Parkin, Selective Conversion of Carbon Dioxide to Formaldehyde via a Bis(silyl)acetal: Incorporation of Isotopically Labeled C<sub>1</sub> Moieties Derived from Carbon Dioxide into Organic Molecules, *J. Am. Chem. Soc.*, 2019, **141**, 17754–17762; (b) D. Zhang, C. Jarava-Barrera and S. Bontemps, Selective Reductive Dimerization of CO<sub>2</sub> into Glycolaldehyde, *ACS Catal.*, 2021, **11**, 4568–4575.

30 S. Desmons, K. Grayson-Steel, N. Nuñez-Dallos, L. Vendier, J. Hurtado, P. Clapés, R. Fauré, C. Dumon and S. Bontemps, Enantioselective Reductive Oligomerization of Carbon Dioxide into L-Erythrulose via a Chemoenzymatic Catalysis, *J. Am. Chem. Soc.*, 2021, **143**, 16274–16283.

31 T. Cai, H. Sun, J. Qiao, L. Zhu, F. Zhang, J. Zhang, Z. Tang, X. Wei, J. Yang, Q. Yuan, W. Wang, X. Yang, H. Chu, Q. Wang, C. You, H. Ma, Y. Sun, Y. Li, C. Li, H. Jiang, Q. Wang and Y. Ma, Cell-free chemoenzymatic starch synthesis from carbon dioxide, *Science*, 2021, **373**, 1523–1527.

32 S. Zhao, H.-Q. Liang, X.-M. Hu, S. Li and K. Daasbjerg, Challenges and Prospects in the Catalytic Conversion of Carbon Dioxide to Formaldehyde, *Angew. Chem., Int. Ed.*, 2022, **61**, e202204008.

33 A. Béthegnies, Y. Escudie, N. Nuñez-Dallos, L. Vendier, J. Hurtado, I. del Rosal, L. Maron and S. Bontemps, Reductive CO<sub>2</sub> Homocoupling: Synthesis of a Borylated C<sub>3</sub> Carbohydrate, *ChemCatChem*, 2019, **11**, 760–765.

34 (a) H. Maciejewski, C. Pietraszuk, P. Pawluć and B. Marciniec, *Hydrosilylation - A Comprehensive Review on Recent Advances*, Springer, Berlin, 2010; (b) B. Marciniec, Catalysis by transition metal complexes of alkene silylation–recent progress and mechanistic implications, *Coord. Chem. Rev.*, 2005, **249**, 2374–2390.



35 C. Hühn, A. Erlebach, D. Mey, L. Wondraczek and M. Sierka, Ab Initio energetics of Si-O bond cleavage, *J. Comput. Chem.*, 2017, **38**, 2349–2353.

36 (a) G. Sussfink and J. Reiner, Anionic Ruthenium Clusters as Catalysts in the Hydrosilylation of Carbon-Dioxide, *J. Organomet. Chem.*, 1981, **221**, C36–C38; (b) H. Koinuma, F. Kawakami, H. Kato and H. Hirai, Hydrosilylation of carbon dioxide catalysed by ruthenium complexes, *J. Chem. Soc., Chem. Commun.*, 1981, 213–214.

37 T. C. Eisenschmid and R. Eisenberg, The iridium complex catalyzed reduction of carbon dioxide to methoxide by alkylsilanes, *Organometallics*, 1989, **8**, 1822–1824.

38 T. Matsuo and H. Kawaguchi, From Carbon Dioxide to Methane: Homogeneous Reduction of Carbon Dioxide with Hydrosilanes Catalyzed by Zirconium–Borane Complexes, *J. Am. Chem. Soc.*, 2006, **128**, 12362–12363.

39 P. Rios, N. Curado, J. Lopez-Serrano and A. Rodriguez, Selective reduction of carbon dioxide to bis(silyl)acetal catalyzed by a PBP-supported nickel complex, *Chem. Commun.*, 2016, **52**, 2114–2117.

40 T. T. Metsänen and M. Oestreich, Temperature-Dependent Chemoselective Hydrosilylation of Carbon Dioxide to Formaldehyde or Methanol Oxidation State, *Organometallics*, 2015, **34**, 543–546.

41 S. N. Riduan, Y. Zhang and J. Y. Ying, Conversion of Carbon Dioxide into Methanol with Silanes over N-Heterocyclic Carbene Catalysts, *Angew. Chem., Int. Ed.*, 2009, **48**, 3322–3325.

42 M. L. Scheuermann, S. P. Semproni, I. Pappas and P. J. Chirik, Carbon Dioxide Hydrosilylation Promoted by Cobalt Pincer Complexes, *Inorg. Chem.*, 2014, **53**, 9463–9465.

43 M. Tolzmann, L. Schürmann, A. Hepp, W. Uhl and M. Layh, Hydrosilylation and Hydrogermylation of  $\text{CO}_2$  and  $\text{CS}_2$  by Al and Ga Functionalized Silanes and Germanes – Cooperative Reactivity with Formation of Silyl Formates and Disilylacetals, *Eur. J. Inorg. Chem.*, 2020, **2020**, 4024–4036.

44 Y. Jiang, O. Blacque, T. Fox and H. Berke, Catalytic  $\text{CO}_2$  Activation Assisted by Rhenium Hydride/ $\text{B}(\text{C}_6\text{F}_5)_3$  Frustrated Lewis Pairs–Metal Hydrides Functioning as FLP Bases, *J. Am. Chem. Soc.*, 2013, **135**, 7751–7760.

45 F. A. LeBlanc, W. E. Piers and M. Parvez, Selective Hydrosilation of  $\text{CO}_2$  to a Bis(silylacetal) Using an Anilido Bipyridyl-Ligated Organoscandium Catalyst, *Angew. Chem., Int. Ed.*, 2014, **53**, 789–792.

46 Z. Lu, H. Hausmann, S. Becker and H. A. Wegner, Aromaticity as Stabilizing Element in the Bidentate Activation for the Catalytic Reduction of Carbon Dioxide, *J. Am. Chem. Soc.*, 2015, **137**, 5332–5335.

47 N. Del Rio, M. Lopez-Reyes, A. Baceiredo, N. Saffon-Merceron, D. Lutters, T. Müller and T. Kato, N-P-Heterocyclic Germylene/ $\text{B}(\text{C}_6\text{F}_5)_3$  Adducts: A Lewis Pair with Multi-reactive Sites, *Angew. Chem., Int. Ed.*, 2017, **56**, 1365–1370.

48 L. Luconi, A. Rossin, G. Tuci, Z. Gafurov, D. M. Lyubov, A. A. Trifonov, S. Cicchi, H. Ba, C. Pham-Huu, D. Yakhvarov and G. Giambastiani, Benzoimidazole-Pyridylamido Zirconium and Hafnium Alkyl Complexes as Homogeneous Catalysts for Tandem Carbon Dioxide Hydrosilylation to Methane, *ChemCatChem*, 2019, **11**, 495–510.

49 W. Huang, T. Roisnel, V. Dorcet, C. Orione and E. Kirillov, Reduction of  $\text{CO}_2$  by Hydrosilanes in the Presence of Formamidinates of Group 13 and 12 Elements, *Organometallics*, 2020, **39**, 698–710.

50 T. González and J. J. García, Catalytic  $\text{CO}_2$  hydrosilylation with  $[\text{Mn}(\text{CO})_5\text{Br}]$  under mild reaction conditions, *Polyhedron*, 2021, **203**, 115242.

51 A. Caise, J. Hicks, M. Ángeles Fuentes, J. M. Goicoechea and S. Aldridge, Partnering a Three-Coordinate Gallium Cation with a Hydroborate Counter-Ion for the Catalytic Hydrosilylation of  $\text{CO}_2$ , *Chem.–Eur. J.*, 2021, **27**, 2138–2148.

52 K. Chang, I. del Rosal, X. Zheng, L. Maron and X. Xu, Hydrosilylative reduction of carbon dioxide by a homoleptic lanthanum aryloxide catalyst with high activity and selectivity, *Dalton Trans.*, 2021, **50**, 7804–7809.

53 S. Park, D. Bézier and M. Brookhart, An Efficient Iridium Catalyst for Reduction of Carbon Dioxide to Methane with Trialkylsilanes, *J. Am. Chem. Soc.*, 2012, **134**, 11404–11407.

54 M. Rauch and G. Parkin, Zinc and Magnesium Catalysts for the Hydrosilylation of Carbon Dioxide, *J. Am. Chem. Soc.*, 2017, **139**, 18162–18165.

55 Q. Zhang, N. Fukaya, T. Fujitani and J.-C. Choi, Carbon Dioxide Hydrosilylation to Methane Catalyzed by Zinc and Other First-Row Transition Metal Salts, *Bull. Chem. Soc. Jpn.*, 2019, **92**, 1945–1949.

56 M.-A. Courtemanche, M.-A. Legare, E. Rochette and F.-G. Fontaine, Phosphazenes: efficient organocatalysts for the catalytic hydrosilylation of carbon dioxide, *Chem. Commun.*, 2015, **51**, 6858–6861.

57 (a) B. H. Rotstein, S. H. Liang, M. S. Placzek, J. M. Hooker, A. D. Gee, F. Dolle, A. A. Wilson and N. Vasdev,  $^{11}\text{C}=\text{O}$  bonds made easily for positron emission tomography radiopharmaceuticals, *Chem. Soc. Rev.*, 2016, **45**, 4708–4726; (b) B. H. Rotstein, S. H. Liang, J. P. Holland, T. L. Collier, J. M. Hooker, A. A. Wilson and N. Vasdev,  $^{11}\text{CO}_2$  fixation: a renaissance in PET radiochemistry, *Chem. Commun.*, 2013, **49**, 5621–5629; (c) M. Ahamed, J. Verbeek, U. Funke, J. Lecina, A. Verbruggen and G. Bormans, Recent Progress in Metal Catalyzed Direct Carboxylation of Aryl Halides and Pseudo Halides Employing  $\text{CO}_2$ : Opportunities for  $^{11}\text{C}$  Radiochemistry, *ChemCatChem*, 2016, **8**, 3692–3700; (d) S. Monticelli, A. Talbot, P. Gotico, F. Caillé, O. Loreau, A. Del Vecchio, A. Malandain, A. Sallustro, W. Leibl, A. Aukauloo, F. Taran, Z. Halime and D. Audisio, Unlocking full and fast conversion in photocatalytic carbon dioxide reduction for applications in radio-carbonylation, *Nat. Commun.*, 2023, **14**, 4451; (e) A. Malandain, M. Molins, A. Hauwelle, A. Talbot, O. Loreau, T. D'Anfray, S. Goutal, N. Tournier, F. Taran, F. Caillé and D. Audisio, Carbon Dioxide Radical Anion by Photoinduced Equilibration between Formate Salts and  $[^{11}\text{C}, ^{13}\text{C}, ^{14}\text{C}]\text{CO}_2$ : Application to Carbon Isotope Radiolabeling, *J. Am. Chem. Soc.*, 2023, **145**,



16760–16770; (f) G. Destro, K. Horkka, O. Loreau, D.-A. Buisson, L. Kingston, A. Del Vecchio, M. Schou, C. S. Elmore, F. Taran, T. Cantat and D. Audisio, Transition-Metal-Free Carbon Isotope Exchange of Phenyl Acetic Acids, *Angew. Chem., Int. Ed.*, 2020, **59**, 13490–13495; (g) G. Destro, O. Loreau, E. Marcon, F. Taran, T. Cantat and D. Audisio, Dynamic Carbon Isotope Exchange of Pharmaceuticals with Labeled CO<sub>2</sub>, *J. Am. Chem. Soc.*, 2019, **141**, 780–784; (h) P. Gotico, A. Del Vecchio, D. Audisio, A. Quaranta, Z. Halime, W. Leibl and A. Aukauloo, Visible-Light-Driven Reduction of CO<sub>2</sub> to CO and Its Subsequent Valorization in Carbonylation Chemistry and <sup>13</sup>C Isotope Labeling, *ChemPhotoChem*, 2018, **2**, 715–719.

58 A. Berkefeld, W. E. Piers and M. Parvez, Tandem Frustrated Lewis Pair/Tris(pentafluorophenyl)borane-Catalyzed Deoxygenative Hydrosilylation of Carbon Dioxide, *J. Am. Chem. Soc.*, 2010, **132**, 10660–10661.

59 A. Berkefeld, W. E. Piers, M. Parvez, L. Castro, L. Maron and O. Eisenstein, Decamethylscandocinium-hydrido-(perfluorophenyl)borate: fixation and tandem tris(perfluorophenyl)borane catalysed deoxygenative hydrosilation of carbon dioxide, *Chem. Sci.*, 2013, **4**, 2152–2162.

60 F. Bertini, M. Glatz, B. Stöger, M. Peruzzini, L. F. Veiros, K. Kirchner and L. Gonsalvi, Carbon Dioxide Reduction to Methanol Catalyzed by Mn(I) PNP Pincer Complexes under Mild Reaction Conditions, *ACS Catal.*, 2019, **9**, 632–639.

61 D. S. Morris, C. Weetman, J. T. C. Wennmacher, M. Cokoja, M. Drees, F. E. Kühn and J. B. Love, Reduction of carbon dioxide and organic carbonyls by hydrosilanes catalysed by the perrhenate anion, *Catal. Sci. Technol.*, 2017, **7**, 2838–2845.

62 X. Zhang, J. Sun, G. Wei, Z. Liu, H. Yang, K. Wang and H. Fei, In Situ Generation of an N-Heterocyclic Carbene Functionalized Metal–Organic Framework by Postsynthetic Ligand Exchange: Efficient and Selective Hydrosilylation of CO<sub>2</sub>, *Angew. Chem., Int. Ed.*, 2019, **58**, 2844–2849.

63 J. Chen, L. Falivene, L. Caporaso, L. Cavallo and E. Y. X. Chen, Selective Reduction of CO<sub>2</sub> to CH<sub>4</sub> by Tandem Hydrosilylation with Mixed Al/B Catalysts, *J. Am. Chem. Soc.*, 2016, **138**, 5321–5333.

64 D. W. Beh, W. E. Piers, B. S. Gelfand and J.-B. Lin, Tandem deoxygenative hydrosilation of carbon dioxide with a cationic scandium hydridoborate and B(C<sub>6</sub>F<sub>5</sub>)<sub>3</sub>, *Dalton Trans.*, 2020, **49**, 95–101.

65 F. Huang, G. Lu, L. Zhao, H. Li and Z.-X. Wang, The Catalytic Role of N-Heterocyclic Carbene in a Metal-Free Conversion of Carbon Dioxide into Methanol: A Computational Mechanism Study, *J. Am. Chem. Soc.*, 2010, **132**, 12388–12396.

66 (a) T. Robert and M. Oestreich, Si–H Bond Activation: Bridging Lewis Acid Catalysis with Brookhart's Iridium(III) Pincer Complex and B(C<sub>6</sub>F<sub>5</sub>)<sub>3</sub>, *Angew. Chem., Int. Ed.*, 2013, **52**, 5216–5218; (b) D. J. Parks, J. M. Blackwell and W. E. Piers, Studies on the Mechanism of B(C<sub>6</sub>F<sub>5</sub>)<sub>3</sub>-Catalyzed Hydrosilation of Carbonyl Functions, *J. Org. Chem.*, 2000, **65**, 3090–3098; (c) V. Gevorgyan, M. Rubin, S. Benson, J.-X. Liu and Y. Yamamoto, A Novel B(C<sub>6</sub>F<sub>5</sub>)<sub>3</sub>-Catalyzed Reduction of Alcohols and Cleavage of Aryl and Alkyl Ethers with Hydrosilanes, *J. Org. Chem.*, 2000, **65**, 6179–6186; (d) D. J. Parks and W. E. Piers, Tris(pentafluorophenyl)boron-Catalyzed Hydrosilation of Aromatic Aldehydes, Ketones, and Esters, *J. Am. Chem. Soc.*, 1996, **118**, 9440–9441.

67 S. Fang, H. Chen and H. Wei, Insight into catalytic reduction of CO<sub>2</sub> to methane with silanes using Brookhart's cationic Ir(III) pincer complex, *RSC Adv.*, 2018, **8**, 9232–9242.

68 M. Wen, F. Huang, G. Lu and Z.-X. Wang, Density Functional Theory Mechanistic Study of the Reduction of CO<sub>2</sub> to CH<sub>4</sub> Catalyzed by an Ammonium Hydridoborate Ion Pair: CO<sub>2</sub> Activation via Formation of a Formic Acid Entity, *Inorg. Chem.*, 2013, **52**, 12098–12107.

69 P. Ríos, A. Rodríguez and J. López-Serrano, Mechanistic Studies on the Selective Reduction of CO<sub>2</sub> to the Aldehyde Level by a Bis(phosphino)boryl (PBP)-Supported Nickel Complex, *ACS Catal.*, 2016, **6**, 5715–5723.

70 T. Stahl, H. F. T. Klare and M. Oestreich, C(sp<sup>3</sup>)-F Bond Activation of CF<sub>3</sub>-Substituted Anilines with Catalytically Generated Silicon Cations: Spectroscopic Evidence for a Hydride-Bridged Ru–S Dimer in the Catalytic Cycle, *J. Am. Chem. Soc.*, 2013, **135**, 1248–1251.

71 H. H. Cramer, S. Ye, F. Neese, C. Werlé and W. Leitner, Cobalt-Catalyzed Hydrosilylation of Carbon Dioxide to the Formic Acid, Formaldehyde, and Methanol Level—How to Control the Catalytic Network?, *JACS Au*, 2021, **1**, 2058–2069.

72 (a) K. Fujiwara, S. Yasuda and T. Mizuta, Reduction of CO<sub>2</sub> to Trimethoxyboroxine with BH<sub>3</sub> in THF, *Organometallics*, 2014, **33**, 6692–6695; (b) I. Knopf and C. C. Cummins, Revisiting CO<sub>2</sub> Reduction with NaBH<sub>4</sub> under Aprotic Conditions: Synthesis and Characterization of Sodium Triformatoborohydride, *Organometallics*, 2015, **34**, 1601–1603.

73 Y. Zhao, X. Liu, L. Zheng, Y. Du, X. Shi, Y. Liu, Z. Yan, J. You and Y. Jiang, One-Pot Methylenation–Cyclization Employing Two Molecules of CO<sub>2</sub> with Arylamines and Enaminones, *J. Org. Chem.*, 2020, **85**, 912–923.

74 (a) O. Jacquet, C. Das Neves Gomes, M. Ephritikhine and T. Cantat, Recycling of Carbon and Silicon Wastes: Room Temperature Formylation of N–H Bonds Using Carbon Dioxide and Polymethylhydrosiloxane, *J. Am. Chem. Soc.*, 2012, **134**, 2934–2937; (b) C. Das Neves Gomes, O. Jacquet, C. Villiers, P. Thuéry, M. Ephritikhine and T. Cantat, A Diagonal Approach to Chemical Recycling of Carbon Dioxide: Organocatalytic Transformation for the Reductive Functionalization of CO<sub>2</sub>, *Angew. Chem., Int. Ed.*, 2012, **51**, 187–190.

75 S. Schreiner, J. Y. Yu and L. Vaska, Reversible homogeneous catalysis of carbon dioxide hydrogenation/reduction at



room temperature and low pressures, *J. Chem. Soc., Chem. Commun.*, 1988, 602–603.

76 M. Khandelwal and R. J. Wehmschulte, Deoxygenative Reduction of Carbon Dioxide to Methane, Toluene, and Diphenylmethane with  $[\text{Et}_2\text{Al}]^+$  as Catalyst, *Angew. Chem., Int. Ed.*, 2012, **51**, 7323–7326.

77 X. Frogneux, E. Blondiaux, P. Thuéry and T. Cantat, Bridging Amines with  $\text{CO}_2$ : Organocatalyzed Reduction of  $\text{CO}_2$  to Aminals, *ACS Catal.*, 2015, **5**, 3983–3987.

78 D.-Y. Zhu, L. Fang, H. Han, Y. Wang and J.-B. Xia, Reductive  $\text{CO}_2$  Fixation via Tandem C–C and C–N Bond Formation: Synthesis of Spiro-indolepyrrolidines, *Org. Lett.*, 2017, **19**, 4259–4262.

79 Y. Zhao, X. Guo, X. Ding, Z. Zhou, M. Li, N. Feng, B. Gao, X. Lu, Y. Liu and J. You, Reductive  $\text{CO}_2$  Fixation via the Selective Formation of C–C Bonds: Bridging Enaminones and Synthesis of 1,4-Dihydropyridines, *Org. Lett.*, 2020, **22**, 8326–8331.

80 W.-D. Li, J. Chen, D.-Y. Zhu and J.-B. Xia, Fe-Catalyzed Pictet-Spengler-Type Cyclization via Selective Four-Electron Reductive Functionalization of  $\text{CO}_2$ , *Chin. J. Chem.*, 2021, **39**, 614–620.

81 D.-Y. Zhu, W.-D. Li, C. Yang, J. Chen and J.-B. Xia, Transition-Metal-Free Reductive Deoxygenative Olefination with  $\text{CO}_2$ , *Org. Lett.*, 2018, **20**, 3282–3285.

82 X.-Y. Li, S.-S. Zheng, X.-F. Liu, Z.-W. Yang, T.-Y. Tan, A. Yu and L.-N. He, Waste Recycling: Ionic Liquid-Catalyzed 4-Electron Reduction of  $\text{CO}_2$  with Amines and Polymethylhydrosiloxane Combining Experimental and Theoretical Study, *ACS Sustain. Chem. Eng.*, 2018, **6**, 8130–8135.

83 Z.-J. Mu, X. Ding, Z.-Y. Chen and B.-H. Han, Zwitterionic Covalent Organic Frameworks as Catalysts for Hierarchical Reduction of  $\text{CO}_2$  with Amine and Hydrosilane, *ACS Appl. Mater. Interfaces*, 2018, **10**, 41350–41358.

84 (a) R. Köster and I. Borverbindungen, Darstellung von Bortrialkylen und ihre Reaktionen mit Olefinen, *Justus Liebigs Ann. Chem.*, 1958, **618**, 31–43; (b) H. C. Brown and G. Zweifel, Hydroboration. VII. Directive Effects in the Hydroboration of Olefins, *J. Am. Chem. Soc.*, 1960, **82**, 4708–4712; (c) H. C. Brown and B. C. S. Rao, A new technique for the conversion of olefins into organoboranes and related alcohols, *J. Am. Chem. Soc.*, 1956, **78**, 5694–5695.

85 (a) E. J. Corey, R. K. Bakshi and S. Shibata, Highly enantioselective borane reduction of ketones catalyzed by chiral oxazaborolidines. Mechanism and synthetic implications, *J. Am. Chem. Soc.*, 1987, **109**, 5551–5553; (b) E. J. Corey and C. J. Helal, Reduction of Carbonyl Compounds with Chiral Oxazaborolidine Catalysts: A New Paradigm for Enantioselective Catalysis and a Powerful New Synthetic Method, *Angew. Chem., Int. Ed.*, 1998, **37**, 1986–2012.

86 A. Suzuki, Cross-Coupling Reactions Of Organoboranes: An Easy Way To Construct C–C Bonds (Nobel Lecture), *Angew. Chem., Int. Ed.*, 2011, **50**, 6722–6737.

87 Y.-R. Luo and Editor, *Comprehensive Handbook of Chemical Bond Energies*, CRC Press, 2007.

88 S. Chakraborty, J. Zhang, J. A. Krause and H. Guan, An Efficient Nickel Catalyst for the Reduction of Carbon Dioxide with a Borane, *J. Am. Chem. Soc.*, 2010, **132**, 8872–8873.

89 F. Huang, C. Zhang, J. Jiang, Z.-X. Wang and H. Guan, How Does the Nickel Pincer Complex Catalyze the Conversion of  $\text{CO}_2$  to a Methanol Derivative? A Computational Mechanistic Study, *Inorg. Chem.*, 2011, **50**, 3816–3825.

90 S. Bontemps, L. Vendier and S. Sabo-Etienne, Borane-Mediated Carbon Dioxide Reduction at Ruthenium: Formation of  $\text{C}_1$  and  $\text{C}_2$  Compounds, *Angew. Chem., Int. Ed.*, 2012, **51**, 1671–1674.

91 S. Bontemps, L. Vendier and S. Sabo-Etienne, Ruthenium-Catalyzed Reduction of Carbon Dioxide to Formaldehyde, *J. Am. Chem. Soc.*, 2014, **136**, 4419–4425.

92 S. Desmons, Y. Zhou, D. Zhang, C. Jarava-Barrera, A. Coffinet, A. Simonneau, L. Vendier, G. Luo and S. Bontemps,  $\text{CO}_2$  Hydroboration: Impact of the Boryl Moieties on the Reactivity of Four Bis(boryl)acetal Compounds toward 2,6-Diisopropylaniline, *Eur. J. Org. Chem.*, 2023, **26**, e202300525.

93 G. Jin, C. G. Werncke, Y. Escudié, S. Sabo-Etienne and S. Bontemps, Iron-Catalyzed Reduction of  $\text{CO}_2$  into Methylene: Formation of C–N, C–O, and C–C Bonds, *J. Am. Chem. Soc.*, 2015, **137**, 9563–9566.

94 L. J. Murphy, H. Hollenhorst, R. McDonald, M. Ferguson, M. D. Lumsden and L. Turculet, Selective Ni-Catalyzed Hydroboration of  $\text{CO}_2$  to the Formaldehyde Level Enabled by New PSiP Ligation, *Organometallics*, 2017, **36**, 3709–3720.

95 H.-W. Suh, L. M. Guard and N. Hazari, Synthesis and reactivity of a masked PSiP pincer supported nickel hydride, *Polyhedron*, 2014, **84**, 37–43.

96 R. Pal, T. L. Groy and R. J. Trovitch, Conversion of Carbon Dioxide to Methanol Using a C–H Activated Bis(imino) pyridine Molybdenum Hydroboration Catalyst, *Inorg. Chem.*, 2015, **54**, 7506–7515.

97 M. R. Espinosa, D. J. Charboneau, A. Garcia de Oliveira and N. Hazari, Controlling Selectivity in the Hydroboration of Carbon Dioxide to the Formic Acid, Formaldehyde, and Methanol Oxidation Levels, *ACS Catal.*, 2019, **9**, 301–314.

98 M. D. Anker, M. Arrowsmith, P. Bellham, M. S. Hill, G. Kociok-Kohn, D. J. Liptrot, M. F. Mahon and C. Weetman, Selective reduction of  $\text{CO}_2$  to a methanol equivalent by  $\text{B}(\text{C}_6\text{F}_5)_3$ -activated alkaline earth catalysis, *Chem. Sci.*, 2014, **5**, 2826–2830.

99 L. Li, H. Zhu, L. Liu, D. Song and M. Lei, A Hydride-Shuttle Mechanism for the Catalytic Hydroboration of  $\text{CO}_2$ , *Inorg. Chem.*, 2018, **57**, 3054–3060.

100 (a) Y. Yang, L. Yan, Q. Xie, Q. Liang and D. Song, Zwitterionic indenylammonium with carbon-centred reactivity towards reversible  $\text{CO}_2$  binding and catalytic reduction, *Org. Biomol. Chem.*, 2017, **15**, 2240–2245; (b) T. Janes, K. M. Osten, A. Pantaleo, E. Yan, Y. Yang and D. Song, Insertion of  $\text{CO}_2$  into the carbon-boron bond of a boronic ester ligand, *Chem. Commun.*, 2016, **52**, 4148–



4151; (c) Y. Yang, M. Xu and D. Song, Organocatalysts with carbon-centered activity for  $\text{CO}_2$  reduction with boranes, *Chem. Commun.*, 2015, **51**, 11293–11296; (d) C. Weetman, A. Porzelt, P. Bag, F. Hanusch and S. Inoue, Dialumenes – aryl vs. silyl stabilisation for small molecule activation and catalysis, *Chem. Sci.*, 2020, **11**, 4817–4827; (e) J. Fan, J.-Q. Mah, M.-C. Yang, M.-D. Su and C.-W. So, A N-Phosphinoamidinato NHC-Diborene Catalyst for Hydroboration, *J. Am. Chem. Soc.*, 2021, **143**, 4993–5002.

101 C. Das Neves Gomes, E. Blondiaux, P. Thuéry and T. Cantat, Metal-Free Reduction of  $\text{CO}_2$  with Hydroboranes: Two Efficient Pathways at Play for the Reduction of  $\text{CO}_2$  to Methanol, *Chem.-Eur. J.*, 2014, **20**, 7098–7106.

102 A. Aloisi, J.-C. Berthet, C. Genre, P. Thuéry and T. Cantat, Complexes of the tripodal phosphine ligands  $\text{PhSi}(\text{XPPH}_2)_3$  ( $\text{X} = \text{CH}_2, \text{O}$ ): synthesis, structure and catalytic activity in the hydroboration of  $\text{CO}_2$ , *Dalton Trans.*, 2016, **45**, 14774–14788.

103 A. Ramos, A. Antinolo, F. Carrillo-Hermosilla, R. Fernandez-Galan, A. Rodriguez-Dieguet and D. Garcia-Vivo, Carbodiimides as catalysts for the reduction of  $\text{CO}_2$  with boranes, *Chem. Commun.*, 2018, **54**, 4700–4703.

104 A. Ramos, A. Antinolo, F. Carrillo-Hermosilla and R. Fernández-Galán,  $\text{Ph}_2\text{PCH}_2\text{CH}_2\text{B}(\text{C}_8\text{H}_{14})$  and Its Formaldehyde Adduct as Catalysts for the Reduction of  $\text{CO}_2$  with Hydroboranes, *Inorg. Chem.*, 2020, **59**, 9998–10012.

105 S. C. Sau, R. Bhattacharjee, P. K. Vardhanapu, G. Vijaykumar, A. Datta and S. K. Mandal, Metal-Free Reduction of  $\text{CO}_2$  to Methoxyborane under Ambient Conditions through Borondiformate Formation, *Angew. Chem., Int. Ed.*, 2016, **55**, 15147–15151.

106 X. Wang, K. Chang and X. Xu, Hydroboration of carbon dioxide enabled by molecular zinc dihydrides, *Dalton Trans.*, 2020, **49**, 7324–7327.

107 M. Frick, J. Horn, H. Wadeppohl, E. Kaifer and H. J. Himmel, Catalyst-Free Hydroboration of  $\text{CO}_2$  With a Nucleophilic Diborane(4), *Chem.-Eur. J.*, 2018, **24**, 16983–16986.

108 J. Li, C. G. Daniliuc, G. Kehr and G. Erker, Preparation of the Borane (Fmes) $\text{BH}_2$  and its Utilization in the FLP Reduction of Carbon Monoxide and Carbon Dioxide, *Angew. Chem. Int. Ed.*, 2019, **58**, 6737–6741.

109 (a) R. Declercq, G. Bouhadir, D. Bourissou, M.-A. Légaré, M.-A. Courtemanche, K. S. Nahi, N. Bouchard, F.-G. Fontaine and L. Maron, Hydroboration of Carbon Dioxide using Ambiphilic Phosphine-Borane Catalysts: On the Role of the Formaldehyde Adduct, *ACS Catal.*, 2015, **5**, 2513–2520; (b) S. Y. F. Ho, C.-W. So, N. Saffon-Merceron and N. Mezailles, Formation of a zwitterionic boronium species from the reaction of a stable carbenoid with borane:  $\text{CO}_2$  reduction, *Chem. Commun.*, 2015, **51**, 2107–2110.

110 M.-A. Courtemanche, A. P. Pulis, E. Rochette, M.-A. Legare, D. W. Stephan and F.-G. Fontaine, Intramolecular B/N frustrated Lewis pairs and the hydrogenation of carbon dioxide, *Chem. Commun.*, 2015, **51**, 9797–9800.

111 J. H. W. LaFortune, Z. W. Qu, K. L. Bamford, A. Trofimova, S. A. Westcott and D. W. Stephan, Double Phosphinoboration of  $\text{CO}_2$ : A Facile Route to Diphospho-Ureas, *Chem.-Eur. J.*, 2019, **25**, 12063–12067.

112 S. Bontemps and S. Sabo-Etienne, Trapping Formaldehyde in the Homogeneous Catalytic Reduction of Carbon Dioxide, *Angew. Chem., Int. Ed.*, 2013, **52**, 10253–10255.

113 (a) C. Dong, M. Ji, X. Yang, J. Yao and H. Chen, Reaction Mechanisms of  $\text{CO}_2$  Reduction to Formaldehyde Catalyzed by Hourglass Ru, Fe, and Os Complexes: A Density Functional Theory Study, *Catalysts*, 2017, **7**, 5; (b) F. Huang, Q. Wang, J. Guo, M. Wen and Z.-X. Wang, Computational mechanistic study of Ru-catalyzed  $\text{CO}_2$  reduction by pinacolborane revealing the  $\sigma$ - $\pi$  coupling mechanism for  $\text{CO}_2$  decarbonylation, *Dalton Trans.*, 2018, **47**, 4804–4819.

114 A. Caise, D. Jones, E. L. Kolychev, J. Hicks, J. M. Goicoechea and S. Aldridge, On the Viability of Catalytic Turnover via Al–O/B–H Metathesis: The Reactivity of  $\beta$ -Diketiminate Aluminium Hydrides towards  $\text{CO}_2$  and Boranes, *Chem.-Eur. J.*, 2018, **24**, 13624–13635.

115 N. Ma, C. Tu, Q. Xu, W. Guo, J. Zhang and G. Zhang, Computational study on the mechanism of hydroboration of  $\text{CO}_2$  catalysed by POCOP pincer nickel thiolate complexes: concerted catalysis and hydride transfer by a shuttle, *Dalton Trans.*, 2021, **50**, 2903–2914.

116 (a) X. Wan, M. Li and R.-Z. Liao, Ligand-assisted Hydride Transfer: A Pivotal Step for  $\text{CO}_2$  Hydroboration Catalyzed by a Mononuclear Mn(I) PNP Complex, *Chem.-Asian J.*, 2021, **16**, 2529–2537; (b) C. Erken, A. Kaithal, S. Sen, T. Weyhermüller, M. Hölscher, C. Werlé and W. Leitner, Manganese-catalyzed hydroboration of carbon dioxide and other challenging carbonyl groups, *Nat. Commun.*, 2018, **9**, 4521.

117 H. Sabet-Sarvestani, M. Izadyar and H. Eshghi, Theoretical evaluation of the organocatalytic behavior of the negatively charged carbon atom in a fused five-member ring in carbon dioxide transformation to methanol, *Energy*, 2017, **134**, 493–503.

118 (a) M.-A. Courtemanche, M.-A. Légaré, L. Maron and F.-G. Fontaine, Reducing  $\text{CO}_2$  to Methanol Using Frustrated Lewis Pairs: On the Mechanism of Phosphine-Borane-Mediated Hydroboration of  $\text{CO}_2$ , *J. Am. Chem. Soc.*, 2014, **136**, 10708–10717; (b) M.-A. Courtemanche, M.-A. Légaré, L. Maron and F.-G. Fontaine, A Highly Active Phosphine-Borane Organocatalyst for the Reduction of  $\text{CO}_2$  to Methanol Using Hydroboranes, *J. Am. Chem. Soc.*, 2013, **135**, 9326–9329.

119 Z.-W. Qu, H. Zhu and S. Grimme, Frustrated Lewis Pair Catalyzed Reduction of Carbon Dioxide Using Hydroboranes: New DFT Mechanistic Insights, *ChemCatChem*, 2020, **12**, 3656–3660.

120 T. Wang and D. W. Stephan, Phosphine catalyzed reduction of  $\text{CO}_2$  with boranes, *Chem. Commun.*, 2014, **50**, 7007–7010.

121 Y. C. A. Sokolovicz, O. Nieto Faza, D. Specklin, B. Jacques, C. S. López, J. H. Z. dos Santos, H. S. Schrekker and S. Dagorne, Acetate-catalyzed hydroboration of  $\text{CO}_2$  for



the selective formation of methanol-equivalent products, *Catal. Sci. Technol.*, 2020, **10**, 2407–2414.

122 Z. M. Heiden and A. P. Lathem, Establishing the Hydride Donor Abilities of Main Group Hydrides, *Organometallics*, 2015, **34**, 1818–1827.

123 H. Gao, J. Jia, C.-H. Tung and W. Wang, Iron-Catalyzed Selective Hydroboration of  $\text{CO}_2$  by Cooperative B–H Bond Activation, *Organometallics*, 2023, **42**, 944–951.

124 W. Huadsai, M. Westerhausen and S. Bontemps, Alkaline Earth Catalyzed  $\text{CO}_2$  Hydroboration into Acetal Derivatives Leading to C–S Bond Formation, *Organometallics*, 2023, **42**, 2921–2926.

125 A. Butlerow, Formation synthétique d'une substance sucrée, *Cr. Acad. Sci.*, 1861, **53**, 145–147.

126 J. Henrique Teles, J.-P. Melder, K. Ebel, R. Schneider, E. Gehrer, W. Harder, S. Brode, D. Enders, K. Breuer and G. Raabe, The Chemistry of Stable Carbenes. Part 2. Benzoin-type condensations of formaldehyde catalyzed by stable carbenes, *Helv. Chim. Acta*, 1996, **79**, 61–83.

127 A. M. Fajardo, N. Queyriaux, A. Camy, L. Vendier, M. Grellier, I. del Rosal, L. Maron and S. Bontemps, A Masked Form of an O-Borylated Breslow Intermediate for the Diastereoselective FLP-Type Activation of Aldehydes, *Chem.-Eur. J.*, 2022, **28**, e202104122.

128 (a) I. V. Delidovich, A. N. Simonov, O. P. Pestunova and V. N. Parmon, Catalytic condensation of glycolaldehyde and glyceraldehyde with formaldehyde in neutral and weakly alkaline aqueous media: Kinetics and mechanism, *Kinet. Catal.*, 2009, **50**, 297–303; (b) J. Castells, F. Geijo and F. López-Calahorra, The “formoin reaction” : A promising entry to carbohydrates from formaldehyde, *Tetrahedron Lett.*, 1980, **21**, 4517–4520.

129 J. J. A. G. Kamps, R. J. Hopkinson, C. J. Schofield and T. D. W. Claridge, How formaldehyde reacts with amino acids, *Commun. Chem.*, 2019, **2**, 126.

130 (a) T. Zhou, J. J. Vallooran, S. Assenza, A. Szekrenyi, P. Clapés and R. Mezzenga, Efficient Asymmetric Synthesis of Carbohydrates by Aldolase Nano-Confined in Lipidic Cubic Mesophases, *ACS Catal.*, 2018, **8**, 5810–5815; (b) A. Szekrenyi, X. Garrabou, T. Parella, J. Joglar, J. Bujons and P. Clapés, Asymmetric Assembly of Aldose Carbohydrates from Formaldehyde and Glycolaldehyde by Tandem Biocatalytic Aldol Reactions, *Nat. Chem.*, 2015, **7**, 724–729; (c) J. A. Castillo, C. Guérard-Hélaine, M. Gutiérrez, X. Garrabou, M. Sancelme, M. Schürmann, T. Inoue, V. Hélaine, F. Charmantray, T. Gefflaut, L. Hecquet, J. Joglar, P. Clapés, G. A. Sprenger and M. Lemaire, A Mutant D-Fructose-6-Phosphate Aldolase (Ala129Ser) with Improved Affinity towards Dihydroxyacetone for the Synthesis of Polyhydroxylated Compounds, *Adv. Synth. Catal.*, 2010, **352**, 1039–1046; (d) S. Güner, V. Wegat, A. Pick and V. Sieber, Design of a synthetic enzyme cascade for the *in vitro* fixation of a C<sub>1</sub> carbon source to a functional C<sub>4</sub> sugar, *Green Chem.*, 2021, **23**, 6583–6590; (e) T. Li, Z. Tang, H. Wei, Z. Tan, P. Liu, J. Li, Y. Zheng, J. Lin, W. Liu, H. Jiang, H. Liu, L. Zhu and Y. Ma, Totally atom-economical synthesis of lactic acid from formaldehyde: combined bio-carboligation and chemo-rearrangement without the isolation of intermediates, *Green Chem.*, 2020, **22**, 6809–6814; (f) J. B. Siegel, A. L. Smith, S. Poust, A. J. Wargacki, A. Bar-Even, C. Louw, B. W. Shen, C. B. Eiben, H. M. Tran, E. Noor, J. L. Gallaher, J. Bale, Y. Yoshikuni, M. H. Gelb, J. D. Keasling, B. L. Stoddard, M. E. Lidstrom and D. Baker, Computational Protein Design Enables a Novel one-Carbon Assimilation Pathway, *Proc. Natl. Acad. Sci. U. S. A.*, 2015, **112**, 3704–3709; (g) S. Poust, J. Piety, A. Bar-Even, C. Louw, D. Baker, J. D. Keasling and J. B. Siegel, Mechanistic Analysis of an Engineered Enzyme that Catalyzes the Formose Reaction, *ChemBioChem*, 2015, **16**, 1950–1954.

131 X. Garrabou, J. A. Castillo, C. Guérard-Hélaine, T. Parella, J. Joglar, M. Lemaire and P. Clapés, Asymmetric Self- and Cross-Aldol Reactions of Glycolaldehyde Catalyzed by D-Fructose-6-phosphate Aldolase, *Angew. Chem., Int. Ed.*, 2009, **121**, 5629–5633.

132 J. Yang, S. Sun, Y. Men, Y. Zeng, Y. Zhu, Y. Sun and Y. Ma, Transformation of Formaldehyde into Functional Sugars via Multi-Enzyme Stepwise Cascade Catalysis, *Catal. Sci. Technol.*, 2017, **7**, 3459–3463.

133 J.-C. Berthet and M. Ephritikhine, Reactions of the uranium (IV) hydride (C<sub>5</sub>H<sub>4</sub>SiMe<sub>3</sub>)<sub>3</sub>UH including the first transformation : 2 [M]–H + CO<sub>2</sub> → [M]–O–CH<sub>2</sub>–O–[M], *New J. Chem.*, 1992, **16**, 767–768.

134 (a) N. E. Schlörer, E. J. Cabrita and S. Berger, Characterization of Reactive Intermediates by Diffusion-Ordered NMR Spectroscopy: A Snapshot of the Reaction of <sup>13</sup>CO<sub>2</sub> with [Cp<sub>2</sub>Zr(Cl)H], *Angew. Chem., Int. Ed.*, 2002, **41**, 107–109; (b) N. E. Schlörer and S. Berger, First Spectroscopical Evidence of a Dioxomethylene Intermediate in the Reaction of CO<sub>2</sub> with Cp<sub>2</sub>Zr(H)Cl: A <sup>13</sup>C NMR Study, *Organometallics*, 2001, **20**, 1703–1704.

135 (a) A. Mendiratta, J. S. Figueroa and C. C. Cummins, Synthesis of a four-coordinate titanium(iv) oxoanion via deprotonation and decarbonylation of complexed formate, *Chem. Commun.*, 2005, 3403–3405; (b) M. A. Rankin and C. C. Cummins, Carbon Dioxide Reduction by Terminal Tantalum Hydrides: Formation and Isolation of Bridging Methylene Diolate Complexes, *J. Am. Chem. Soc.*, 2010, **132**, 10021–10023.

136 J. Ballmann, F. Pick, L. Castro, M. D. Fryzuk and L. Maron, Reduction of Carbon Dioxide Promoted by a Dinuclear Tantalum Tetrahydride Complex, *Inorg. Chem.*, 2013, **52**, 1685–1687.

137 O. Tardif, D. Hashizume and Z. Hou, Hydrogenation of Carbon Dioxide and Aryl Isocyanates by a Tetranuclear Tetrahydrido Yttrium Complex. Isolation, Structures, and CO<sub>2</sub> Insertion Reactions of Methylene Diolate and  $\mu$ 3-Oxo Yttrium Complexes, *J. Am. Chem. Soc.*, 2004, **126**, 8080–8081.

138 (a) K.-C. Lau, B. J. Petro, S. Bontemps and R. F. Jordan, Comparative Reactivity of Zr- and Pd-Alkyl Complexes with Carbon Dioxide, *Organometallics*, 2013, **32**, 6895–6898; (b) M. Hill and O. F. Wendt, Reactivity of Carbon



Dioxide toward Zirconocene Cations, *Organometallics*, 2005, **24**, 5772–5775; (c) N. Hazari and J. E. Heimann, Carbon Dioxide Insertion into Group 9 and 10 Metal-Element  $\sigma$  Bonds, *Inorg. Chem.*, 2017, **56**(22), 13655–13678; (d) A. P. Deziel, M. R. Espinosa, L. Pavlovic, D. J. Charboneau, N. Hazari, K. H. Hopmann and B. Q. Mercado, Ligand and solvent effects on CO<sub>2</sub> insertion into group 10 metal alkyl bonds, *Chem. Sci.*, 2022, **13**, 2391–2404.

139 (a) S. Gambarotta, S. Strologo, C. Floriani, A. Chiesi-Villa and C. Guastini, Stepwise reduction of carbon dioxide to formaldehyde and methanol: reactions of carbon dioxide and carbon dioxide like molecules with hydridochlorobis(cyclopentadienyl)zirconium(IV), *J. Am. Chem. Soc.*, 1985, **107**, 6278–6282; (b) G. Fachinetti, C. Floriani and S. Pucci, Stoichiometric reduction of CO and CO<sub>2</sub> to methanol: evidence for carbon monoxide insertion into zirconium–hydrogen bond, *J. Chem. Soc., Chem. Commun.*, 1978, 269–270; (c) J. A. Labinger, Titanium, zirconium and hafnium: Annual survey covering the year 1976, *J. Organomet. Chem.*, 1977, **138**, 185–210; (d) G. Fachinetti, C. Floriani, A. Chiesi-Villa and C. Guastini, Carbon dioxide activation. Deoxygenation and disproportionation of carbon dioxide promoted by bis(cyclopentadienyl)titanium and -zirconium derivatives. A novel bonding mode of the carbonato and a trimer of the zirconyl unit, *J. Am. Chem. Soc.*, 1979, **101**, 1767–1775.

140 D. Spencer and T. Henshall, The Kinetics and Mechanism of the Reaction of Formaldehyde with Dimedone. Part I, *J. Am. Chem. Soc.*, 1955, **77**, 1943–1948.

141 C. C. Chong and R. Kinjo, Hydrophosphination of CO<sub>2</sub> and Subsequent Formate Transfer in the 1,3,2-Diazaphospholene-Catalyzed N-Formylation of Amines, *Angew. Chem., Int. Ed.*, 2015, **54**, 12116–12120.

142 D. Gudat, in *Encyclopedia of Inorganic and Bioinorganic Chemistry*, 2018, pp. 1–23, DOI: [10.1002/9781119951438.eibc2642](https://doi.org/10.1002/9781119951438.eibc2642).

143 J. Wei, R. Yao, Y. Han, Q. Ge and J. Sun, Towards the development of the emerging process of CO<sub>2</sub> heterogenous hydrogenation into high-value unsaturated heavy hydrocarbons, *Chem. Soc. Rev.*, 2021, **50**, 10764–10805.

144 M. M. T. Khan, S. B. Halligudi and S. Shukla, Reduction of CO<sub>2</sub> by molecular hydrogen to formic acid and formaldehyde and their decomposition to CO and H<sub>2</sub>O, *J. Mol. Catal.*, 1989, **57**, 47–60.

145 D.-K. Lee, D.-S. Kim and S.-W. Kim, Selective formation of formaldehyde from carbon dioxide and hydrogen over PtCu/SiO<sub>2</sub>, *Appl. Organomet. Chem.*, 2001, **15**, 148–150.

146 S. Carenco, C.-H. Wu, A. Shavorskiy, S. Alayoglu, G. A. Somorjai, H. Bluhm and M. Salmeron, Synthesis and Structural Evolution of Nickel–Cobalt Nanoparticles Under H<sub>2</sub> and CO<sub>2</sub>, *Small*, 2015, **11**, 3045–3053.

147 F. L. Chan, G. Altinkaya, N. Fung and A. Tanksale, Low temperature hydrogenation of carbon dioxide into formaldehyde in liquid media, *Catal. Today*, 2018, **309**, 242–247.

148 L. Deng, X. Liu, J. Xu, Z. Zhou, S. Feng, Z. Wang and M. Xu, Transfer hydrogenation of CO<sub>2</sub> into formaldehyde from aqueous glycerol heterogeneously catalyzed by Ru bound to LDH, *Chem. Commun.*, 2021, **57**, 5167–5170.

149 U. Kleeberg and W. Klinger, Sensitive formaldehyde determination with NASH's reagent and a 'tryptophan reaction', *J. Pharmacol. Methods*, 1982, **8**, 19–31.

150 J. Zhang, C. Xing, B. Tiwari and Y. R. Chi, Catalytic Activation of Carbohydrates as Formaldehyde Equivalents for Stetter Reaction with Enones, *J. Am. Chem. Soc.*, 2013, **135**, 8113–8116.

151 (a) K. Thenert, K. Beydoun, J. Wiesenthal, W. Leitner and J. Klankermayer, Ruthenium-Catalyzed Synthesis of Dialkoxymethane Ethers Utilizing Carbon Dioxide and Molecular Hydrogen, *Angew. Chem., Int. Ed.*, 2016, **55**, 12266–12269; (b) B. G. Schiewek and J. Klankermayer, Tailor-made Molecular Cobalt Catalyst System for the Selective Transformation of Carbon Dioxide to Dialkoxymethane Ethers, *Angew. Chem., Int. Ed.*, 2017, **56**, 10854–10857.

152 (a) F. A. Long and D. McIntyre, Acid-catalyzed Hydrolysis of Methylal. II. Kinetic and Equilibrium Salt Effects and Correlation with H<sub>0</sub>, *J. Am. Chem. Soc.*, 1954, **76**, 3243–3247; (b) D. McIntyre and F. A. Long, Acid-catalyzed Hydrolysis of Methylal. I. Influence of Strong Acids and Correlation with Hammett Acidity Function, *J. Am. Chem. Soc.*, 1954, **76**, 3240–3242.

153 (a) S. Dabral and T. Schaub, The Use of Carbon Dioxide (CO<sub>2</sub>) as a Building Block in Organic Synthesis from an Industrial Perspective, *Adv. Synth. Catal.*, 2019, **361**, 223–246; (b) Z. Wei, X. Tian, M. Bender, M. Beller and H. Jiao, Mechanisms of CoII and Acid Jointly Catalyzed Domino Conversion of CO<sub>2</sub>, H<sub>2</sub>, and CH<sub>3</sub>OH to Dialkoxymethane: A DFT Study, *ACS Catal.*, 2021, 6908–6919.

154 M. Siebert, M. Seibicke, A. F. Siegle, S. Kräh and O. Trapp, Selective Ruthenium-Catalyzed Transformation of Carbon Dioxide: An Alternative Approach toward Formaldehyde, *J. Am. Chem. Soc.*, 2019, **141**, 334–341.

155 M. Siebert, G. Krennrich, M. Seibicke, A. F. Siegle and O. Trapp, Identifying high-performance catalytic conditions for carbon dioxide reduction to dimethoxymethane by multivariate modelling, *Chem. Sci.*, 2019, **10**, 10466–10474.

156 M. Seibicke, M. Siebert, A. F. Siegle, S. M. Gutenthaler and O. Trapp, Application of Hetero-Triphos Ligands in the Selective Ruthenium-Catalyzed Transformation of Carbon Dioxide to the Formaldehyde Oxidation State, *Organometallics*, 2019, **38**, 1809–1814.

157 R. Konrath, K. Sekine, I. Jevtoklj, R. A. Paciello, A. S. K. Hashmi and T. Schaub, Performance enhancing additives for reusable ruthenium-triphos catalysts in the reduction of CO<sub>2</sub> to dimethoxymethane, *Green Chem.*, 2020, **22**, 6464–6470.

158 K. Beydoun and J. Klankermayer, Ruthenium-Catalyzed Synthesis of Cyclic and Linear Acetals by the Combined Utilization of CO<sub>2</sub>, H<sub>2</sub>, and Biomass Derived Diols, *Chem.-Eur. J.*, 2019, **25**, 11412–11415.



159 C. A. Huff and M. S. Sanford, Cascade Catalysis for the Homogeneous Hydrogenation of  $\text{CO}_2$  to Methanol, *J. Am. Chem. Soc.*, 2011, **133**, 18122–18125.

160 N. M. Rezayee, C. A. Huff and M. S. Sanford, Tandem Amine and Ruthenium-Catalyzed Hydrogenation of  $\text{CO}_2$  to Methanol, *J. Am. Chem. Soc.*, 2015, **137**, 1028–1031.

161 M. Leopold, M. Siebert, A. F. Siegle and O. Trapp, Reaction Network Analysis of the Ruthenium-Catalyzed Reduction of Carbon Dioxide to Dimethoxymethane, *ChemCatChem*, 2021, **13**, 2807–2814.

162 J. D. Erickson, A. Z. Preston, J. C. Linehan and E. S. Wiedner, Enhanced Hydrogenation of Carbon Dioxide to Methanol by a Ruthenium Complex with a Charged Outer-Coordination Sphere, *ACS Catal.*, 2020, 7419–7423.

163 (a) S. Wesselbaum, V. Moha, M. Meuresch, S. Brosinski, K. M. Thenert, J. Kothe, T. vom Stein, U. Englert, M. Holscher, J. Klankermayer and W. Leitner, Hydrogenation of carbon dioxide to methanol using a homogeneous ruthenium-Triphos catalyst: from mechanistic investigations to multiphase catalysis, *Chem. Sci.*, 2015, **6**, 693–704; (b) S. Wesselbaum, T. vom Stein, J. Klankermayer and W. Leitner, Hydrogenation of Carbon Dioxide to Methanol by Using a Homogeneous Ruthenium-Phosphine Catalyst, *Angew. Chem., Int. Ed.*, 2012, **51**, 7499–7502; (c) K. Beydoun, G. Ghattas, K. Thenert, J. Klankermayer and W. Leitner, Ruthenium-Catalyzed Reductive Methylation of Imines Using Carbon Dioxide and Molecular Hydrogen, *Angew. Chem., Int. Ed.*, 2014, **53**, 11010–11014; (d) K. Beydoun, T. vom Stein, J. Klankermayer and W. Leitner, Ruthenium-Catalyzed Direct Methylation of Primary and Secondary Aromatic Amines Using Carbon Dioxide and Molecular Hydrogen, *Angew. Chem., Int. Ed.*, 2013, **52**, 9554–9557; (e) Y. Li, T. Yan, K. Junge and M. Beller, Catalytic Methylation of C–H Bonds Using  $\text{CO}_2$  and  $\text{H}_2$ , *Angew. Chem., Int. Ed.*, 2014, **126**, 10644–10648; (f) Y. Li, I. Sorribes, T. Yan, K. Junge and M. Beller, Selective Methylation of Amines with Carbon Dioxide and  $\text{H}_2$ , *Angew. Chem., Int. Ed.*, 2013, **52**, 12156–12160.

164 A. N. Simonov, L. G. Matvienko, O. P. Pestunova, V. N. Parmon, N. A. Komandrova, V. A. Denisenko and V. E. Vas'kovskii, Selective synthesis of erythrulose and 3-pentulose from formaldehyde and dihydroxyacetone catalyzed by phosphates in a neutral aqueous medium, *Kinet. Catal.*, 2007, **48**, 550–555.

165 E. Boutin and M. Robert, Molecular Electrochemical Reduction of  $\text{CO}_2$  beyond Two Electrons, *Trends Chem.*, 2021, **3**, 359–372.

166 (a) H. Nagao, T. Mizukawa and K. Tanaka, Carbon–Carbon Bond Formation in the Electrochemical Reduction of Carbon Dioxide Catalyzed by a Ruthenium Complex, *Inorg. Chem.*, 1994, **33**, 3415–3420; (b) N. Hirotaka, M. Tetsunori and T. Koji, Carbon–Carbon Bond Formation in Multi-electron Reduction of Carbon Dioxide Catalyzed by  $[\text{Ru}(\text{bpy})(\text{trpy})(\text{CO})]^{2+}$  ( $\text{bpy} = 2,2'\text{-bipyridine}$ ;  $\text{trpy} = 2,2':6',2''\text{-terpyridine}$ ), *Chem. Lett.*, 1993, **22**, 955–958.

167 D. Xiang, D. Magana and R. B. Dyer,  $\text{CO}_2$  Reduction Catalyzed by Mercaptopteridine on Glassy Carbon, *J. Am. Chem. Soc.*, 2014, **136**, 14007–14010.

168 M. Girardi, S. Blanchard, S. Griveau, P. Simon, M. Fontecave, F. Bedioui and A. Proust, Electro-Assisted Reduction of  $\text{CO}_2$  to CO and Formaldehyde by  $(\text{TOA})_6[\alpha\text{-SiW}_{11}\text{O}_{39}\text{Co}(\text{L})]$  Polyoxometalate, *Eur. J. Inorg. Chem.*, 2015, **2015**, 3642–3648.

169 S. Gonglach, S. Paul, M. Haas, F. Pillwein, S. S. Sreejith, S. Barman, R. De, S. Müllegger, P. Gerschel, U.-P. Apfel, H. Coskun, A. Aljabour, P. Stadler, W. Schöfberger and S. Roy, Molecular cobalt corrole complex for the heterogeneous electrocatalytic reduction of carbon dioxide, *Nat. Commun.*, 2019, **10**, 3864.

170 J. A. Ramos Sende, C. R. Arana, L. Hernandez, K. T. Potts, M. Keshevarz-K and H. D. Abruna, Electrocatalysis of  $\text{CO}_2$  Reduction in Aqueous Media at Electrodes Modified with Electropolymerized Films of Vinylterpyridine Complexes of Transition Metals, *Inorg. Chem.*, 1995, **34**, 3339–3348.

171 K. Kusuda, R. Ishihara, H. Yamaguchi and I. Izumi, Electrochemical investigation of thin films of cobalt phthalocyanine and cobalt-4,4',4'',4'''-tetracarboxyphthalocyanine and the reduction of carbon monoxide, formic acid and formaldehyde mediated by the  $\text{Co}(\text{I})$  complexes, *Electrochim. Acta*, 1986, **31**, 657–663.

172 E. Boutin, A. Salamé, L. Merakeb, T. Chatterjee and M. Robert, On the Existence and Role of Formaldehyde During Aqueous Electrochemical Reduction of Carbon Monoxide to Methanol by Cobalt Phthalocyanine, *Chem.–Eur. J.*, 2022, **28**, e202200697.

173 A. Singh, A. Zamader, R. Khakpour, K. Laasonen, M. Busch and M. Robert, Molecular electrochemical catalysis of  $\text{CO}_2$  to-formaldehyde conversion with a Cobalt complex, *J. Am. Chem. Soc.*, 2024, **146**(32), 22129–22133.

174 (a) K. Nakata, T. Ozaki, C. Terashima, A. Fujishima and Y. Einaga, High-Yield Electrochemical Production of Formaldehyde from  $\text{CO}_2$  and Seawater, *Angew. Chem., Int. Ed.*, 2014, **53**, 871–874; (b) D. Luo, S. Liu, K. Nakata and A. Fujishima, Electrochemical reduction of  $\text{CO}_2$  and degradation of KHP on boron-doped diamond electrodes in a simultaneous and enhanced process, *Chin. Chem. Lett.*, 2019, **30**, 509–512.

175 J. Bin Yeo, J. Ho Jang, Y. In Jo, J. Woo Koo and K. Tae Nam, Paired Electrosynthesis of Formaldehyde Derivatives from  $\text{CO}_2$  Reduction and Methanol Oxidation, *Angew. Chem., Int. Ed.*, 2024, **63**, e202316020.

176 (a) M. Shibata and N. Furuya, Electrochemical synthesis of urea at gas-diffusion electrodes: Part VI. Simultaneous reduction of carbon dioxide and nitrite ions with various metallophthalocyanine catalysts, *J. Electroanal. Chem.*, 2001, **507**, 177–184; (b) M. Shibata, K. Yoshida and N. Furuya, Electrochemical synthesis of urea on reduction of carbon dioxide with nitrate and nitrite ions using Cu-loaded gas-diffusion electrode, *J. Electroanal. Chem.*, 1995, **387**, 143–145.



177 Y. Wu, Z. Jiang, Z. Lin, Y. Liang and H. Wang, Direct electrosynthesis of methylamine from carbon dioxide and nitrate, *Nat. Sustain.*, 2021, **4**, 725–730.

178 (a) B. Kumar, M. Llorente, J. Froehlich, T. Dang, A. Sathrum and C. P. Kubiak, Photochemical and Photoelectrochemical Reduction of CO<sub>2</sub>, *Annu. Rev. Phys. Chem.*, 2012, **63**, 541–569; (b) J. Wu, Y. Huang, W. Ye and Y. Li, CO<sub>2</sub> Reduction: From the Electrochemical to Photochemical Approach, *Adv. Sci.*, 2017, **4**, 1700194; (c) A. U. Pawar, C. W. Kim, M.-T. Nguyen-Le and Y. S. Kang, General Review on the Components and Parameters of Photoelectrochemical System for CO<sub>2</sub> Reduction with in Situ Analysis, *ACS Sustain. Chem. Eng.*, 2019, **7**, 7431–7455; (d) P. R. Yaashikaa, P. Senthil Kumar, S. J. Varjani and A. Saravanan, A review on photochemical, biochemical and electrochemical transformation of CO<sub>2</sub> into value-added products, *J. CO<sub>2</sub> Util.*, 2019, **33**, 131–147.

179 T. D. Nguyen, T. Van Tran, S. Singh, P. T. T. Phuong, L. G. Bach, S. Nanda and D.-V. N. Vo, in *Conversion of Carbon Dioxide into Hydrocarbons Vol. 2 Technology*, ed. Inamuddin, A. M. Asiri and E. Lichtfouse, Springer International Publishing, Cham, 2020, ch. 6, pp. 159–183, DOI: [10.1007/978-3-030-28638-5\\_6](https://doi.org/10.1007/978-3-030-28638-5_6).

180 M. Bonchio, J. Bonin, O. Ishitani, T.-B. Lu, T. Morikawa, A. J. Morris, E. Reisner, D. Sarkar, F. M. Toma and M. Robert, Best practices for experiments and reporting in photocatalytic CO<sub>2</sub> reduction, *Nat. Catal.*, 2023, **6**, 657–665.

181 E. C. C. Baly, I. M. Heilbron and W. F. Barker, CX.—Photocatalysis. Part I. The synthesis of formaldehyde and carbohydrates from carbon dioxide and water, *J. Chem. Soc., Trans.*, 1921, **119**, 1025–1035.

182 T. Inoue, A. Fujishima, S. Konishi and K. Honda, Photoelectrocatalytic reduction of carbon dioxide in aqueous suspensions of semiconductor powders, *Nature*, 1979, **277**, 637–638.

183 B. Aurian-Blajeni, M. Halmann and J. Manassen, Photoreduction of carbon dioxide and water into formaldehyde and methanol on semiconductor materials, *Sol. Energy*, 1980, **25**, 165–170.

184 M. Ulman, A. H. A. Tinnemans, A. Mackor, B. Aurian-Blajeni and M. Halmann, Photoreduction of Carbon Dioxide to Formic Acid, Formaldehyde, Methanol, Acetaldehyde and Ethanol Using Aqueous Suspensions of Strontium Titanate with Transition Metal Additives, *Int. J. Sol. Energy*, 1982, **1**, 213–222.

185 S. M. Aliwi and K. F. Al-Jubori, Photoreduction of CO<sub>2</sub> by metal sulphide semiconductors in presence of H<sub>2</sub>S, *Sol. Energy Mater.*, 1989, **18**, 223–229.

186 F. Solymosi and I. Tombácz, Photocatalytic reaction of H<sub>2</sub>O+CO<sub>2</sub> over pure and doped Rh/TiO<sub>2</sub>, *Catal. Lett.*, 1994, **27**, 61–65.

187 E. Bahadori, A. Tripodi, A. Villa, C. Pirola, L. Prati, G. Ramis, N. Dimitratos, D. Wang and I. Rossetti, High pressure CO<sub>2</sub> photoreduction using Au/TiO<sub>2</sub>: unravelling the effect of co-catalysts and of titania polymorphs, *Catal. Sci. Technol.*, 2019, **9**, 2253–2265.

188 S. Zeng, E. Vahidzadeh, C. G. VanEssen, P. Kar, R. Kisslinger, A. Goswami, Y. Zhang, N. Mahdi, S. Riddell, A. E. Kobryn, S. Gusalov, P. Kumar and K. Shankar, Optical control of selectivity of high rate CO<sub>2</sub> photoreduction via interband- or hot electron Z-scheme reaction pathways in Au-TiO<sub>2</sub> plasmonic photonic crystal photocatalyst, *Appl. Catal., B*, 2020, **267**, 118644.

189 F. Galli, M. Compagnoni, D. Vitali, C. Pirola, C. L. Bianchi, A. Villa, L. Prati and I. Rossetti, CO<sub>2</sub> photoreduction at high pressure to both gas and liquid products over titanium dioxide, *Appl. Catal., B*, 2017, **200**, 386–391.

190 I. Moriya, Converting of CO<sub>2</sub> into low-molecular-weight organic compounds with the TiO<sub>2</sub>/ZrO<sub>2</sub> composites under solar irradiation, *Sci. Rep.*, 2017, **7**, 14446.

191 J. M. Mora-Hernandez, A. M. Huerta-Flores and L. M. Torres-Martínez, Photoelectrocatalytic characterization of carbon-doped NaTaO<sub>3</sub> applied in the photoreduction of CO<sub>2</sub> towards the formaldehyde production, *J. CO<sub>2</sub> Util.*, 2018, **27**, 179–187.

192 M. Lashgari and S. Soodi, Photocatalytic Conversion of CO<sub>2</sub> into Oxygenate Fuels/Chemicals Using Efficient, Eco-Friendly, Titania/Hematite-Based Nanostructured Solar-Energy Materials, *J. Nanosci. Nanotechnol.*, 2019, **19**, 3237–3243.

193 Z. Zhao, J. Fan, S. Liu and Z. Wang, Optimal design and preparation of titania-supported CoPc using sol-gel for the photo-reduction of CO<sub>2</sub>, *Chem. Eng. J.*, 2009, **151**, 134–140.

194 A. Kumar and R. Ananthakrishnan, Visible light-assisted reduction of CO<sub>2</sub> into formaldehyde by heteroleptic ruthenium metal complex-TiO<sub>2</sub> hybrids in an aqueous medium, *Green Chem.*, 2020, **22**, 1650–1661.

195 B. Kim, D. Kwon, J.-O. Baeg, M. Austeria P, G. H. Gu, J.-H. Lee, J. Jeong, W. Kim and W. Choi, Dual-Atom-Site Sn-Cu/C<sub>3</sub>N<sub>4</sub> Photocatalyst Selectively Produces Formaldehyde from CO<sub>2</sub> Reduction, *Adv. Funct. Mater.*, 2023, **33**, 2212453.

196 G. Guan, T. Kida, T. Harada, M. Isayama and A. Yoshida, Photoreduction of carbon dioxide with water over K<sub>2</sub>Ti<sub>6</sub>O<sub>13</sub> photocatalyst combined with Cu/ZnO catalyst under concentrated sunlight, *Appl. Catal., A*, 2003, **249**, 11–18.

197 M. Guo, F. Gu, L. Meng, Q. Liao, Z. Meng and W. Liu, Synthesis of formaldehyde from CO<sub>2</sub> catalyzed by the coupled photo-enzyme system, *Sep. Purif. Technol.*, 2022, **286**, 120480.

198 S. N. Habisreutinger, L. Schmidt-Mende and J. K. Stolarczyk, Photocatalytic Reduction of CO<sub>2</sub> on TiO<sub>2</sub> and Other Semiconductors, *Angew. Chem., Int. Ed.*, 2013, **52**, 7372–7408.

199 X. Chang, T. Wang, P. Yang, G. Zhang and J. Gong, The Development of Cocatalysts for Photoelectrochemical CO<sub>2</sub> Reduction, *Adv. Mater.*, 2019, **31**, 1804710.

200 B. Aurian-Blajeni, I. Taniguchi and J. O. M. Bockris, Photoelectrochemical reduction of carbon dioxide using polyaniline-coated silicon, *J. Electroanal. Chem.*, 1983, **149**, 291–293.



201 M. Zafrir, M. Ulman, Y. Zuckerman and M. Halmann, Photoelectrochemical reduction of carbon dioxide to formic acid, formaldehyde and methanol on p-gallium arsenide in an aqueous V(II)-V(III) chloride redox system, *J. Electroanal. Chem.*, 1983, **159**, 373–389.

202 G. Qin, Y. Zhang, X. Ke, X. Tong, Z. Sun, M. Liang and S. Xue, Photocatalytic reduction of carbon dioxide to formic acid, formaldehyde, and methanol using dye-sensitized  $\text{TiO}_2$  film, *Appl. Catal., B*, 2013, **129**, 599–605.

203 J. F. de Brito, A. R. Araujo, K. Rajeshwar and M. V. B. Zanoni, Photoelectrochemical reduction of  $\text{CO}_2$  on  $\text{Cu}/\text{Cu}_2\text{O}$  films: Product distribution and pH effects, *Chem. Eng. J.*, 2015, **264**, 302–309.

204 C. W. Kim, M. J. Kang, S. Ji and Y. S. Kang, Artificial Photosynthesis for Formaldehyde Production with 85% of Faradaic Efficiency by Tuning the Reduction Potential, *ACS Catal.*, 2018, **8**, 968–974.

205 A. U. Pawar, U. Pal, J. Y. Zheng, C. W. Kim and Y. S. Kang, Thermodynamically controlled photo-electrochemical  $\text{CO}_2$  reduction at  $\text{Cu}/\text{rGO}/\text{PVP}/\text{Nafion}$  multi-layered dark cathode for selective production of formaldehyde and acetaldehyde, *Appl. Catal., B*, 2022, **303**, 120921.

206 S. Das, S. Biswas, T. Balaraju, S. Barman, R. Pochamoni and S. Roy, Photochemical reduction of carbon dioxide coupled with water oxidation using various soft-oxometalate (SOM) based catalytic systems, *J. Mater. Chem. A*, 2016, **4**, 8875–8887.

207 D. J. Boston, C. Xu, D. W. Armstrong and F. M. MacDonnell, Photochemical Reduction of Carbon Dioxide to Methanol and Formate in a Homogeneous System with Pyridinium Catalysts, *J. Am. Chem. Soc.*, 2013, **135**, 16252–16255.

208 D. J. Boston, Y. M. F. Pachón, R. O. Lezna, N. R. de Tacconi and F. M. MacDonnell, Electrocatalytic and Photocatalytic Conversion of  $\text{CO}_2$  to Methanol using Ruthenium Complexes with Internal Pyridyl Cocatalysts, *Inorg. Chem.*, 2014, **53**, 6544–6553.

209 A. Alissandratos and C. J. Easton, Biocatalysis for the application of  $\text{CO}_2$  as a chemical feedstock, *Beilstein J. Org. Chem.*, 2015, **11**, 2370–2387.

210 E. C. C. Baly, I. M. Heilbron and D. P. Hudson, CXXXI. Photocatalysis. Part II. The photosynthesis of nitrogen compounds from nitrates and carbon dioxide, *J. Chem. Soc., Trans.*, 1922, **121**, 1078–1088.

211 J. A. Bassham, A. A. Benson, L. D. Kay, A. Z. Harris, A. T. Wilson and M. Calvin, The Path of Carbon in Photosynthesis. XXI. The Cyclic Regeneration of Carbon Dioxide Acceptor, *J. Am. Chem. Soc.*, 1954, **76**, 1760–1770.

212 (a) L. F. Li, L. Ljungdahl and H. G. Wood, Properties of Nicotinamide Adenine Dinucleotide Phosphate-Dependent Formate Dehydrogenase from *Clostridium thermoaceticum*, *J. Bacteriol.*, 1966, **92**, 405–412; (b) L. Calzadiaz-Ramirez and A. S. Meyer, Formate dehydrogenases for  $\text{CO}_2$  utilization, *Curr. Opin. Biotechnol.*, 2022, **73**, 95–100.

213 K. Murashima, H. Yoneda, H. Sumi and Y. Amao, Electrocatalytic production of formaldehyde with formaldehyde dehydrogenase using a viologen redox mediator, *New J. Chem.*, 2022, **46**, 10004–10011.

214 J. Shi, Y. Jiang, Z. Jiang, X. Wang, X. Wang, S. Zhang, P. Han and C. Yang, Enzymatic conversion of carbon dioxide, *Chem. Soc. Rev.*, 2015, **44**, 5981–6000.

215 (a) M. Miller, W. E. Robinson, A. R. Oliveira, N. Heidary, N. Kornienko, J. Warnan, I. A. C. Pereira and E. Reisner, Interfacing Formate Dehydrogenase with Metal Oxides for the Reversible Electrocatalysis and Solar-Driven Reduction of Carbon Dioxide, *Angew. Chem., Int. Ed.*, 2019, **58**, 4601–4605; (b) B. S. Jayathilake, S. Bhattacharya, N. Vaidehi and S. R. Narayanan, Efficient and Selective Electrochemically Driven Enzyme-Catalyzed Reduction of Carbon Dioxide to Formate using Formate Dehydrogenase and an Artificial Cofactor, *Acc. Chem. Res.*, 2019, **52**, 676–685.

216 (a) S. K. Kuk, R. K. Singh, D. H. Nam, R. Singh, J.-K. Lee and C. B. Park, Photoelectrochemical Reduction of Carbon Dioxide to Methanol through a Highly Efficient Enzyme Cascade, *Angew. Chem., Int. Ed.*, 2017, **56**, 3827–3832; (b) K. Ma, O. Yehezkel, E. Park and J. N. Cha, Enzyme Mediated Increase in Methanol Production from Photoelectrochemical Cells and  $\text{CO}_2$ , *ACS Catal.*, 2016, **6**, 6982–6986; (c) R. K. Yadav, G. H. Oh, N.-J. Park, A. Kumar, K.-j. Kong and J.-O. Baeg, Highly Selective Solar-Driven Methanol from  $\text{CO}_2$  by a Photocatalyst/Biocatalyst Integrated System, *J. Am. Chem. Soc.*, 2014, **136**, 16728–16731.

217 R. Cazelles, J. Drone, F. Fajula, O. Ersen, S. Moldovan and A. Galarneau, Reduction of  $\text{CO}_2$  to methanol by a polyenzymatic system encapsulated in phospholipids-silica nanocapsules, *New J. Chem.*, 2013, **37**, 3721–3730.

218 W. Liu, Y. Hou, B. Hou and Z. Zhao, Enzyme-catalyzed Sequential Reduction of Carbon Dioxide to Formaldehyde, *Chin. J. Chem. Eng.*, 2014, **22**, 1328–1332.

219 J. Shi, L. Zhang and Z. Jiang, Facile Construction of Multicompartment Multienzyme System through Layer-by-Layer Self-Assembly and Biomimetic Mineralization, *ACS Appl. Mater. Interfaces*, 2011, **3**, 881–889.

220 J. Shi, X. Wang, Z. Jiang, Y. Liang, Y. Zhu and C. Zhang, Constructing spatially separated multienzyme system through bioadhesion-assisted bio-inspired mineralization for efficient carbon dioxide conversion, *Bioresour. Technol.*, 2012, **118**, 359–366.

221 J. Shi, X. Wang, W. Zhang, Z. Jiang, Y. Liang, Y. Zhu and C. Zhang, Synergy of Pickering Emulsion and Sol-Gel Process for the Construction of an Efficient, Recyclable Enzyme Cascade System, *Adv. Funct. Mater.*, 2013, **23**, 1450–1458.

222 P. S. Nabavi Zadeh, M. Zazzi do Valle Gomes, B. Åkerman and A. E. C. Palmqvist, Förster Resonance Energy Transfer Study of the Improved Biocatalytic Conversion of  $\text{CO}_2$  to Formaldehyde by Coimmobilization of Enzymes in Siliceous Mesostructured Cellular Foams, *ACS Catal.*, 2018, **8**, 7251–7260.

223 J. Zhou, S. Yu, H. Kang, R. He, Y. Ning, Y. Yu, M. Wang and B. Chen, Construction of multi-enzyme cascade



biomimetic carbon sequestration system based on photocatalytic coenzyme NADH regeneration, *Renewable Energy*, 2020, **156**, 107–116.

224 P. Bauler, G. Huber, T. Leyh and J. A. McCammon, Channeling by Proximity: The Catalytic Advantages of Active Site Colocalization Using Brownian Dynamics, *J. Phys. Chem. Lett.*, 2010, **1**, 1332–1335.

225 (a) J. Liu and M. Antonietti, Bio-inspired NADH regeneration by carbon nitride photocatalysis using diatom templates, *Energy Environ. Sci.*, 2013, **6**, 1486–1493; (b) A. Weckbecker, H. Gröger and W. Hummel, in *Biosystems Engineering I: Creating Superior Biocatalysts*, ed. C. Wittmann and R. Krull, Springer Berlin Heidelberg, Berlin, Heidelberg, 2010, pp. 195–242.

